PUBLIC VENTURA COUNTY WORKS

COUNTY of VENTURA

Jeff Pratt
Agency Director

David Fleisch
Assistant Director

Central Services
Joan Araujo, Director

Engineering Services
Christopher Cooper, Director

Roads & Transportation
Christopher Kurgan, Director

Water & Sanitation
Joseph Pope, Director

Watershed Protection
Glenn Shephard, Director

Arroyo Las Posas Stormwater Diversion Feasibility Study and Percolation Test

By:

Craig Ulrich, Sebastian Uhlemann, Michelle Newcomer and Peter Fiske

BERKELEY LAB
Bringing Science Solutions to the World

EARTH & ENVIRONMENTAL SCIENCES

PUBLIC VENTURA COUNTY WORKS

VENTURA COUNTY WATERWORKS DISTRICTS

VENTURA COUNTY WATERWORKS DISTRICT NO. 1
MOORPARK

Executive Summary

Background

Water users are facing increasing constraints in the amount of groundwater they can withdraw due to the slow rate of natural recharge. With climate change exacerbating the duration of droughts and the intensity of precipitation during wet periods, water managers are seeking ways of capturing a greater fraction of precipitation that would normally run off to the ocean to accelerate aquifer recharge. In California, recent regulations require that all Groundwater Sustainability Agencies become compliant with their newly formulated groundwater sustainability plans. Local water districts and other entities are currently working together to identify methods to capture these elevated flood flows before they reach the Pacific Ocean and use the captured water for aquifer recharge. Eighty to 90% of the flood flows in the Arroyo Las Posas River are estimated to discharge to the Pacific Ocean every year. Ventura County Waterworks District No. 1 (VCWWD) along with other water entities intend to utilize the existing percolation ponds at the Moorpark Water Reclamation Facility to capture some of the yearly flood flows for managed aquifer recharge (MAR). VCWWD estimates the project could potentially recharge up to 3,000 acre-feet of captured runoff per year. However, the realization of that potential depends on how much water can be infiltrated quickly during large storm events, making the performance of the ponds a key factor in overall benefit.

Study Scope and Objectives

The objective of the feasibility study and percolation test is to utilize novel technology that may optimize percolation pond design, which potentially could be replicated across the Metropolitan service area. VCWWD and Lawrence Berkeley National Lab (LBNL) will conduct a geophysical study of the structure and permeability of the subsurface soils below percolation ponds located in the Arroyo Las Posas region, at the Moorpark Facility, using state-of-the-art electrical resistivity tomography (ERT) and other methods. Areas of low permeability and high permeability will be identified and methods to increase the overall permeability of each basin will be developed.

The goals of this study were as follows:

1. Develop an approach using geophysical methods and other sensors to characterize the subsurface soils and quantify recharge in selected percolation ponds during controlled recharge events.
2. Identify the potential to improve recharge in the selected ponds.
3. Determine if water was leaking (“leakage”) or lost from the ponds directly into the adjacent Arroyo or recharging the aquifer.
4. Determine if this approach is transferable to any other location within Metropolitan’s service area.

To achieve these goals, LBNL characterized the top 2 m (6 ft) of soil in ponds 8 to 13 and based on those results selected two ponds that represented contrasting soil types to perform the controlled recharge experiments. After ponds 9 and 10 were selected deeper sensing geophysical tools were used to capture the spatial distribution of soil types. The geophysical data was used to place the location of four 15 m (50 ft) deep soil borings to log all the soil types observed in the geophysical data.

Once the geology beneath ponds 9 and 10 was characterized the geologic model was then used to strategically place soil moisture, soil temperature, and water level sensors for the recharge experiments. Prior to the recharge experiments background data for the timelapse resistivity tomography (used to image the migration of water in the subsurface), soil moisture, soil temperature and saturated hydraulic conductivity (at strategic locations) was collected for comparison.

Timelapse resistivity data showed the tortuosity of fluid movement in the subsurface that was controlled by high permeability fast paths across both ponds. Little to no infiltration was observed in half of pond 9 compared to pond 10 and was controlled by soil texture. All of the timelapse and characterization data was used in two hydrological models (Hydrus and Min3P) to simulate and evaluate current spatial recharge rates. Recharge at strategic locations were also monitored with novel vertical thermal probes and used in a 1D thermal flux model to estimate recharge rates. These probes were tested as a simple cost-effective tool to monitor recharge performance.

The Hydrus model was used to evaluate the potential to improve recharge in the top 2 m (6ft) of ponds 8 through 13. The results from this modeling approach required limited data (resistivity and saturated hydraulic conductivity) measured in each pond to simulate pond modifications' that would improve recharge. In one example, removal of the 2ft thick low permeability soils in half of pond 9 to expose the sandy soils below would improve recharge rates by 185% from *2186 m^3 (1.77 AF) to 6224 m^3 (5.04 AF)* over a 24hr period!

The successes of this study were numerous and provide an approach that can be tailored and used at any site to characterize the subsurface, image water movement over time and confirm deep percolation, quantify recharge rates and volumes, and provide insights for system modification to improve and maximize recharge. The following are a list of key findings and lessons learned.

The results from this study have currently resulted in one peer-reviewed publication and others are currently being developed.

Uhlemann, Sebastian, Craig Ulrich, Michelle Newcomer, Peter Fiske, Jeewoong Kim, and Joseph Pope. "3D hydrogeophysical characterization of managed aquifer recharge basins." *Frontiers in Earth Science* 10 (2022): 942737. https://doi.org/10.3389/feart.2022.942737

Key Findings and Lessons Learned

The results from this pilot study have identified an approach that incorporates a suite of geophysics and point sensors that can be successfully designed to characterize, monitor and estimate recharge at a MAR site.

Key Findings and Lessons Learned:

1. The study approach overall was able to image water recharge deep into the subsurface confirming aquifer recharge.
2. This study provides a dynamic approach that can be tailored to the project needs and the site dimensions. This *'cookbook'* is highlighted as a guide for the water user in the Conclusion section.
3. The streamside electrical resistivity monitored the potential for "leakage" from the infiltration ponds back into the river and **no evidence of leakage** was observed during the study period. These are site specific results and all recharge next to rivers should evaluated.
4. The soil spatial variability in all ponds was quickly mapped to a depth of 2 m using electromagnetic induction and took roughly 2 – 3 hours to cover six ponds. This is a cost-effective way to identify areas of low and high soil permeability.
5. Time-lapse electrical resistivity coupled with soil hydrogeological sensors (soil moisture and soil temperature) was able to image preferential flow paths conveying water deep to the aquifer (15 m or 50 ft).
6. Hydrus 1D was coupled with hydraulic conductivity values to create infiltration estimates across all ponds on a 1 m x 1 m grid without a flooding event and provide insight on basin modifications to improve infiltration rates.
7. All direct and indirect sensing data from the geophysical and hydrogeological sensors was able to be incorporated into the 1D and 3D models. This data can be incorporated into other hydrological models.
8. All estimates of infiltration from the 1D and 3D models agreed and fit the soil type distributions. Silty clayey soils had a less than 0.5 cm/h infiltration rates compared to sandy soils that were as high as 26 cm/h.
9. Infiltration estimates could be improved for the 1D temperature sensor method using VFLUX by extending the flooding duration longer than 24 hours.
10. More measurements of the saturated hydraulic conductivity throughout each pond would improve the estimates of infiltration for both the 1D and 3D models.

Recommendations

Based on this pilot study the follow recommendations have been identified:

1. Observations of soil layer thickness from the geophysics and soil cores identified a 1 m thick silty clayey layer at the north end of Pond 9 with low infiltration rates (<0.5 cm/h). Hydrus 1D modeling showed removal of this low permeability layer increased infiltration rates up to 6 - 26 cm/h. This increase means that Pond 9 total recharge (24 hr) would **increase by 185%** from *2186 m^3 (1.77 AF) to 6224 m^3 (5.04 AF)!*
2. Pond 8 shows a thin layer of low permeability soils with sandy soils below, like Pond 9,

and could be improved with dramatic affects by removal of the thin clayey soil layer.

3. Ponds 12 – 13 show a deeper (~1 m) lower permeability layer below the surface sandy soils which could make these ponds more suitable as settling basins to remove fines as part of an operation and maintenance plan, or the installation of drywells could be used to convey the water to the deeper sandier soils to improve site recharge capabilities.

Partners/Stakeholders role and relationship to the study

Funding Agency: *Metropolitan Water District*
Member Agency: *Calleguas Municipal Water District*
Water District, Site Owner, Proposal Partner: *Ventura County Public Works*

This project consists of four entities including LBNL. Metropolitan is the funding agency and performs oversite and review of all progress reports and invoicing. Calleguas is the member agency of Metropolitan and performs oversight of the project ensuring that all deliverables are met at the proposed time intervals, and also is the liason for Ventura and LBL with Metropolitan. Ventura is the owner of the site where the experiment will be performed. Ventura coordinates with LBL for site access and assistance with performing the experiment where needed. LBNL's role was to perform the research to evaluate the goals proposed in the FSA Agreement 188682.

Table of Contents

Tables

Figures

the pond fills. At +16.9 hours the broken pump was fixed and water application commenced. After the pond is filled fairly uniform infiltration is observed at +21.9 hours. Until the southern end sandy soils take over and recharge more of the water at +40.9 hours. The northwest corner clayey soils zone never infiltrated water.

Figure 16. Recharge Phase DTP locations in Ponds 9, 10 and 11. Ponds 9 and 10 had fifteen DTPs installed before the recharge events and Pond 11 had five DTP probes to investigate the lateral flow through the sand channel during the Pond 10 flooding event.

Figure 17. Pond 9 DTP thermal response examples from silty clay no recharge (A & C, northern end) and sandy fast recharge (B & D, southern end). The start and stop of water application is shown in A and B by the green and red lines, and the pond empty is shown by the blue line. Little to no infiltration is observed in the clayey soils (C, red dashed line) compared to very fast and deep infiltration in the sandy soils (D, red dashed line).

Figure 18. Shows the locations of the water level sensors (red dots) and the soil moisture sensors (black dots) with the associated datalogger number. At each soil moisture location, a vertical profile of three soil moisture sensors were installed at 15 cm, 30 cm, and 60 cm bgs.

Figure 19. Shows the Pond 9 soil volumetric soil moisture responses at A) 15cm depth, B) 30cm depth, and C) 60cm depth. On the secondary axis is the water levels at two locations.

Figure 20. Pond 9 Neutron Probe soil moisture responses for B-1 and B-2. B-1 was located in the little to no infiltration zone containing fine grain sediments and B-2 was in the southern sandier soils. These plots show both the volumetric water content and the percent moisture content with the same scales for interchangeable comparison. Little to no change observed in B-1 at all depths except 0 – 1 m. B-2 shows fast, deep infiltration down to 10 m. In some locations, for instance from 4 – 6 m background soil moisture was at 10% or less and increase up to 20%+ over time.

Figure 21. The filling of Pond 10 with 407k gallons (1.5 AF). The pond was never filled due to the high infiltration rates that were similar to the pump outflow rates.

Figure 22. Shows the time-lapse ERT infiltration in Pond 10 as a percent change in resistivity. The background resistivity model prior to water application is shown as a reference. The time after the start of water application is shown in the lower left of each image. Many fast flow paths are observed and connect and reconnect to different zones as the pond fills. Deep recharge is observed over 15m deep. Negative percent change means a decrease in resistivity associated with an increase in saturation.

Figure 23. Pond 10 DTP thermal response examples in sandy soils. The start and stop of water application is shown in (A) and (B) by the green and red lines, and the pond empty is shown by the blue line. DTP probes show tortuosity in the heat migration through the subsurface (C) likely due to horizontal flow observed in the ERT data. Compared to linear heat movement through the subsurface (D) indicating vertical flow.

Figure 24. Shows the Pond 10 soil volumetric soil moisture responses at A) 15cm depth, B) 30cm depth, and C) 60cm depth. All sensors for 1495 show no change in moisture content because it was not inundated. 1491 sensors are located adjacent to the water output pipe but the soils from the EMI show it is in a silty type of soil and a delayed soil moisture increase occurs due to slow infiltration. 1782 and 1817 sensors are located in sandy soil and fast increases in moisture content are observed to 60cm depth.

Figure 25. Pond 10 Neutron Probe soil moisture responses for B-3 and B-4. Both B-3 and B-4 are located in sandy soils but B-3 was in the area of the topographic high and was never inundated. Therefore, no changes are observed in the soil moisture along borehole B-3. B-4 shows deep infiltration (red dashed line). Soil moisture increases from ~10% to ~22% from 0-9m bgs. Below 9m soil moisture is somewhat constant.

Figure 26. shows the location of the streamside ERT profile to monitor for water flow back into the river. Eleven time series datasets were collected from June 24th to July 1st and are shown as a percent

change from the baseline dataset collected June 24th before all water applications. The top of the ERT profile is at the same elevation of the ponds and the river elevation is shown as a dashed blue line. The small percent change in resistivity indicate no water flow back into the river when compared to changes during the flooding events in Figures 14 and 21.

Figure 27. Estimated infiltration rates based on groundwater recharge modeling (Hydrus 1D) for 1 m ×1 m grid cells within each pond, using the Ksat distribution estimated from the EMI data.

Figure 28. Pond 9 simulated infiltration over 36 hours shown in north-south cross sections. The majority of the infiltration happens at the south end of the Pond 9 through the sandy soils. Saturation below the north end of the pond are 5% or less. Red dashed box shows the southwest corner infiltrates more water than the southeast corner.

Figure 29. Pond 9 estimated infiltration rate distributions from 3D modeling at elevation 117 m (A) and 110 m (B). Note the pond bottom is at 118 m). Downward infiltration rates (positive) in the north end of the pond increase with depth (B) and stay relatively the same on the south end with depth.

Figure 30. Electrical resistivity models obtained from the EMI and ERT. Shown are slices through the 3D models for ponds 9 and 10, and the 2D transects that were acquired in pond 11. For ponds 9 and 10, resistivities > 200 □m is shown, which represent the sandy layers. Note that at the northern part of pond 9, this layer is overlain by a ~1m thick layer of low resistivity (blue colors).

Figure 31. LBNL Recharge Cookbook guidance document for planning groundwater recharge site development, monitoring, improvement, etc. based on goals and budget.

Acronyms and Abbreviations

AF – Acre-feet
bgs – Below Ground Surface
cm/h – Centimeters/hour
DTP – Distributed Temperature Probe
EMI – Electromagnetic Induction
ERT – Electrical Resistivity Tomography
Facility – Moorpark Water Reclamation Facility
K_{sat} – Saturated Hydraulic Conductivity
LADWP – Los Angeles Department of Water and Power
LBNL - Lawrence Berkeley National Laboratory
MAR – Managed Aquifer Recharge
m – Meters
m^3 – cubic meters
Mgal – million gallons
Metropolitan– Metropolitan Water District of Southern California
CMWD – Calleguas Municipal Water District
VCWWD – Ventura County Waterworks District No. 1

1.0 Introduction, Site Background and Methods

1.1 Introduction

Historically, Southern California has relied on imported water to meet the water demands for almost a decade because the demand is greater than the amount of water produced locally. Metropolitan provides roughly 50% of the supplies to its service from the Colorado Aqueduct and State Water Project, 40% to 60% depending on hydrology. The remainder comes from local supplies such as groundwater, surface water, recycling and desalination, as well as the LADWP's aqueduct. In the face of climate change, continued droughts, and future water uncertainty Southern California water agencies, along with the rest of the State of California, is looking towards MAR as part of the solution to local groundwater sustainability. Diverting stormwater flows for local aquifer replenishment during the wet winter months appears to be a potential avenue to ease the reliance on imported water. Further still, METROPOLITAN is investing money in pilot programs through its Future Supply Actions Funding Program to "promote technical advances to better prepare the region to adapt to future water supply uncertainties".

Local water districts like VCWWD and CMWD, and other entities are currently working together to identify methods to divert elevated flood flows before they reach the Pacific Ocean and use the captured water for MAR. VCWWD estimated 80% to 90% of the flood flows in the Arroyo Las Posas River are estimated to discharge to the Pacific Ocean every year. VCWWD estimates the project could potentially recharge up to 3,000 acre-feet of captured runoff per year. However, the realization of that potential depends on how much water can be infiltrated quickly during large storm events, making the performance of the ponds a key factor in overall benefit.

The focus of this pilot study was to use a suite of geophysical technologies to characterize the beneath selected basins, and use that information to perform controlled recharge tests in order to monitor subsurface water movement and fate, estimate infiltration rates across the selected percolation ponds and determine if infiltration could be improved, and ultimately develop an approach that can be utilized at other locations performing MAR.

1.2 Site Background

The study site is located at VCWWD's Moorpark Reclamation Facility (Facility) in Moorpark, CA (Figure 1). The Facility is located along the Arroyo Las Posas River in the Little Simi Valley between the Arroyo and East Los Angeles Avenue. The Facility contains approximately 32 percolation ponds of which six ponds (#8-13) were selected to be evaluated for the percolation experiment. The layout of ponds 8 – 13 are shown in Figure 2.

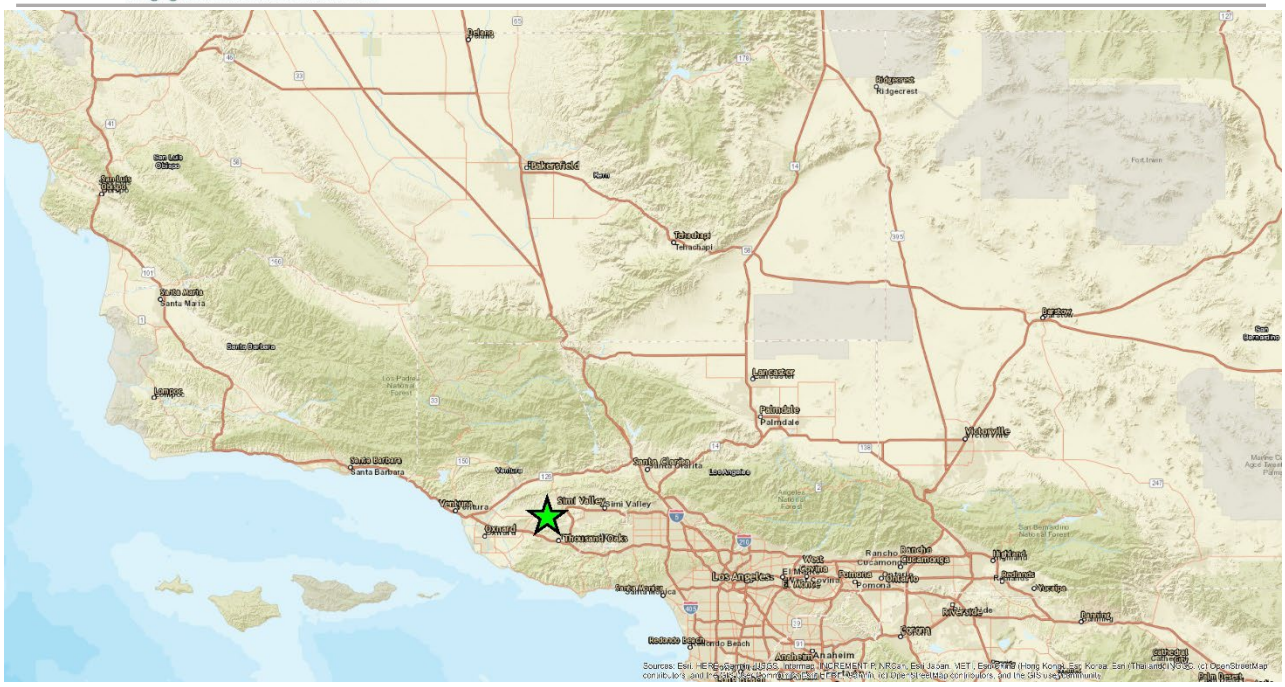

Figure 1. Site location (green star) at the Moorpark Water Reclamation Facility in Moorpark, California.

Figure 2. Moorpark Water Reclamation Facility showing Ponds (P) 8 – 13 that will be part of the Percolation Test study adjacent to the Arroyo Las Posas.

1.3 Methods

In order to achieve the goals of the project LBNL's geophysical team used a suite of geophysical methods, point sensors (some novel), and soil cores to characterize, monitor, and quantify recharge using recycled water from the Facility. To capture the amount of water applied to each pond an in-line flow meter was secured to the outlet pipe at the edge of the pond during water application.

During the characterization phase an Electromagnetic Induction (EMI) method was used, which is walkable and provides fast reconnaissance data. This method measures the electrical conductivity of the ground, which is sensitive to soil moisture, texture and salinity. The chosen instrument can map the subsurface properties and their spatial variability to a depth of about 2m bgs. The EMI instrument generates an electromagnetic field that migrates from the transmitter into the ground causing current to flow through the soil which produces a secondary electromagnetic field that is sensed by the receiver coils. As the system is traversed across the ponds an image of the electrical conductivity variations is produced. The CMD-MiniExplorer 6L is a 6-coil system operating at 24.74 kHz that images the soil conductivity at apparent depths of 0.30, 0.5, 0.80, 1.1, 1.6, and 2.3 m (using a horizontal coplanar coil orientation). Similarly, for deep soil characterization and recharge monitoring Electrical Resistivity Tomography (ERT) was used, which measures the electrical resistivity of the ground (the inverse of the conductivity) and is also sensitive to soil moisture, texture, and salinity. The ERT system collects data through galvanic

conduction with the ground via metal stakes (electrodes), which are hammered approximately 30 cm into the ground, and connected to the system through a multi-core cable. A data collection unit will inject current between a pair of electrodes which induces an electrical field in the ground and the resulting voltage change of that field is mapped with the other electrodes not used for injecting current. In order to map the subsurface in 3D a series of parallel lines were collected to map the shallow and deep (20m) soil resistivity. Note, resistivity and conductivity are the inverse (e.g. resistivity = 1/conductivity) of each other and interchangeable. During the characterization and recharge phases of this study, an MPT-DAS1 system was used. More information about the theory of these two methods can be found in textbooks, such as Reynolds (2011) "An introduction to Applied and Environmental Geophysics".

To capture the water level change in the pond over time we used the METER CDT5 pressure sensors and to monitor shallow (<1m) soil moisture changes the METER Terros 12 moisture sensors. To monitor deep (0 m – 15 m) soil moisture changes we used the InstroTek Inc. 503 Elite Hydroprobe, which is a sealed source neutron probe that emits high-energy neutrons that interact with hydrogen molecules in the soil pore-water and thermalize (slow down). The hydroprobe has a slow (thermal) neutron detector that counts the slow neutrons. An increase in soil moisture results in a proportional increase in slow neutrons. The soil moisture is then estimated using an internal calibration curve.

Saturated hydraulic conductivity (K_{sat}) measurements were made in the top 30 cm below the surface of the ponds with a SOILMOISTURE Equipment Corp. Guelph Permeameter. This system is an in-hole constant-head permeameter that involves measuring the steady-state rate of water infiltration into unsaturated soil in a cylindrical hole. The measurement is made by filling the borehole with a known height of water, once the water bulb in the surrounding soil has been sufficiently formed a steady-state flow of water will occur. This flow rate with the know dimensions of the borehole and water depth permits the K_{sat} measurement.

Initial infiltration rates were collected using a modified seepage meter. One-third of a 55-gallon drum is used to create a seepage meter and is inserted about 1.5 – 2.5 cm into the ground, the top of the drum was cut open to pour a known volume of water into the drum to simulate an infiltration ring or above-ground percolation test. Water was poured into the drum and then timed until all the water had infiltrated.

A vertical array of thermistors (DTP) developed at LBNL was inserted into the ground (0 – 1.2m) and the thermistors were set to 1 min measurement intervals to capture the migration of the daily diurnal thermal flux into the subsurface. These soil temperature measurements combined with soil property measurements from the soil cores at LBNL's soil lab (e.g. soil thermal conductivity) were used in a soil thermal model to estimate 1D infiltration rates between any vertical pair of thermal sensors.

We measured the daily evaporation rate during the recharge phase using five known volume containers. Two liters of water were put into each container and each container's volume of water was measured periodically throughout the duration of the recharge phase (week long).

Lastly, Gregg Drilling was contracted to perform soil coring with a track mounted Geoprobe rig to collect standard direct-push soil cores at 1.5 m increments. The LBNL team logged the cores and collected soil samples for analysis in the LBNL soil lab.

Photos of these instruments in use are shown through the following sections.

2.0 Study Results and Analysis

A summary of the different tasks/phases of the project are listed below:

- **Scoping and Design Phase**: The goal of the scoping and design phase was to meet with VCWWD at the facility to discuss the potential percolation ponds and any historical data that could aid in pond(s) selection. This information will be used to design the characterization and recharge phases.
- **Characterization Phase**: The goal of the characterization phase was to map the geological structure (low and high permeability) beneath a series of selected percolation ponds using different geophysical methods. These results would be used to place soil borings to log the different soil types identified throughout the ponds. Combining these data sets provide a 3D model of the spatial geology beneath the selected ponds.
- **Recharge Phase**: The goal of the recharge phase was to use the characterization data to place a variety of sensors (water level, soil moisture, permeameter, etc.) in different soil types to quantify recharge during a controlled recharge experiment. The controlled recharge experiment was performed with facility recycled water and used to flood an entire basin. During the experiment water movement would be imaged to understand lithologic controls of water movement and sensors to quantify recharge.
- **Data Analysis Phase**: The goal of the data analysis phase was to check the quality of all of the data collected and process (inversion, etc.) the data for assimilation and interpretation.
- **Data Interpretation and Recommendation Phase**: The goal of the data interpretation and recommendation phase was to assess the current recharge potential of each site from the characterization and recharge phases. These data sets would be used to assess if improvements (via pond modification) could be made to increase the recharge potential of the selected ponds.

2.1 Characterization Phase

On August 31st, 2020 the LBNL geophysics team mobilized to Moorpark Water Reclamation Facility to initiate the characterization phase of the project. The goals of this phase of the project were to characterize the shallow subsurface soil structure across Ponds 8 through 13 and then use those results to down-select two ponds that will be used in a controlled flooding experiment (Recharge Phase) to quantify recharge and better understand the recharge process for guidance in later stormwater diversion and MAR. Based on the results reported below, Ponds 9 and 10 were selected for further characterization for the Recharge Phase.

2.1.1 Methods used in characterization phase

During the Characterization Phase the LBNL team used EMI, ERT and DTPs (Figure 3) to characterize the subsurface. The EMI system is a small handheld system that is carried at a constant height just above the ground surface (EMI photo in Figure 2). Data were collected by walking at close spacing in the north-south direction with tie-lines running East-West. This allowed for a dense sampling of the subsurface, and for assessing drift of the instrument. The EMI acquisition took approximately 3 hours to cover Ponds 8 – 13, and the data were collected at 4852 locations.

ERT data (ERT photo in Figure 3) were collected in Ponds 9, 10, and 11. ERT profiles were spaced 3 m apart with a 1.5 m electrode spacing, which resulted in 32 electrodes per profile with 11 profiles in Pond 9, 12 profiles in Pond 10, and 3 profiles in Pond 11. Data were acquired using a dipole-dipole electrode arrangement, with dipole lengths n of 1.5, 3.0, 4.5, 6.0, and 7.5 m, and a dipole separation a of 1 to 8n. Each profile took approximately 0.5 hours to collect, and a total of 43728 measurements were taken. These data were then inverted using the PNNL E4D 3D inversion code. Data quality was evaluated using full reciprocal datasets and all of the inversions converged to a $\chi^2 = 1$, meaning the inversion model fit the data within their errors.

DTP probes (DTP photo in Figure 3) were used to test their response in the pond soils for later use in the Recharge Phase. Ten probes were placed in each of Ponds 9 and 10, and left to collect data for 24 hours. This test was conducted to check the performance of these recently developed sensors for water recharge applications.

The modified seepage meters were used at four locations in each of Ponds 9 and 10. A DTP probe was installed in the center of the seepage meter as a test to capture the temperature change as the water moved into the subsurface (Infiltration test photo Figure 3).

Although collected immediately prior to the recharge phase, saturated hydraulic conductivity was measured as part of the characterization of ponds 8 to 13. The EM data was used as a guide to to perform the tests. Within each pond three to four 7.62 cm diameter auger holes were excavated to a depth of about 30 - 40 cm below ground. The Guelph permeameter was installed in each hole and a constant head infiltration test was performed. For each location saturated hydraulic conductivity was calculated from the measured infiltration rates.

Figure 4 shows the locations where ERT electrodes were deployed and where DTP, percolation tests, and Guelph Permeameter data were acquired.

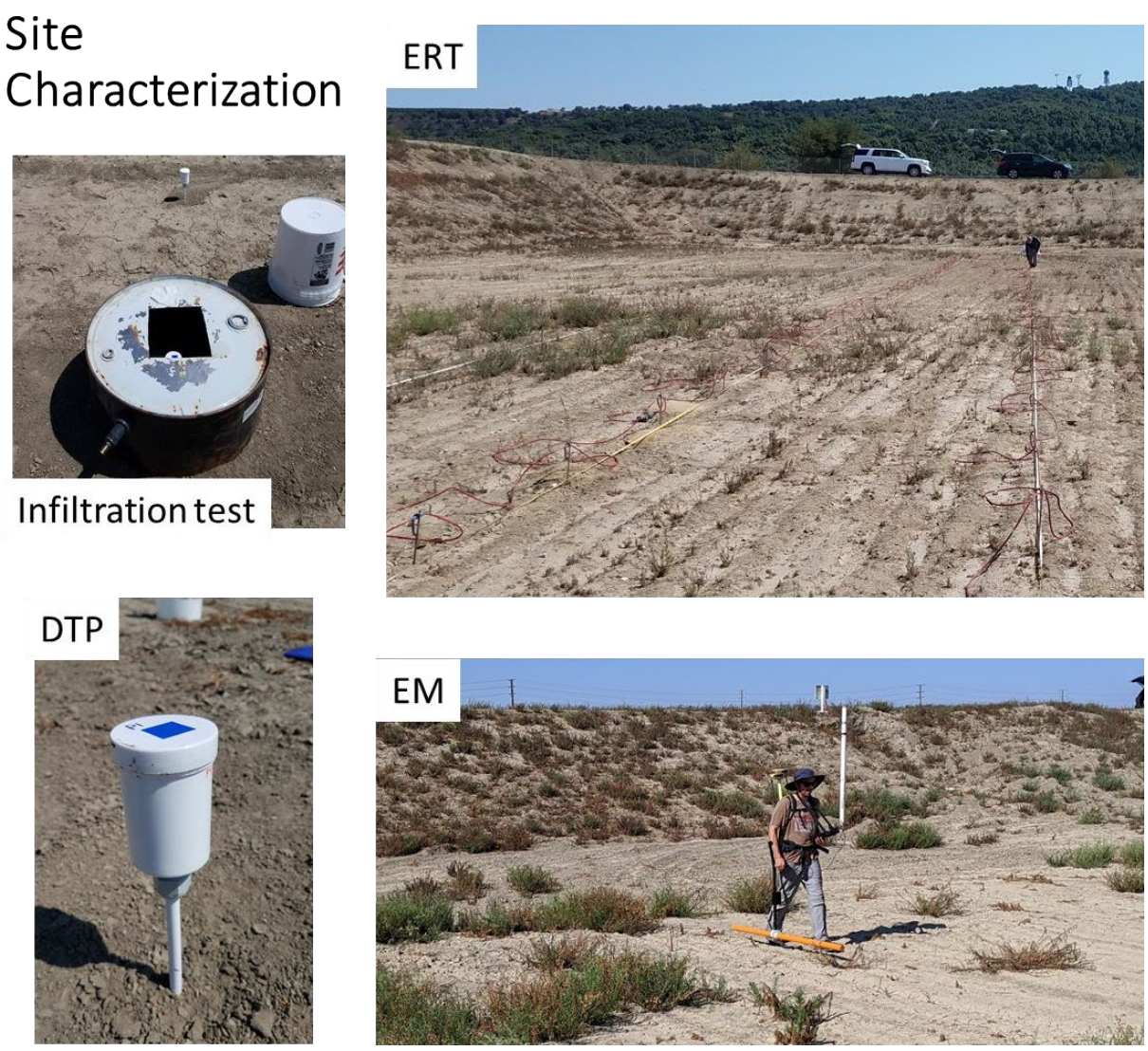

Figure 3. Characterization methods include EMI (EM photo), ERT, DTP, and modified seepage meters for infiltration tests.

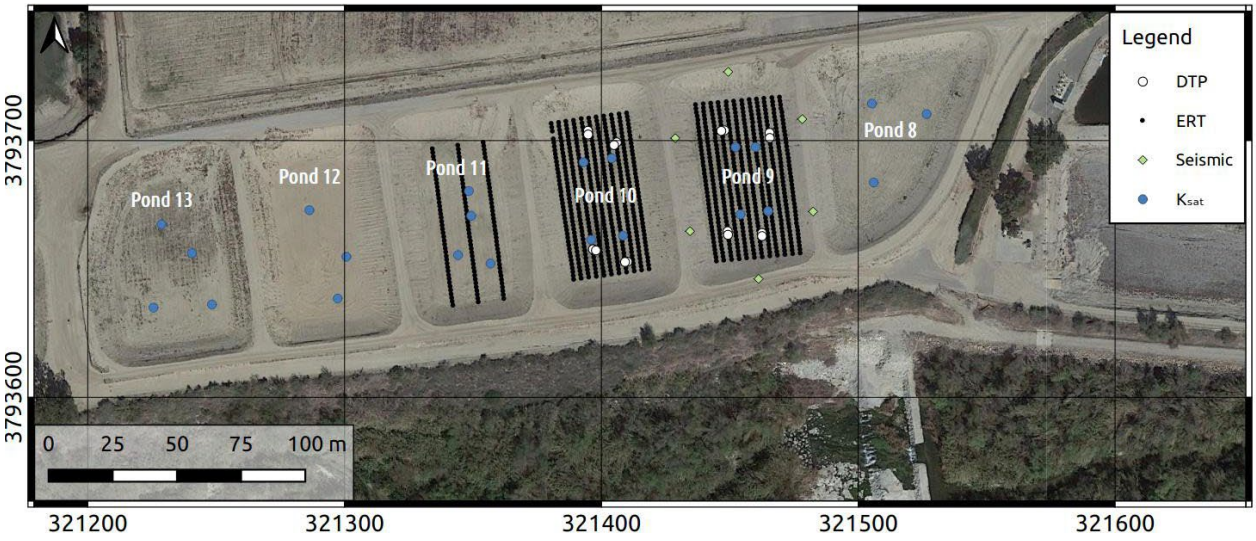

Figure 4. Overview map of data acquired for the characterization phase. Shown are the locations of ERT electrodes (ERT), DTP, and Guelph permeameter readings (K_{sat}). Also shown are locations where ambient seismic noise data were recorded, however, these are not reported on here.

2.1.2 Electromagnetic Induction (EMI) Results

Apparent conductivities recorded using the EMI instruments show that soil electrical conductivities vary spatially in each pond. Figure 5 shows the soil apparent electrical conductivity (ECa) for all sensor depths across all six ponds (Fig. 5A – F). The electrical conductivity ranges from close to zero to 50 milli-Siemens/m (mS/m). Very low conductivity (typically associated with coarse-grain soils) is observed across all ponds in Figure 5A at 0.3 m depth except in the northern parts of P8 and P9. The red colored data points indicate a dry sandy soil, while yellow to blueish colors in the northern portions of P8 and P9 likely relate to soils with higher silt and clay content. For all ponds ECa increases with increasing depth, indicating an increase in soil moisture or fine-grain soils with depth. Data from deeper depths, show more distinct and spatially continuous subsurface features. A potential sandy channel is observed trending northeast-southwest across pond P10 (north side) into P11 and into P12 (red zone middle of pond) passing through the southeast corner of P13. This is a distinct feature extending from 0.5 m to 1.6 m (Figs. 5B-E), but has only a faint signature at 2.3 m depth (Fig. 5F). Another, low conductivity feature can be seen with the same orientation within P8 and P9.

One of the goals of this study is to assess the recharge rates of the ponds of the Moorpark facility, and to determine whether water is short-circuiting back to the river. While Ponds 11 – 13 show reasonably homogeneous soil properties, Ponds 9 and 10 show contrasting properties. One part of Pond 9 shows high electrical conductivity (which can be related to low hydraulic conductivity fine soils), while the other part has low electrical conductivity (related to high hydraulic conductivity coarse soils); and, Pond 10 shows low electrical conductivity (sandy soils) throughout. Because of those pronounced differences between and within Ponds 9 and 10, they were chosen to be the focus of the recharge phase and additional characterization. Therefore, Ponds 9 and 10 were further characterized with DTPs, Guelph permeameter readings (K_{sat}) and the ERT.

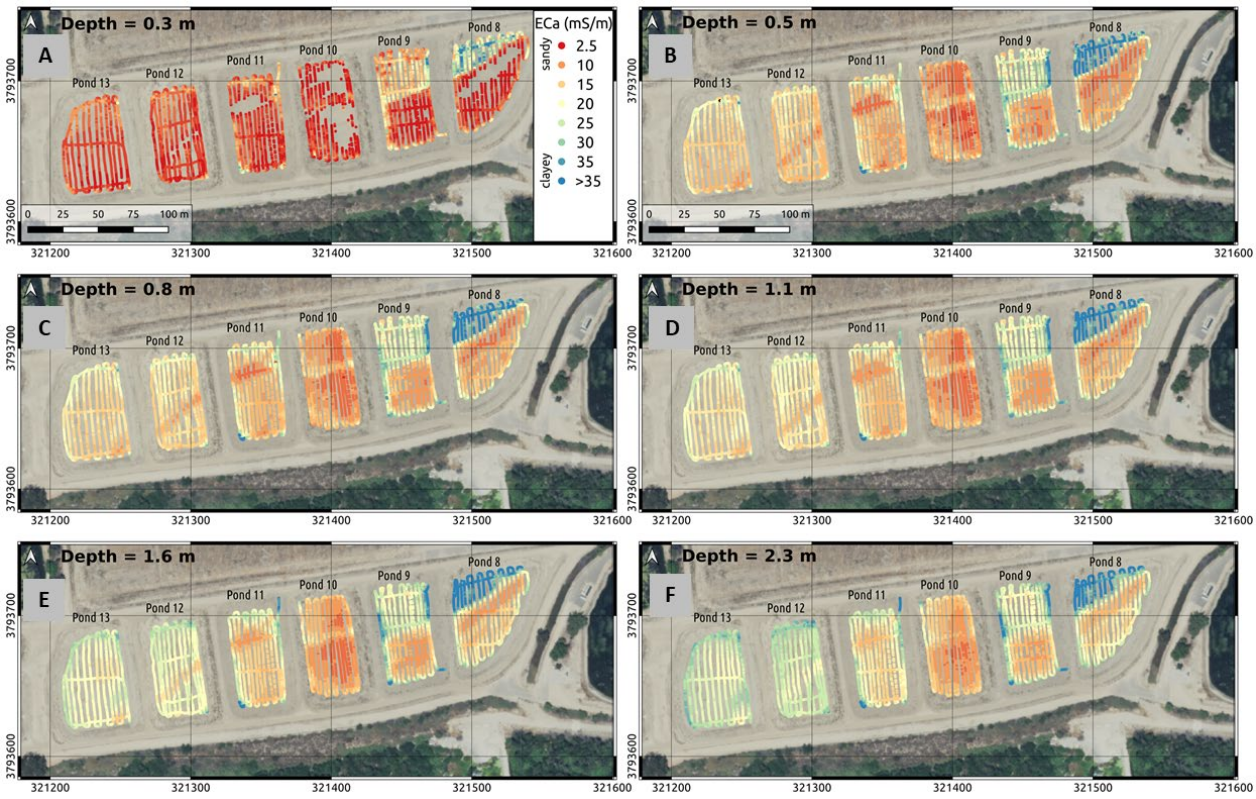

Figure 5. EMI apparent conductivities collected in all ponds (P8-P13) at six coil spacings relating to effective investigation depths of 0.3, 0.5, 0.8, 1.1, 1.6, and 2.3 m. High electrical conductivity (blueish colors) indicate clayey soil types, while low electrical conductivity (reddish colors) indicate sandier soils.

2.1.3 Electrical Resistivity Tomography (ERT) Results

On September 1st through 3rd, ERT data were collected in Ponds 9, 10, and 11. The locations of the electrodes for each profile are shown in Figure 6. Three ERT profiles were collected in Pond 11 to capture the vertical extents of expected sandy channel feature connecting ponds 11 to 13 observed in the EM data (Figure 5). Figure 7 shows the 3D ERT results in Ponds 9 to 11. In Pond 9, a clear boundary can be seen between the low resistivity (blue colors), likely fine clayey soils, in the north end of the pond compared to the drier and coarser sandy soils (yellow – red colors) of the southern part of the pond. The vertical extent of the low resistivity, likely clayey- dominated fine-grained soils, appears to be limited to 1 to 2 meters depth. This layer is underlain by higher resistivity soils (> 150 Ωm), which is likely of a more silty-sand texture. The expected sandy soils in the southern end of Pond 9 are underlain by a layer of moderate resistivity (80 - 200Ωm), with increasing resistivity with depth. This can be interpreted as a silty-sand layer with increasing grain size with depth. Because of the strong contrast between the northern and southern end of Pond 9, we expect considerably different recharge performance within this pond.

Pond 10 shows a continuous up to 3-5 m thick surficial layer of high resistivity (> 200 Ωm), which can be interpreted as a continuous layer of sandy soils (Figure 7, red-yellow colors). Below, resistivities decrease indicating a fining of the subsurface materials, which is more pronounced in the northern part of the pond. Although more uncertain, at a depth of 15 - 17 m, resistivities

increase again, indicating potentially coarser grained material. In the center of Pond 10 there is a narrow, low resistivity zone (green-blue east-west colors in Figure 7), which we suspect corresponds to silty-clayey soils, which link to the lower resistivities imaged at depth in the northern part of this pond.

The resistivity data of Pond 11 shows a resistive (> 200 Ωm), shallow anomaly at the location where a sandy channel was mapped by the EMI data. This channel feature appears to widen towards Pond 12 and is less than 2 m deep. In general, the resistivity data of Pond 11 shows a thin (<1 m), high resistivity layer, which is interpreted to be a sandy soil, overlaying a less resistive layer (<60 Ωm) of 1 - 2 m thickness. Below this layer, resistivities increase again to values > 100 Ωm. This can be interpreted as a sequence of sandy soils overlaying silty-sand above a sandy layer.

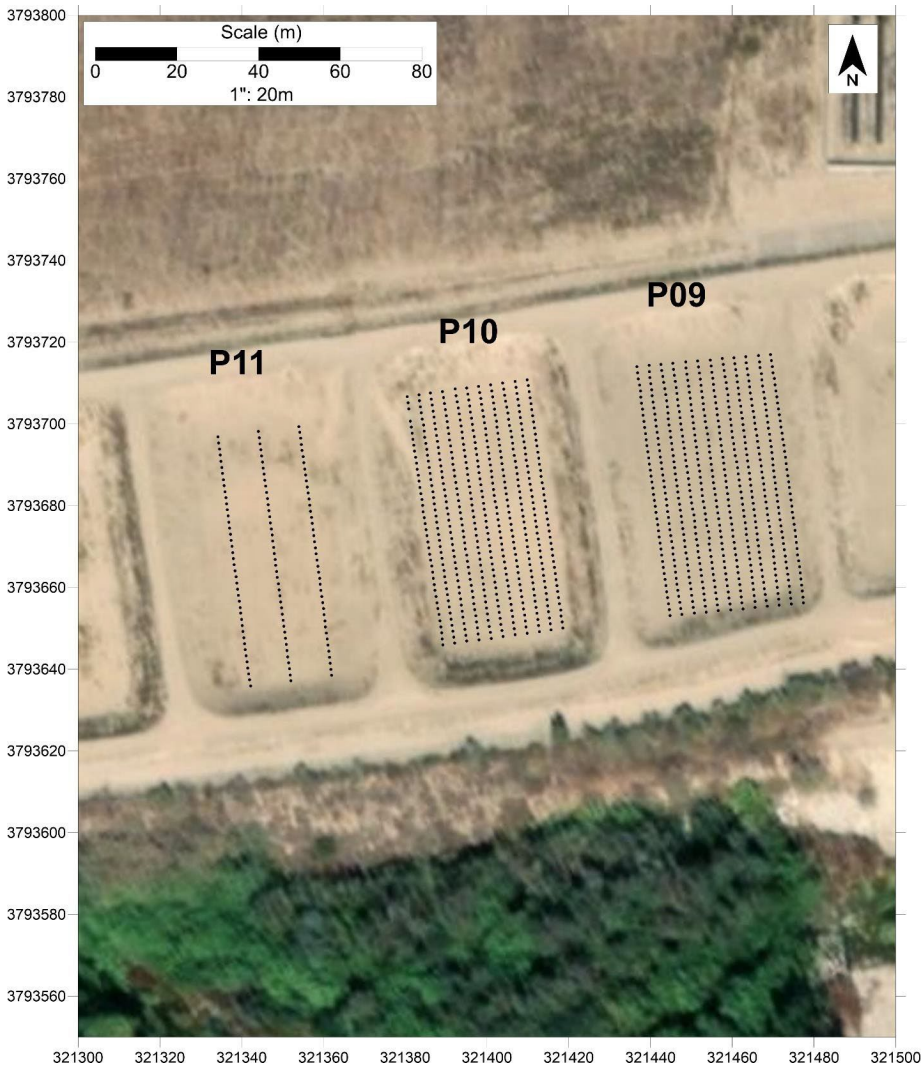

Figure 6. Ponds 9 and 10, 3D ERT grid layout. Black dots show the location of the electrodes. Pond 9 had 12 ERT profiles and Pond 10 had 11 ERT profiles. Three ERT profiles in Pond 11 were collected to better delineate the linear sand feature observed in the EM results.

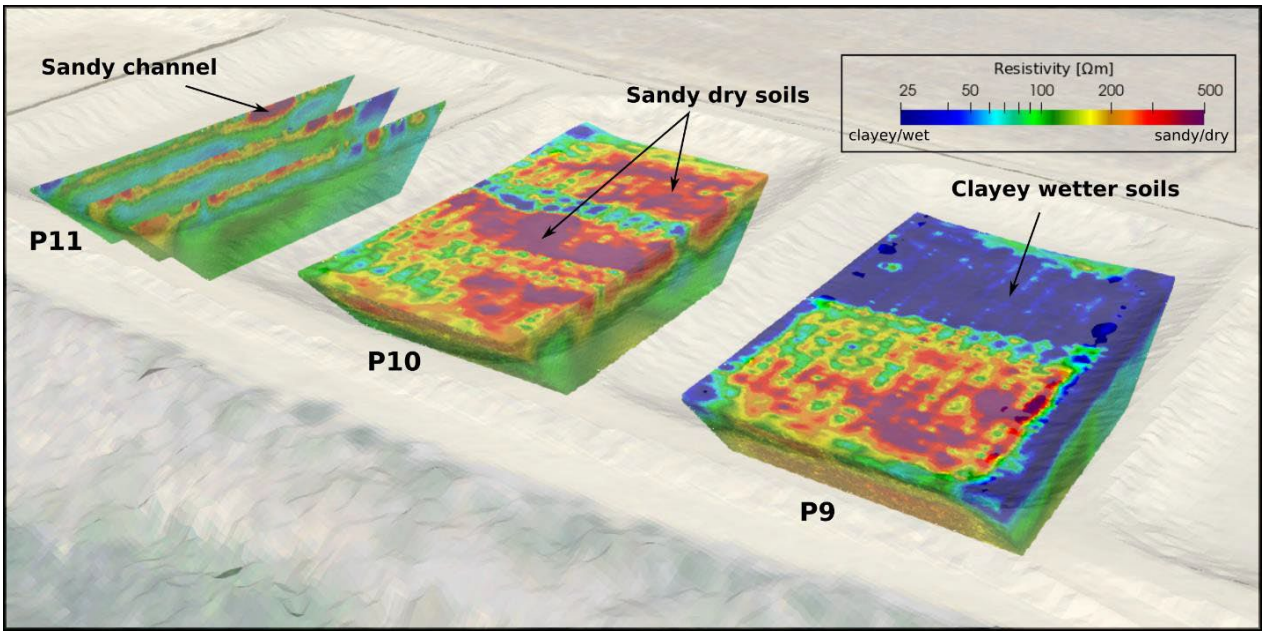

Figure 7. ERT results for ponds 9 – 11. Sandy soils shown in reddish colors, silty sands and silts in greenish-yellow colors, and clayey soils in blue. Variable surficial soils are roughly 1.5 m thick in all ponds then transition to more a more similar silty sand at depth.

2.1.4 EMI Calibration and Inversion

To get an accurate estimate of the subsurface electrical properties, the EMI data has to be calibrated. Often, co-located ERT data is used for this. To calibrate the EMI data, a resistivity profile was extracted from the ERT data at 231 locations, and the response of the EMI to these subsurface models was calculated. By comparing the measured and calculated EMI response, we developed a linear relationship for each coil spacing that was used to correct the measured EMI data. The EMI data was inverted using a cumulative sensitivity method, where the subsurface resistivity model is iteratively changed until the difference between modeled and measured subsurface response is minimal. This process allows to go from the measured apparent conductivities (i.e. a depth average value) to a depth-resolved subsurface resistivity (or conductivity) model. Figure 8 shows the final misfit between modeled and observed data and highlights the importance of the calibration. While in the not calibrated case there is a constant offset between observed and modeled response, this offset is eliminated by the calibration and the data falls almost perfectly along the 1:1 line.

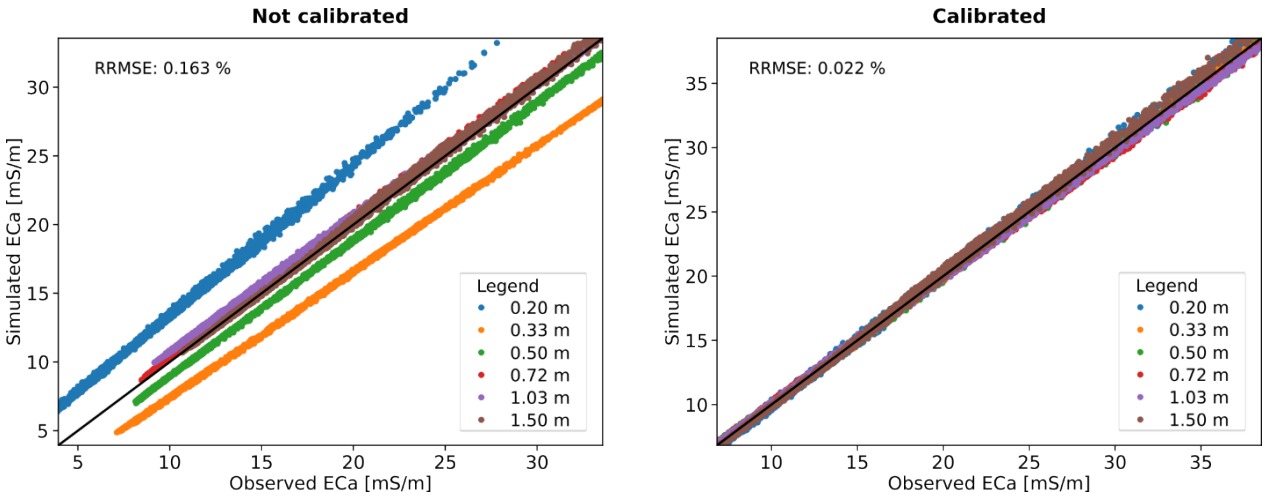

Figure 8. Misfit between modelled and measured electrical conductivity (EMI) after inversion for the non-calibrated (left) and ERT-calibrated EMI data. Note the much smaller misfit for all coil spacings in the calibrated case.

The inverted EMI resistivity models (Figure 9A) show the same observations for the 0 to 2.5 m depths for Ponds 9 to 11 as discussed for the ERT data (Figure 7). Figure 9A shows the full EMI dataset with some transparency to highlight the changes with depth. Figures 9B show the resistivity distributions across all ponds at a depth of 0.1m and 9C at 1.0 m depth; and permits observations of the soil distributions in high resolution and how the soils change spatially.

For instance, in Pond 8 the shallow soil structure (Figure 9A & B), which is characterized by a conductive northern part and a resistive southern part, continues throughout the depth of investigation of the EMI (~2.5 m), with slightly decreasing resistivities with depth. In contrast, for Ponds 12 and 13, the surface shows high resistivities (> 150 Ωm, Figure 9B), this resistive layer (sandy soils) appears to be thin, and at 1 m depth resistivities are considerably smaller (< 50 Ωm, Figure 8C), associated with clayey soils. This indicates that Ponds 12 and 13 are characterized by a thin sandy soil cover, with likely more silty-clayey material below that will limit recharge capabilities.

From those data in Figure 9, we expect Pond 10 to have the highest recharge potential, as this pond shows the highest resistivities throughout. Even though ponds 8 and 9 have a shallow low resistivity layer (clayey soils) in the northern part, which is likely of low hydraulic conductivity, this layer is thin, and below resistivities are comparably high indicating sandier soils. Similarly, Pond 11 shows moderate resistivities throughout. Hence, we expect Ponds 8, 9, and 11 to have moderate recharge potential. Ponds 12 and 13, even though characterized by a thin resistive soil layer, which is likely high in sand content, have likely low recharge potential because of the low resistivity layer that underlays this thin top layer.

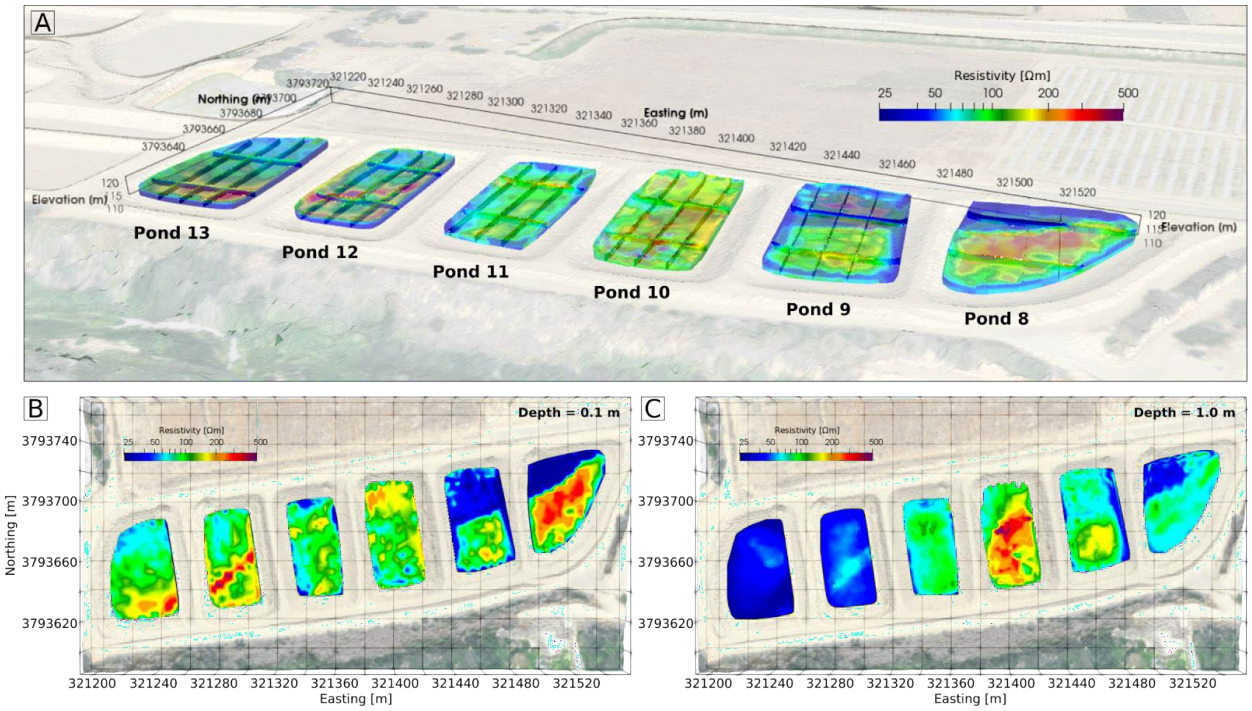

Figure 9. Calibrated and inverted EMI data. P8 and P9 have clayey soils (~1.5-2 m thick) overlying sandy soils. Note that although Ponds 12 and 13 show resistive (i.e. sandy) soil cover, in 1 m depth resistivities are very low, indicating silty/clayey material. This is likely limiting their recharge potential.

2.1.5 Hydraulic Conductivity

Saturated hydraulic conductivity was measured using a Guelph permeameter. The results (Fig. 10) show variable hydraulic conductivities for each pond, with the biggest range in Pond 10 (average of 3.8*10-5), where K_{sat} varies between 6.49*10-7 m/s to 9.9*10-5 m/s. The largest average K_{sat} values were observed for Ponds 11 and 8 (1.33*10-4 m/s and 7.04*10-5 m/s, respectively), followed by Pond 10 (3.19*10-5). Ponds 12 and 13 showed the smallest average K_{sat} (6.61*10-6 and 4.23*10-6 m/s, respectively). These results are summarized in Table 1.

Since the average of each pond is defined by 3 to 4 sampling points only, these averages may not necessarily represent the true heterogeneity of each pond. Nevertheless, this highlights again the relatively homogeneous conditions of pond 10, and the rather poor potential recharge performance of ponds 12 and 13. The considerable difference between Ponds 9 and 10, supports their choice for the follow up recharge experiments.

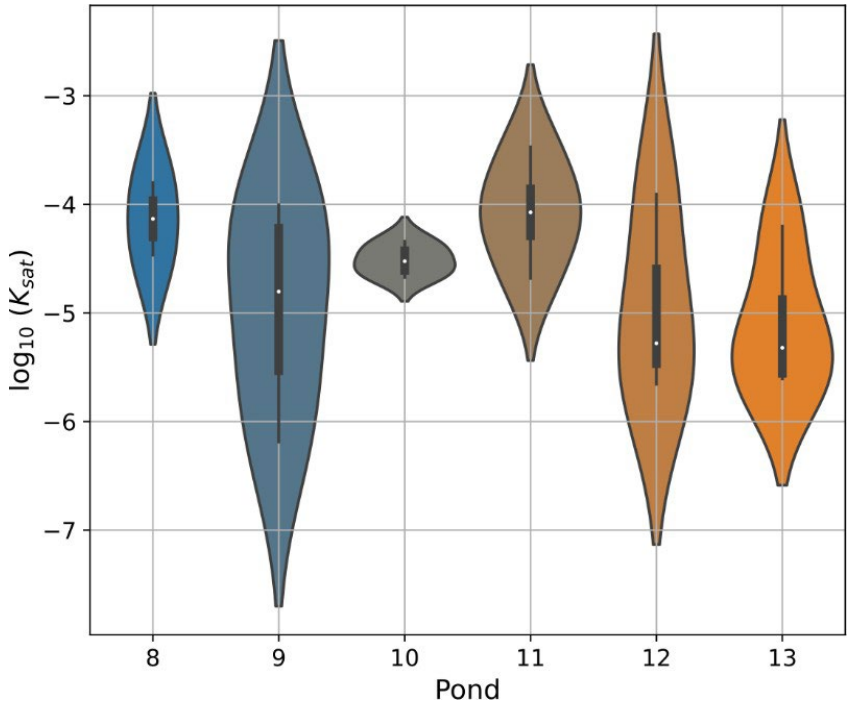

Figure 10. Measured saturated hydraulic conductivity showing the range of values for each pond. Note the large variability of pond 9 and the small average values for ponds 12 and 13.

Table 1. Summary of the minimum, mean, and max K_{sat} and log10(K_{sat}) values in Ponds 8 – 13.

Pond	K_{sat}				Log10(K_{sat})		
	Min	Mean	Max		Min	Mean	Max
8	1.83E-05	7.03E-05	1.58E-04		-4.334	-4.737	-3.799
9	6.49E-07	3.88E-05	9.9E-05		-6.187	-4.949	-4.004
10	2.13E-05	3.19E-05	4.57E-05		-4.671	-4.514	-4.340
11	2.08E-05	1.32E-04	3.37E-04		-4.681	-4.074	-3.471
12	2.21E-06	4.36E-05	1.23E-04		-5.655	-4.947	-3.908
13	2.48E-06	1.90E-05	6.30E-05		-5.605	-5.111	-4.201

In order to provide an estimate of the spatial heterogeneity of K_{sat} throughout the ponds, we established a relationship between electrical conductivity (obtained from the EMI) and measured K_{sat}. This is possible since the electrical conductivity of soils is known to be a function of grain size, which in turn relates to the hydraulic conductivity. A linear relationship was found to fit the data reasonably well (Fig. 11). Based on this, we translated the measured 3D models of electrical conductivity into K_{sat}. These distributions build the basis for a numerical estimation of recharge rates shown in Figure 11. In Figure 11A the spatial distribution of K_{sat} is relatively high (yellow colors) for surface soils down to 0.1 m across all ponds with the exception of low K_{sat} (dark blue color) soils on the north sides of Ponds 8 and 9. At deeper depths, Ponds 8 and 9 K_{sat} improve (Figure 11B) compared to Ponds 12 and 13.

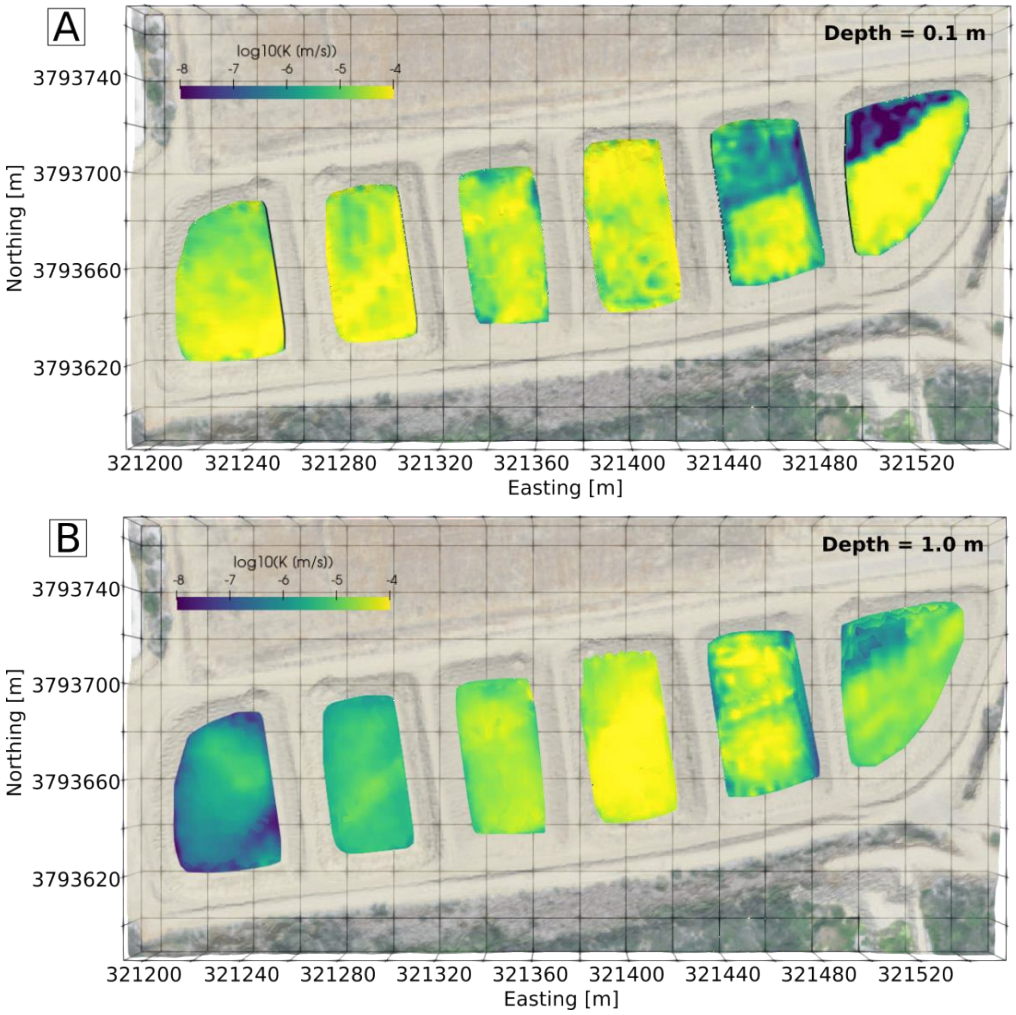

Figure 11. Spatial variability of hydraulic conductivity derived from a linear relationship established between observed K_{sat} and EMI measured electrical conductivity. Shown are two depth slices at (A) 0.1 m depth and (B) 1.0 m depth. Higher K_{sat} are shown in yellow and lower in dark blues.

2.2 Recharge Phase

Due to continued constraints posed by the on-going COVID-19 pandemic in 2020 and 2021 the Recharge Phase could not be initiated until June 2021. On June 21st, 2021 the LBNL geophysics team mobilized back to the MWRF to initiate the Recharge Phase of the project. The goals for this phase were to correlate the ERT and EMI results acquired during the characterization phase with soil cores collected during drilling, and use a suite of geophysical and point sensor methods to monitor and quantify infiltration during the controlled flooding of Ponds 9 and 10. The Recharge Phase used recycled water from the MWRF during the recharge tests in lieu of diverted stormwater. Two recharge events (one in Pond 9 and 10) occurred between June 21st and July 2nd, 2021. After the soil borings were completed, all instrumentation was installed and background datasets were collected prior to inundating the ponds.

2.2.1 Methods used in Recharge Phase

The methods used during the Recharge Phase are highlighted in Figure 12 and some are described in the above Sections 1.3 and 3.1.1. Lessons learned from a previous recharge experiment indicated the need to accurately capture the amount of water applied to close the water budget to determine the amount of water infiltrated. Therefore, a flow meter was installed in-line with the piping to measure the amount of water applied on each pond and the evaporation rate was measured for all days at the site. To monitor and quantify recharge, 3D time-lapse ERT, DTPs, soil moisture sensing, and water elevation was collected in each pond before and during water application until after all the water had infiltrated. A single profile of ERT between the Arroyo and the ponds was collected to determine if infiltrated water was leaking back into the Arroyo, essentially short-circuiting. Soil moisture was measured with both METER shallow soil moisture sensors and deep soil moisture was measured with the InstroTek neutron probe.

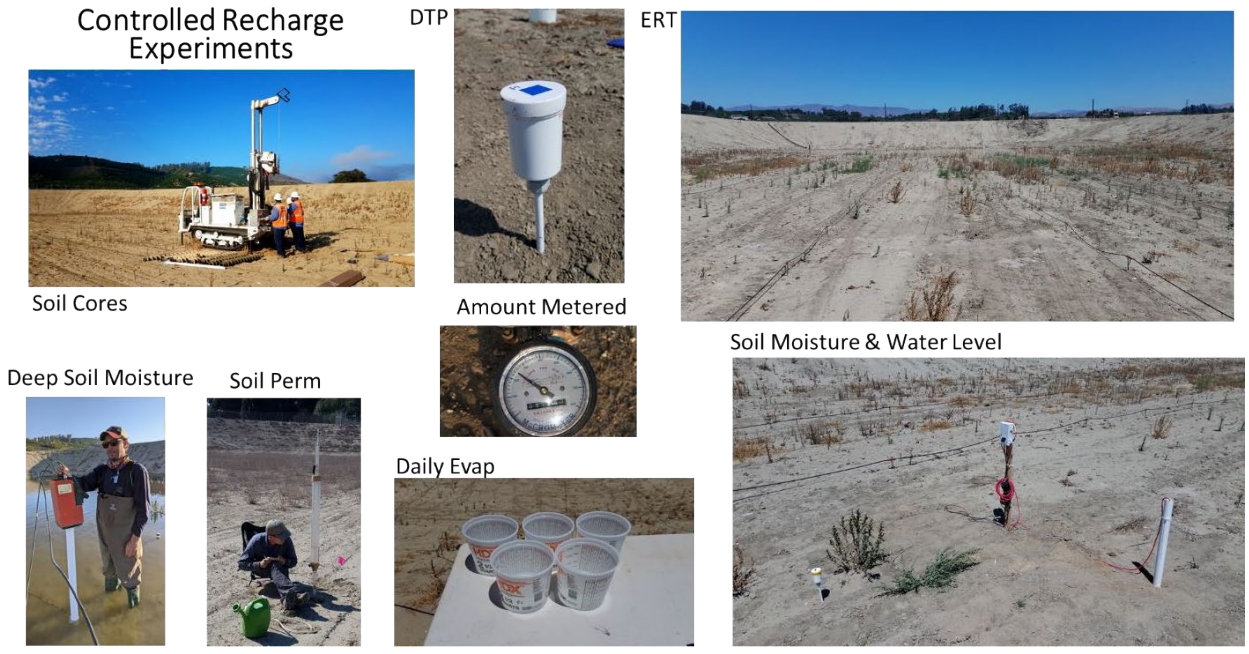

Figure 12. Recharge experiment methods.

2.2.2 *Pond 9 Results*

2.2.2.1 Soil Borings Results

Gregg Drilling was contracted to install four soil borings using direct push technology to a depth of 15 m. Two locations were chosen in Pond 9 and two in Pond 10 based on the characterization results. Soil profiles were collected between three general soil type zones identified in the EMI results. Borings B-1 and B-2 were collected in Pond 9 and, borings B-3 and B-4 in Pond 10 (Figure 12). The following is a verbal description of the soils identified in each boring.

B-1 was in a low resistivity zone (Figure 12) and showed a random sequence of silty sands and silty clays from 0 – 1.1 m, followed by random alternating silty sand and sand from 1.1 – 6.3 m, and fine – coarse sands to 15 m.

B-2 was in a higher resistivity zone (Figure 12) and contained more sand than silty sands from 0 – 1.5 m, with a silty clay lens from 2.8 – 2.94 m, followed by alternating silty sands and fine sands to 5.1 m, where coarser sands and gravels started to appear. The coarsening continued until 11.85 m where some gray clay was observed and drilling stopped at 12 m.

B-3 in Pond 10 was in a high resistivity zone (Figure 13) and consisted of mostly fine-medium sands with some random silty sand and very thin silty clay lenses from 0 – 15 m. At some depths gravelly sands were encountered.

B-4 in Pond 10 was also in a high resistivity zone (Figure 13) showed predominantly fine-medium sands with some coarse sands to 15 m. A small silty clayey lens was observed at 11.55 m. Examples of the drilling and core are also shown in Figure 15.

Examples of the drill rig and core are shown in pictures on the right of Figure 13. After all four boreholes were completed, solid 2-inch PVC pipe was installed in each borehole as an access pipe for the neutron probe soil moisture measurements (Figure 13, center photo).

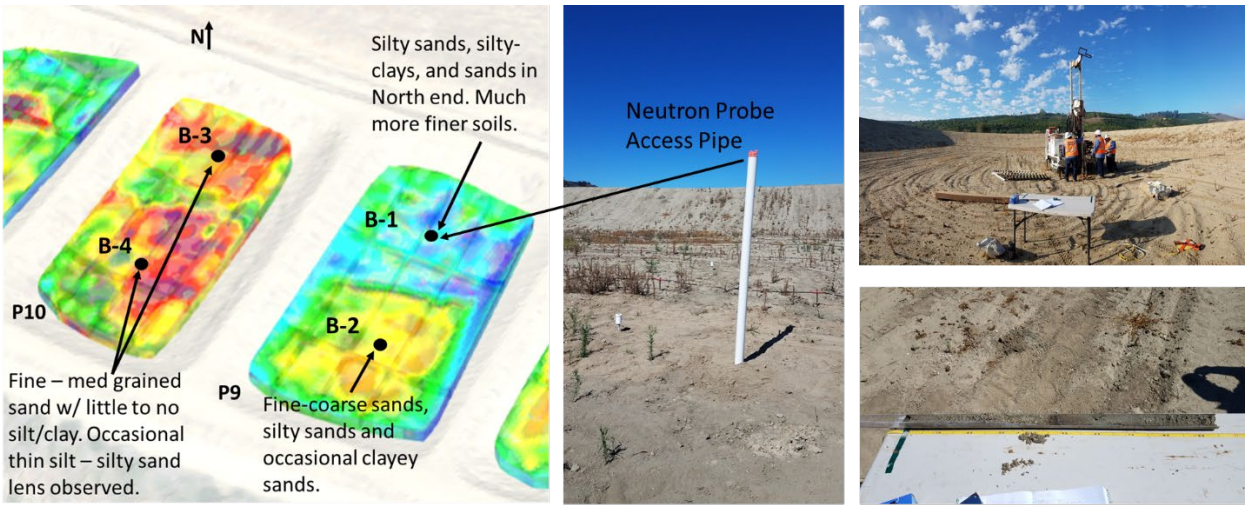

Figure 13. Soils were drilled to 15 m at four locations (B-1 to B-4) chosen from the EMI results. Pond 9 observed a mix of silty sands and clayey sands on the North end and sandy soils on the south end. Pond 10 observed primarily sands with little silt lenses. Examples of the drill rig and core are shown in pictures on the right. After the cores were drilled a PVC pipe was installed as an access pipe for soil moisture measurements with the neutron probe.

2.2.2.2 ERT Results

A total of seventy-one time-lapse ERT images were collected in Pond 9 and for this report we selected seven images from before, during and after flooding to highlight the water movement in the subsurface, a video of the full infiltration at each timestep can be found on LBL's Water Recharge website under the Ventura Groundwater Basin Recharge project webpage (https://waterrecharge.lbl.gov/projects/ventura-percolation-basin-recharge-study/).

Pond 9 was inundated with 230k gallons (0.85 AF) of water (Figure 14). The background ERT dataset was collected prior to any water application for time-lapse comparison (Figure 15, Background Model). As water flowed into the pond from the northwest corner it followed the microtopography across the pond (clockwise) resulting in uneven water application until the pond was completely covered (shown in a composite move at the link above). The time since the start of water application is shown in the bottom left of each image in Figure 15 and the percent change in resistivity ranges from +50% to -50%, with a negative change representing the soil becoming more saturated (decrease in resistivity). In the northwest corner at +6.9 hours no appreciable infiltration is observed in the clayey soils adjacent to the pipe outlet, but other preferential fast flow paths are starting to be observed. At +21.9 hours the pond is completely full and fairly uniform infiltration is observed except in the northern clayey area. The pump was stopped at 24 hours and the ERT captures the bulk of the water moving deeper into the subsurface through the sandier soils in the southern end of the pond (Figure 15, +40.9 hours). After +63 hours, deep infiltration in the southern end of the pond is observed to depths over 15 m. Conversely, the clayey soil zone in northwest corner has yet to infiltrate water (Figure 15, +63 hours). These results highlight infiltration controlled by preferential flow through the coarser sediments and detrimental effects on recharge from fine-grained soils.

Figure 14. Pond 9 water application of 230k gallons (0.85 AF) at start (top) and after full (bottom).

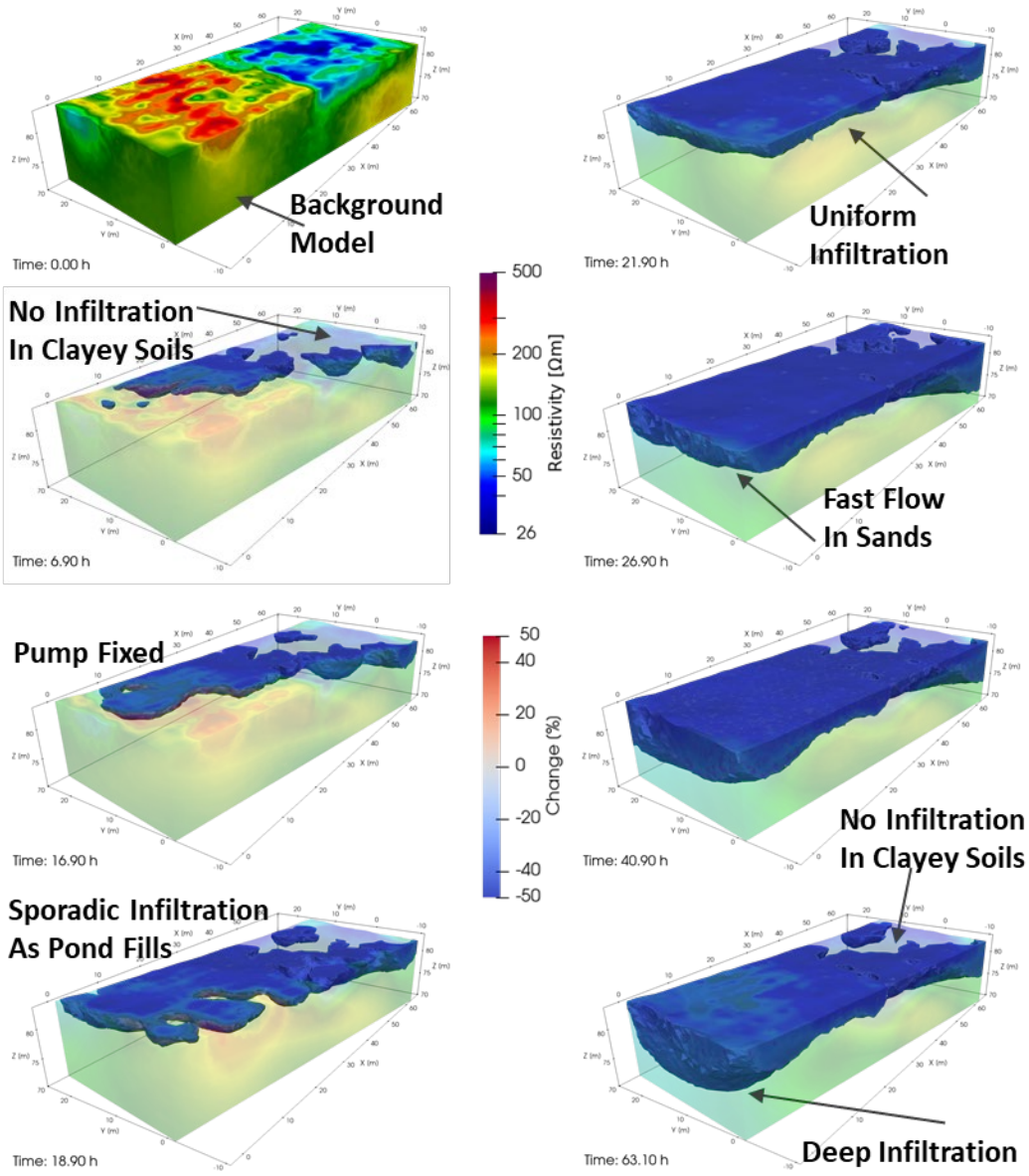

Figure 15. Pond 9 water infiltration mapping in percent change resistivity with the background resistivity model shown and then transparency applied. Sporadic fast path infiltration is observed as the pond fills. At +16.9 hours the broken pump was fixed and water application commenced. After the pond is filled fairly uniform infiltration is observed at +21.9 hours. Until the southern end sandy soils take over and recharge more of the water at +40.9 hours to a depth of 15 m. The northwest corner clayey soils zone never infiltrated water.

2.2.2.3 DTP Results

Fifteen DTP probes were installed in Pond 9 shown in Figure 16. These probes were a new design from the characterization phase probes and had an additional four thermal (16 total) sensors spaced 5 cm apart. Complex subsurface flow was observed in the earlier ERT results. This was confirmed

by the DTP results too and all of the thermal response images are shown in Appendix B. The ERT data showed no infiltration in the northwest corner of Pond 9, and the DTP probe in that location also showed little to no infiltration (Figure 17, A & C). The start and stop time of water application are indicated by green and red lines, respectively (Figure 17 A & B). While the time that the pond was emptied is shown as a blue line. The deeper sensors in Figure 17A appear as a horizontal series of lines indicating a constant temperature, over time fewer and fewer of these lines remain constant indicating very slow water infiltration with some water never reaching 1m. Compare this response to the response in the sandy sediments in Figure 17B and within a couple hours after the start of water application water has infiltrated 1.2 m deep causing all the thermal sensor to collapse to diurnal signal when the pond was fully flooded. Figure 19C thermal waterfall display illustrates this fast, deep infiltration very well and is starkly different from the response in the clayey soils shown in 17B. The responses in Figure 17 B and C show a linear move-out with depth making these probes good candidates to apply a 1D thermal model to estimate the slow and fast infiltration rates.

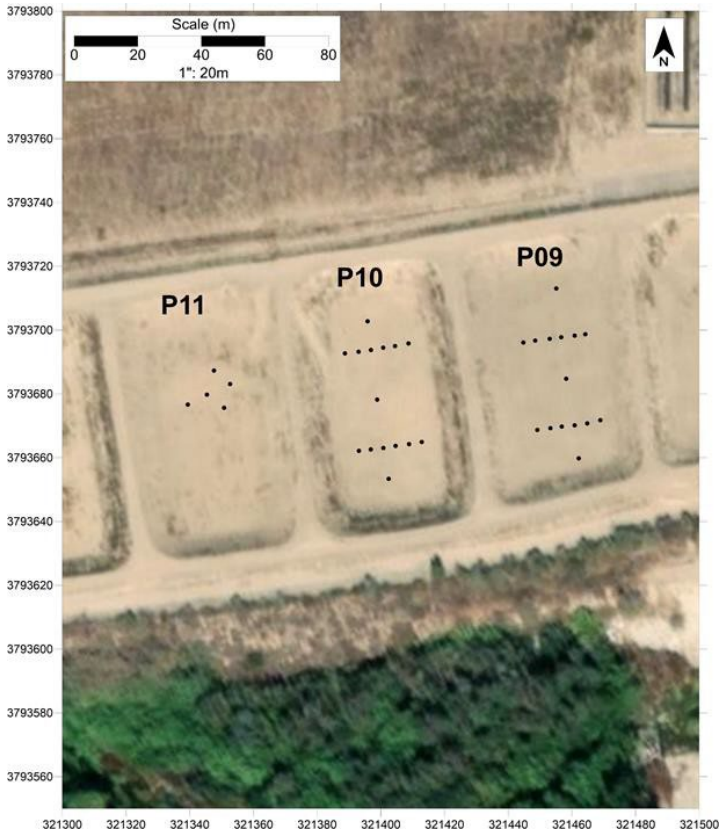

Figure 16. Recharge Phase DTP locations in Ponds 9, 10 and 11. Ponds 9 and 10 had fifteen DTPs installed before the recharge events and Pond 11 had five DTP probes to investigate the lateral flow through the sand channel during the Pond 10 flooding event.

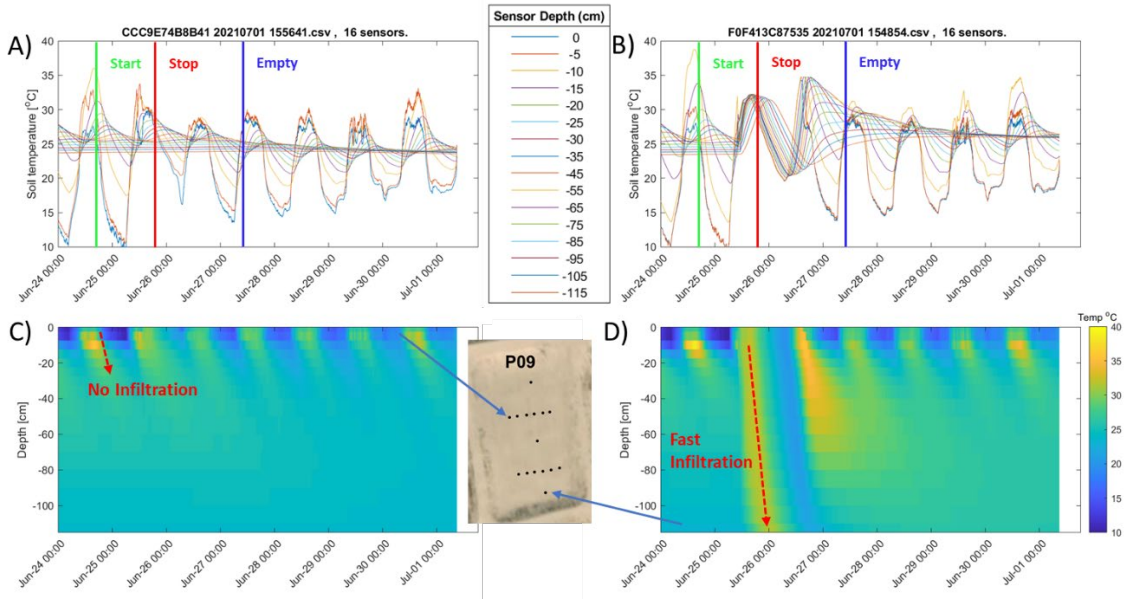

Figure 17. Pond 9 DTP thermal response examples from silty clay no recharge (A & C, northern end) and sandy fast recharge (B & D, southern end). The start and stop of water application is shown in A and B by the green and red lines, and the pond empty is shown by the blue line. Little to no infiltration is observed in the clayey soils (C, red dashed line) compared to very fast and deep infiltration in the sandy soils (D, red dashed line).

2.2.2.4 METER Soil Moisture and Water Level Results

Four METER EM60 dataloggers were installed in Pond 9 (Figure 18) and each datalogger had three soil moisture sensors installed at 15, 30, and 60 cm bgs (black dots) and two water level sensors (red dots) were installed to monitor water Pond 9 water levels during the recharge event. During water application the water followed the microtopography clockwise around the pond until it was completely inundated. That is why the 1495 water level sensors increases before the 1130 sensors and have a longer duration, because the southwest portion of the pond was the last area to be covered. This can be observed in the soil moisture sensor response at 1130 (blue lines, Figure 19) increase at the same time as the grey dashed line of the adjacent water level sensor. Interestingly, sensors at 1480 (magenta lines, Figure 19) in the northwest corner of the pond adjacent to the water output pipe show no initial soil moisture increase but instead is delayed until hours later at all depth intervals due to the clayey soils in that region of the pond. At datalogger 1459 (green lines) soil moisture increase quickly to 35-40% (v/v*100) at 15cm (Figure 19A), and at all depth retain the soil moisture over time due to the fine-grained sediments in that area. The same is observed at datalogger 1480 when compared to the sandier sediments at locations 1130 and 1507. Location 1507 appears to have mostly sandy sediments when observing the soil moisture response curves (red lines, Figure 19) because it captures the initial water application and then when the pump was stopped due to a malfunction overnight allowing the soil moisture to decrease at all depths in the early morning hours on June 25th. After the pump was fixed and the water application continued the soil moisture increases again to its prior levels at all depths (Figure

19). All sensors continued to monitor soil moisture levels for days after Pond 9 had emptied, these soil moisture values beyond June 28th give us an idea of the field capacity of these soils and insight about when the next water application could occur since all soils had drained. These results also highlight the infiltration complexity in different soil types and that most infiltration happens through preferential flow paths controlled by sandy soils. These soil moisture curves can also provide information the porosity of the sediments, after the soil moisture initial increase and all of the soil moisture curves become constant over time. If we assume that during that the plateaued (flat max) part of the curve represents full saturation of the soils then the water content is equal to the porosity. Following this logic, the soils in Pond 9 range in porosity from 30 – 40% for the sandy soils. In some cases, the curves in Figure 19 do not stay constant for very long and those should not be used to estimate the porosity.

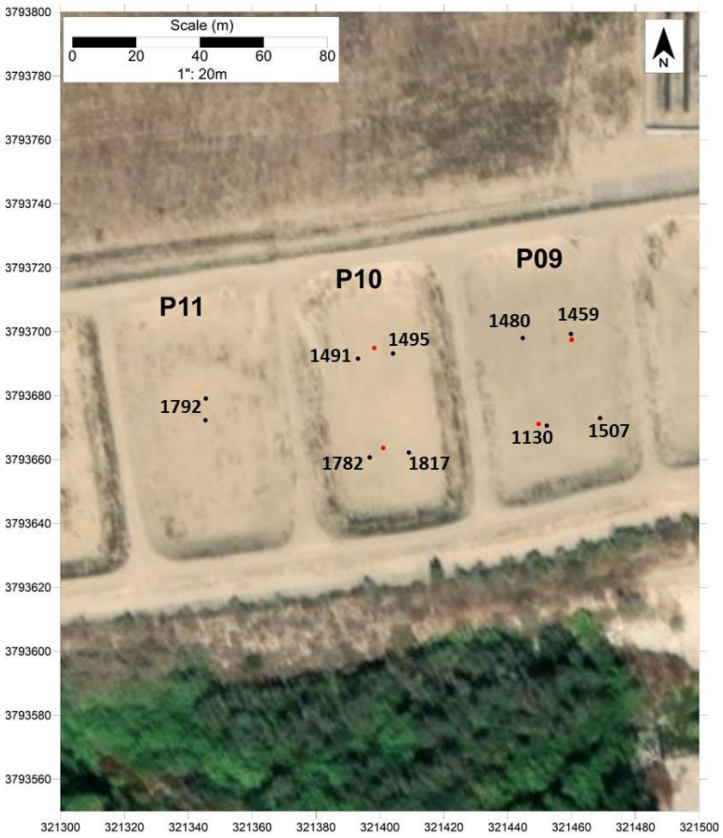

Figure 18. Shows the locations of the water level sensors (red dots) and the soil moisture sensors (black dots) with the associated datalogger number. At each soil moisture location, a vertical profile of three soil moisture sensors were installed at 15 cm, 30 cm, and 60 cm bgs.

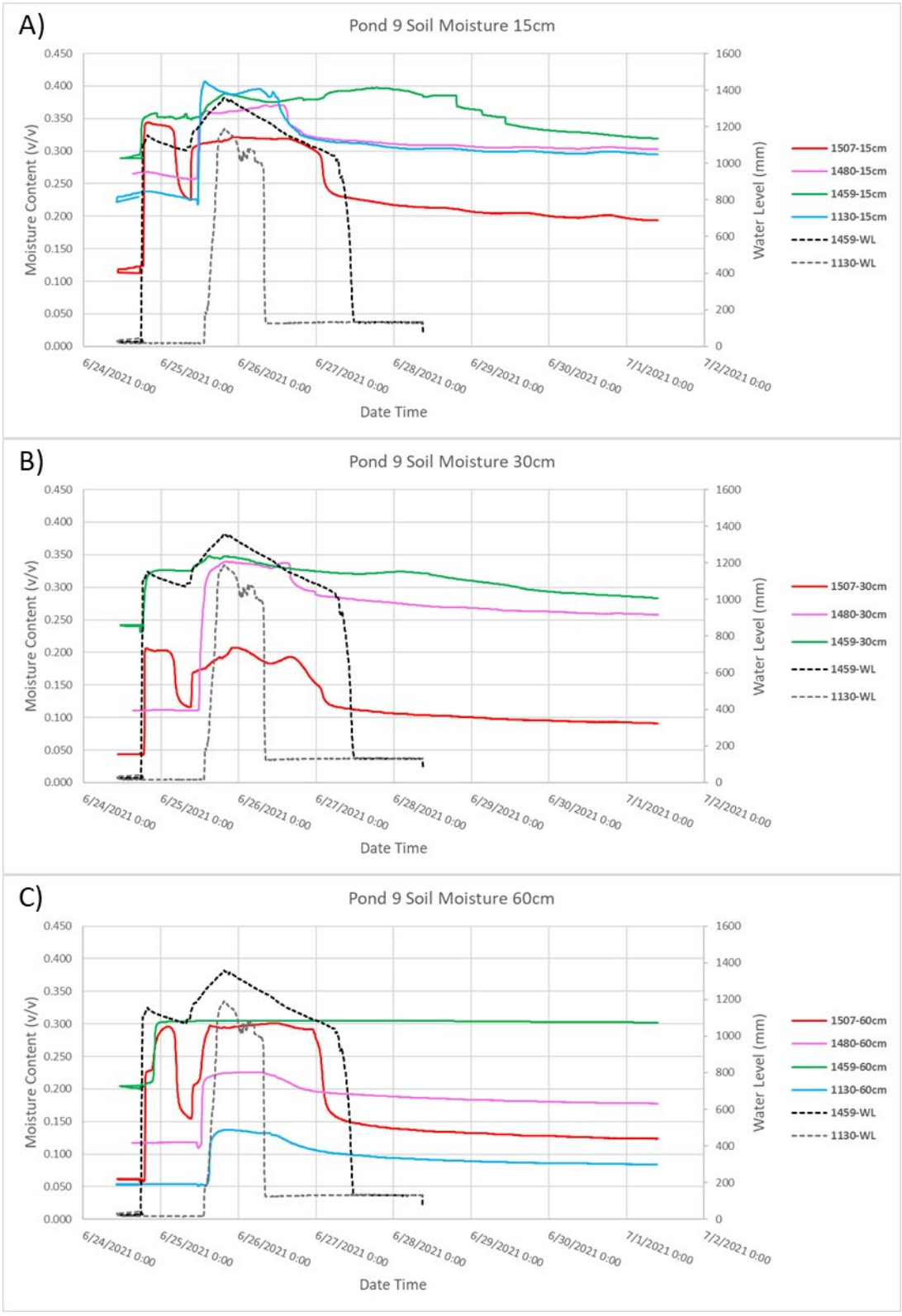

Figure 19. Shows the Pond 9 soil volumetric soil moisture responses at A) 15cm depth, B) 30cm depth, and C) 60cm depth. On the secondary axis is the water levels at two locations.

2.2.2.5 Neutron Probe Deep Soil Moisture Results

The neutron probe was lowered down the access pipe at 0.5m intervals to observe the changes in soil moisture in depth and over time. Figure 19 shows the location of the two neutron probe access holes in Pond 9 (B-1 and B-2). B-1 was located in the silty clayey northern end sediments and B-2 was located in the sandier southern end sediments. The soil moisture plots in Figure 20 show the change in volumetric soil moisture and moisture content in percent, plotted on the same scale. The x-axis shows the displays the times from before, during, and after inundation. B-1 observed little to no infiltration and B-2 observed changes in soil moisture from 10 to 20+%. Interestingly, quick infiltration is observed from 0-2 m, then a slight delay from 2-6m (but almost instantaneous response times). Between 4 and 6 m an increase of soil moisture up to 22% is observed and decreases over time and as that zone starts to decrease we see a slow increase in soil moisture from ~10% to ~14% between 6-11 m. A review of the B-2 soil log shows a silty, fine sand layer from 5.85 – 5.95 m. We suspect this finer sediment, low permeability layer causes the buildup of moisture observed from 4-6 m, but it slowly drains over the next few days as observed soil moisture increases over time in the depths between 6-11 m well after the all the water has infiltrated below the base of the pond.

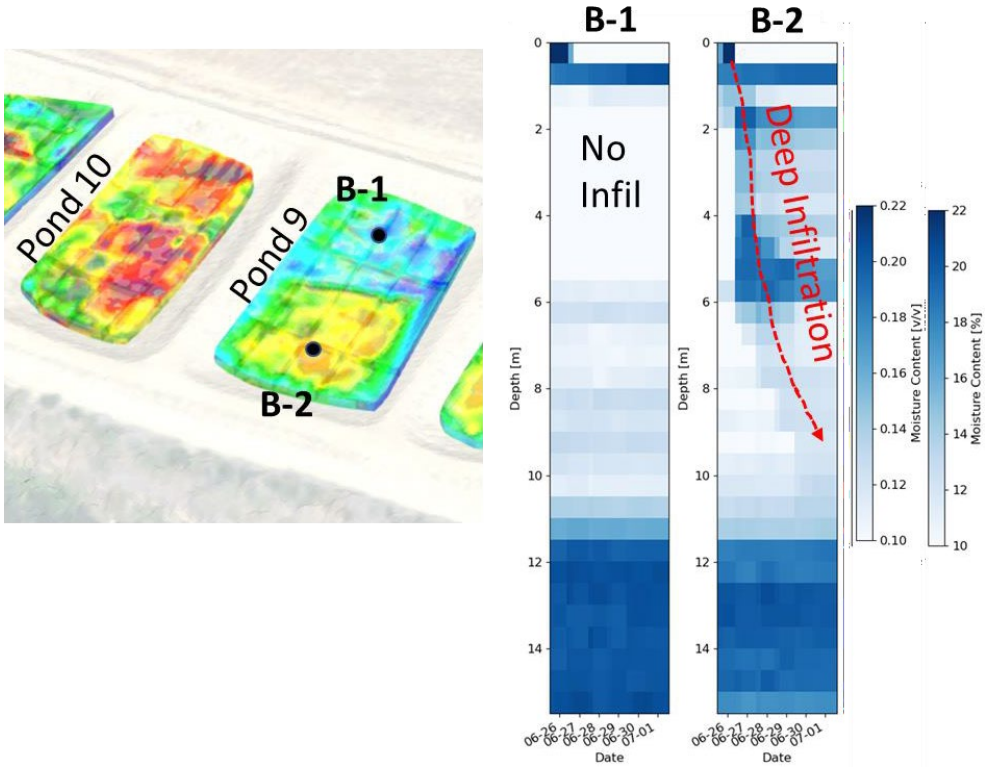

Figure 20. Pond 9 Neutron Probe soil moisture responses for B-1 and B-2. B-1 was located in the little to no infiltration zone containing fine grain sediments and B-2 was in the southern sandier soils. These plots show both the volumetric water content and the percent moisture content with

the same scales for interchangeable comparison. Little to no change observed in B-1 at all depths except 0 – 1 m. B-2 shows fast, deep infiltration down to 10 m. In some locations, for instance from 4 – 6 m background soil moisture was at 10% or less and increase up to 20%+ over time.

2.2.3 *Pond 10 Results*

2.2.3.1 Soil Borings Results

Soil borings B-3 and B-4 were collected in Pond 10 (Figure 13).

B-3 consisted of sands and silty sands from 0-4m, then a silty clay lens from 4 - 4.4 m, followed by large sand zones with thin silts and silty sands down to 15m. Below 5m occasional small gravels were mixed with sand zones.

B-4 consisted of medium sands with occasional silty sands lenses down to 10 m where the sands coarsened to 11.55 m. A silty clay lens was observed from 11.55 – 11.65 m followed by fine-medium sands to 15 m.

2.2.3.2 ERT Results

Figure 21 shows the photos of Pond 10 being filled. In the lower photo (looking north) the northwest corner is a topographic high (although minute) and the sandy soil infiltration rates were so high that they almost matched the pump inflow rates which cause the pond to never be fully inundated. Therefore, almost double the amount of water was applied to Pond 10 as compared to Pond 9.

Time lapse resistivity data was collected in 3D over Pond 10 and the resulting changes in resistivity area shown in Figure 22 as percent change. The percent change ranges from +50% to -50% and an increase in a negative percent indicates that the soil is becoming wetter and the resistivity decreases. The first image in Figure 22 shows the background resistivity model collected in the hours prior to water application. The time since the start of water application is shown in the bottom left of each image for reference in Figure 22. As the pond begins to fill preferential flow paths or fast paths are observed conveying water deep into the subsurface at +6 hours. As the pond continues to fill these fast paths connect, disconnect and then reconnect as other soil begins to saturate, +15 hours. These high infiltration rates in these sandy soils were perfect for conveying water deep (>15-20m) into the subsurface +45 hours well after Pond 10 had emptied. The ERT captured perfectly the complex nature of infiltration in Pond 10 and imaged the water movement deep in to the subsurface.

Figure 21. The filling of Pond 10 with 407k gallons (1.5 AF). The pond was never filled due to the high infiltration rates that were similar to the pump outflow rates.

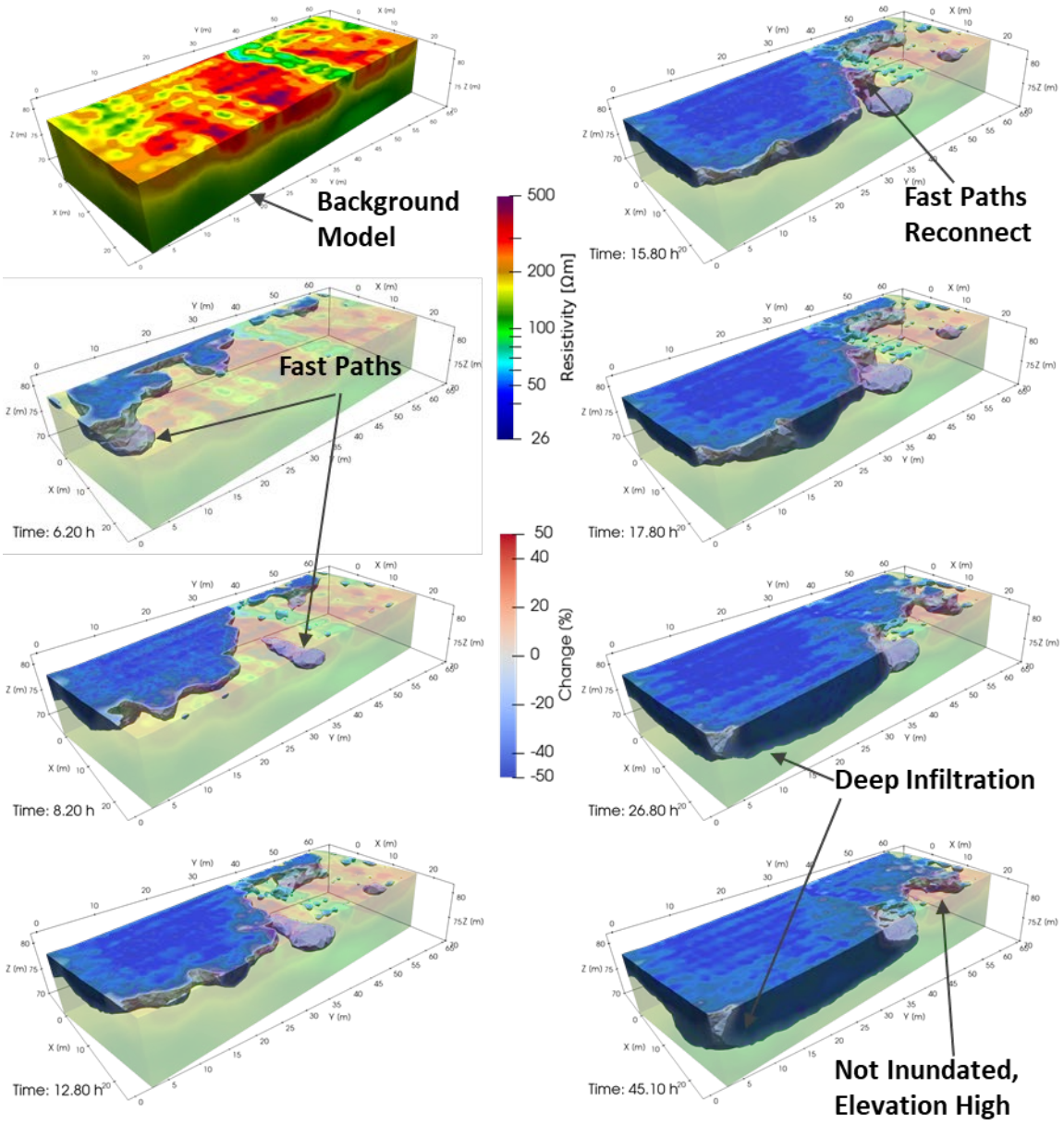

Figure 22. Shows the time-lapse ERT infiltration in Pond 10 as a percent change in resistivity. The background resistivity model prior to water application is shown as a reference. The time after the start of water application is shown in the lower left of each image. Many fast flow paths are observed and connect and reconnect to different zones as the pond fills. Deep recharge is observed over 15m deep. Negative percent change means a decrease in resistivity associated with an increase in saturation.

2.2.3.3 DTP Results

Fifteen DTP probes were installed in Pond 10 shown in Figure 18. Again, these probes were a new design from the characterization phase probes and had an additional four thermal (16 total) sensors all spaced 5 cm apart. Complex subsurface flow was observed in the earlier ERT results (Figure 22). This was confirmed by the DTP results too and all of the thermal response images are shown in Appendix B. The start and stop time of water application are indicated by green and red lines, respectively (Figure 23 A & B), while the time that the pond was completely empty is shown as a blue line. The tortuosity of the heat pulse through the subsurface in Figure 23C (curvy red dashed line) is likely the result of horizontal water movement in addition to vertical flow. This result is exciting because it captures complex water movement in the subsurface, but it cannot be used for estimating 1D infiltration rates from the thermal sensors because it is not purely vertical flow; but, given the cheap cost of these probes many probes can be placed throughout the ponds to ensure that only vertical flow is captured (Figure 23D) in order to estimate infiltration rates.

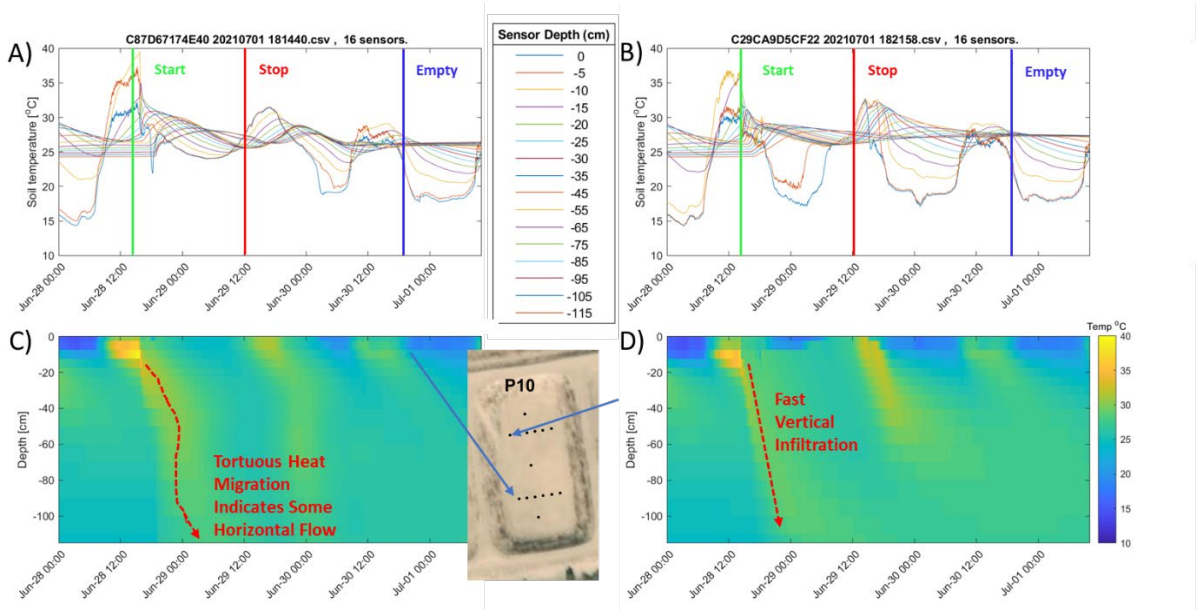

Figure 23. Pond 10 DTP thermal response examples in sandy soils. The start and stop of water application are shown in (A) and (B) by the green and red lines, and the pond empty is shown by the blue line. DTP probes show tortuosity in the heat migration through the subsurface (C) likely due to horizontal flow observed in the ERT data. Compared to linear heat movement through the subsurface (D) indicating vertical flow.

2.2.3.4 METER Soil Moisture and Water Level Results

Four METER EM60 dataloggers were installed in Pond 10 (Figure 18) and each datalogger had three soil moisture sensors installed at 15, 30, and 60 cm bgs (black dots) and two water level sensors (red dots) were installed to monitor Pond 10 water levels during the recharge event. Unfortunately, both water level sensors failed, likely came unplugged due to sensor movement during water application. During water application the water followed the microtopography counterclockwise around the pond. The northeast corner of the pond is a topographic high and was never inundated, therefore 1495 sensors show now change in soil moisture. Interestingly, station

1495 was adjacent to the water outlet pipe but is in what appears to be silty soils (in the EMI data) which causes very slow infiltration resulting in delayed (almost 24 hours compared to the other sensors) soil moisture increases at all sensors depths (Figure 24, red lines). Both stations 1782 and 1817 are located in sandy soils and quick soil moisture increases are observed, green and blue lines, respectively. Overall, initial soil moisture values are approximately 5 – 15% (v/v*100) and increase to 30 – 40% except for 1491 at 60cm bgs. At almost all depths, once the pond is emptied the soils drain very quickly due to the high sand content. Those that drain slower contain more fine-grained material. Unfortunately, these sensors were not permitted to monitor long enough to observe the soil moisture contents go back to field capacity. Following the same logic that we did for Pond 9 porosity estimates, Pond 10 soils range in porosity from 30 – 40% for the sandy soils.

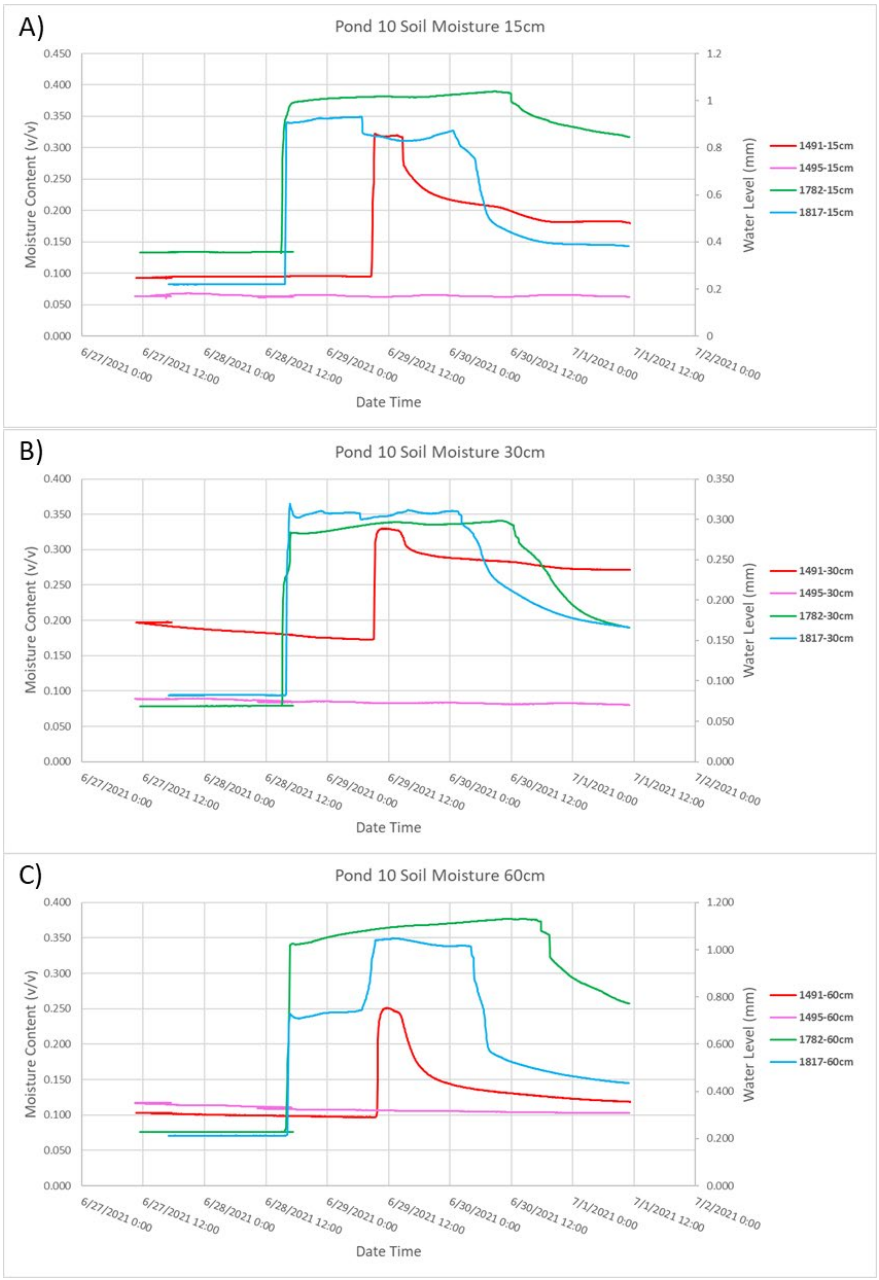

Figure 24 Shows the Pond 10 soil volumetric soil moisture responses at A) 15cm depth, B) 30cm depth, and C) 60cm depth. All sensors for 1495 show no change in moisture content because it was not inundated. 1491 sensors are located adjacent to the water output pipe but the soils from the EMI show it is in a silty type of soil and a delayed soil moisture increase occurs due to slow infiltration. 1782 and 1817 sensors are located in sandy soil and fast increases in moisture content are observed to 60cm depth.

2.2.3.5 Neutron Probe Soil Moisture Results

As discussed in the previous ERT section, the northeast corner of Pond 10 was never inundated which resulted in B-3 never being under water to monitor soil moisture changes due to recharge (Figure 25). B-4 was inundated and like the ERT showed fast, deep infiltration (red dashed line,

Figure 25). Soil moisture increase from 10% (background) up to ~22% were observed down to 9m. B-4 was on the boundary of the sandy zone that covered the southeast portion of the pond and contained slightly more fine sediments that reduced infiltration depths. When looking at the ERT +45 hours in Figure 21 the deepest infiltration is observed in the southeast corner. B-4 was on the transition to the finer soils on the southwestern side of Pond 10. The ERT response there shows infiltration down to ~10m which agrees with these neutron probe soil moisture results.

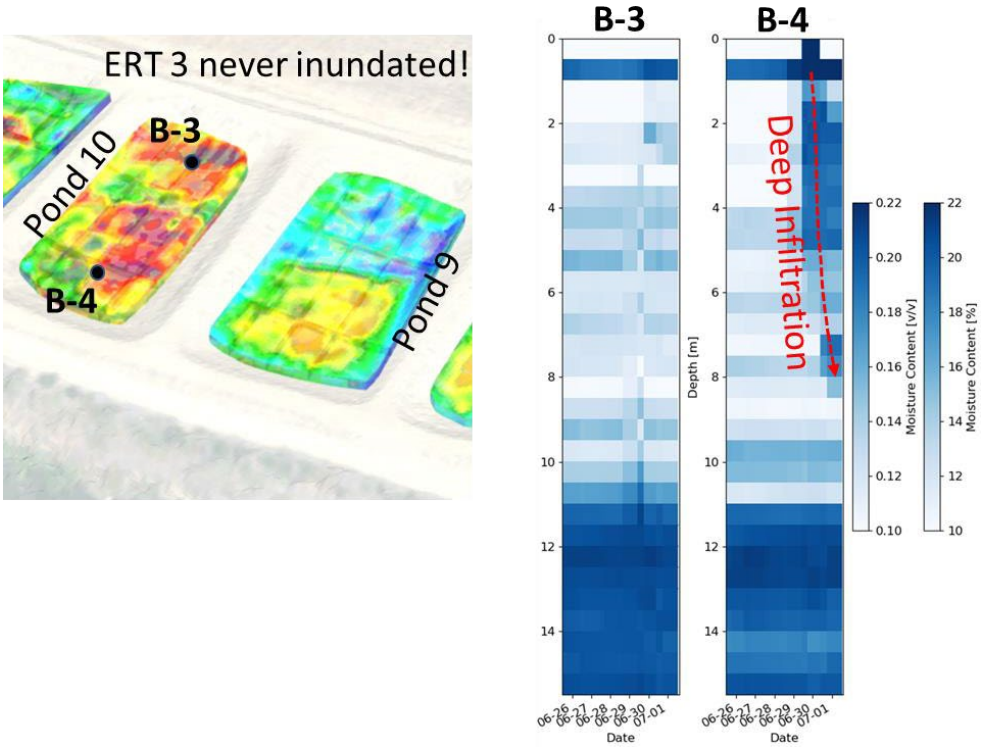

Figure 25. Pond 10 Neutron Probe soil moisture responses for B-3 and B-4. Both B-3 and B-4 are located in sandy soils but B-3 was in the area of the topographic high and was never inundated. Therefore, no changes are observed in the soil moisture along borehole B-3. B-4 shows deep infiltration (red dashed line). Soil moisture increases from ~10% to ~22% from 0-9m bgs. Below 9m soil moisture is somewhat constant.

2.2.4 *Pond 11 Results*

Six METER soil moisture sensors (Figure 18) and five DTP probes (Figure 16) were installed in the sandy channel observed in the EMI and ERT results to evaluate additional leakage from Pond 10 during the recharge event. Nothing was observed in all of the data that would indicate water migrating from Pond 10 into the sandy channel and across Ponds 11, 12, and 13.

2.2.5 Streamside ERT

The location of the streamside ERT profile is shown in Figure 26, which is located on the steep bank between the Arroyo and the ponds. Eleven time-lapse images were collected from before, during and after all flooding events, but only four images throughout the study area shown in Figure 26 for simplicity. The top of the ERT profile is at the same elevation as the base of the ponds. The river elevation is shown as a dashed blue line on the percent change in resistivity panels in Figure 26.

The river elevation is 10 – 12m below the base of the ponds. Results from the ERT timeseries show no indication of water flowing from the ponds to the river during water infiltration. Given the amount of water applied during both experiments, and the percent change of greater than 50% in Figures 15 and 22 observed during both flooding events, we would expect to see large changes in the resistivity values between the ponds and the river if the recharged water was migrating into the river. The maximum changes in Figure 26 throughout the whole two weeks was less than 10%. Furthermore, we would expect to see a large feature visible within the plane, but only sporadic small changes are observed. These results indicate that the infiltrated water does not migrate directly back into the river.

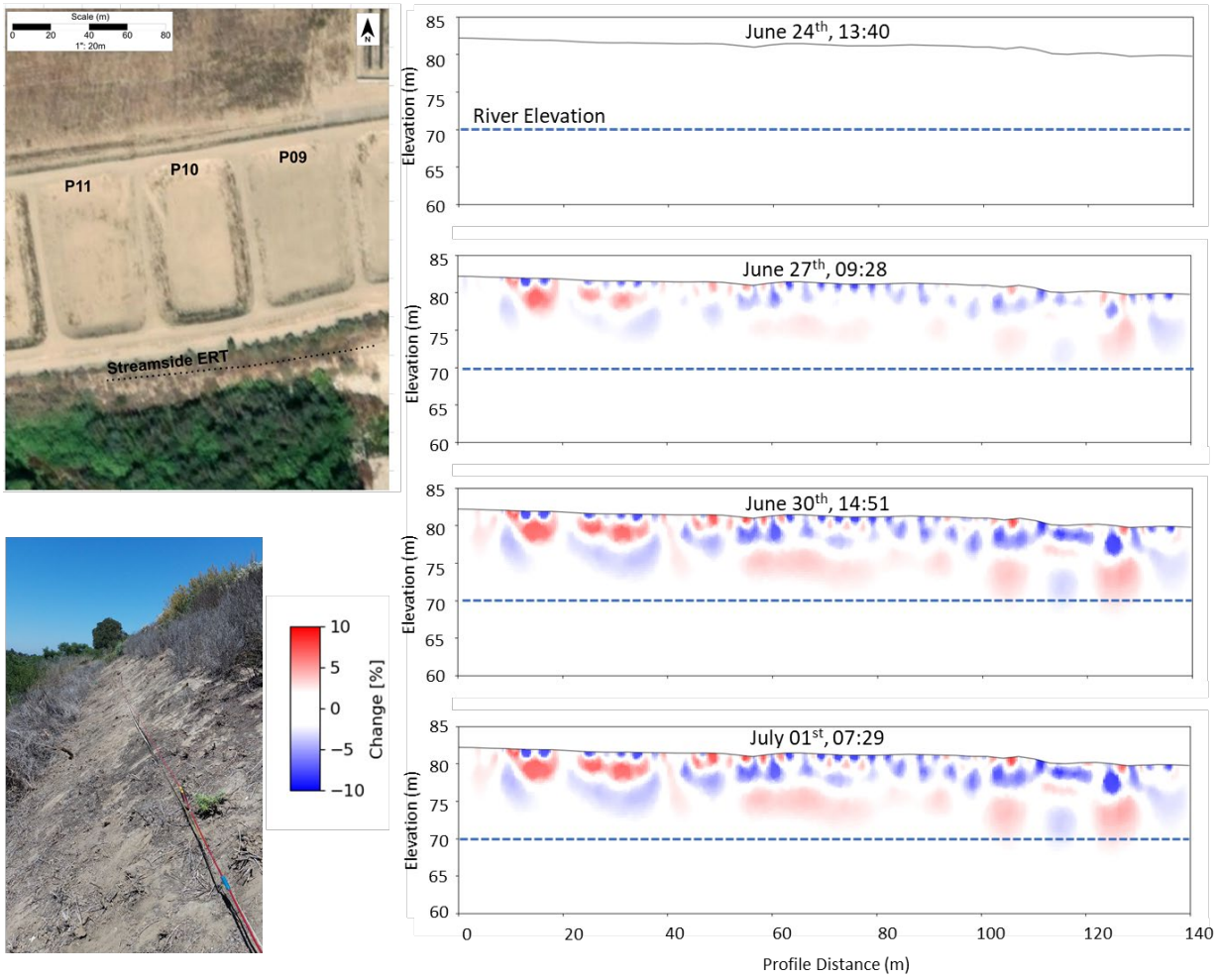

Figure 26. shows the location of the streamside ERT profile to monitor for water flow back into the river. Eleven time series datasets were collected from June 24th to July 1st and are shown as a percent change from the baseline dataset collected June 24th before all water applications. The top of the ERT profile is at the same elevation of the ponds and the river elevation is shown as a dashed blue line. The small percent change in resistivity indicate no water flow back into the river when compared to changes during the flooding events in Figures 15 and 22.

3.0 Infiltration Rate Estimation

3.1 DTP Infiltration Rates

Vertical 1D infiltration rates were estimated through saturated porous media using an analytical heat transport model. These heat transport equations use a number of known heat transport models such as Hatch and Keery for example. For ease of use these models have been incorporated into a Matlab gui interface called Vertical Fluid Heat Transfer Solver or VFLUX. These models rely on a number of input parameters and sensor geometry. Common input parameters are oscillation period of the sampling time window, soil thermal conductivity, fluid density, soil porosity, soil volumetric heat capacity, and fluid volumetric heat capacity to name a few.

Data from the DTP sensors were run through a quality control process, formatted, and then ran through VFLUX to estimate the infiltration rates. These models have the flexibility to evaluate the infiltration rates between temperature sensors with different spacings in order to evaluate effects from small soil layers (5cm) to a look at a larger volume (0 – 110cm).

For simplicity, a handful of sensors were evaluated and tabulated in Table 2 from Ponds 9 and 10. The sensors selected represent the different types of soil observed in the ponds and the observed max infiltration rates. The silty clayey soils at the north end of Pond 9 had a max infiltration rate of 0.72 cm/h which 3x slower compared to the sandy soils in the south end (2.16 cm/h) and 1.6x slower than the silty sands in the center (1.15 cm/h). The sandy soils in Pond 10 saw similar infiltration rates (2.88 and 1.44 cm/h, respectively) to the center and south of Pond 9.

Note, infiltration calculations were complicated by the short duration of the infiltration experiment. Ponds were done filling at the end of the day when saturated conditions were met, but the pond was empty within 24 hours after shut off. This resulted in either a single full diurnal cycle or slightly less. The accuracy of these estimates would be improved if the ponded water was kept at a constant level for greater than 24 hours, ensuring more than one full diurnal pulse was observed.

Table 2. Vertical infiltration rates from DTP sensors using VFLUX.

Sensor #	Max Infiltration (cm/h)	Location/soil type
P9E34D	0.72	P9 North end/silty clayey soil
P9F2FC	2.16	P9 South end/sandy soil
P9C3C0	1.15	P9 Center/sandy soil w/ some silty sands
P10F855	1.44	P10 South end/sandy soil w/some silty sands
P10D3F6	2.88	P10 Center/sandy soils

3.2 1D Hydrus Infiltration Rates

To assess potential infiltration rates, we used the derived spatial distribution of hydraulic conductivities (Fig. 11) to parameterize a simple 1D vertical groundwater flow model. Each pond, was subdivided into 1m×1m grid cells, and we extracted K_{sat} for each of those cells at 0.5 m intervals from 0 to 2.5 m depth. Recharge was simulated by applying a 50 cm head to this area over a period of 12 h. The model itself was run for a duration of 72 h. We extracted the infiltration rate 10 h after start of the infiltration to ensure saturated conditions.

Similar to the K_{sat} observations, Ponds 8 and 9 show a clear division in potential infiltration rates (Fig. 27). Note, the grey areas in Figure 27 are where the infiltration rates are well below 0.5 cm/h (red color) indicating no infiltration. The northern parts of Ponds 8 and 9 have little to no infiltration (<0.5 cm/h or 31.7 gal/day) compared to the southern ends which ranged from 6.5 cm/h up to >26 cm/h (412 – 1686 gal/day). Pond 10 showed the highest infiltration rates that ranged from 6.5 – >26 cm/h and Pond 11 ranged from 6.5 – 13 cm/h (412 – 824 gal/day). Ponds 12 and 13 showed the lowest infiltration rates, below ~ 2.1 cm/h (133 gal/day) for Pond 12 and 0 – 0.5 cm/h for Pond 13.

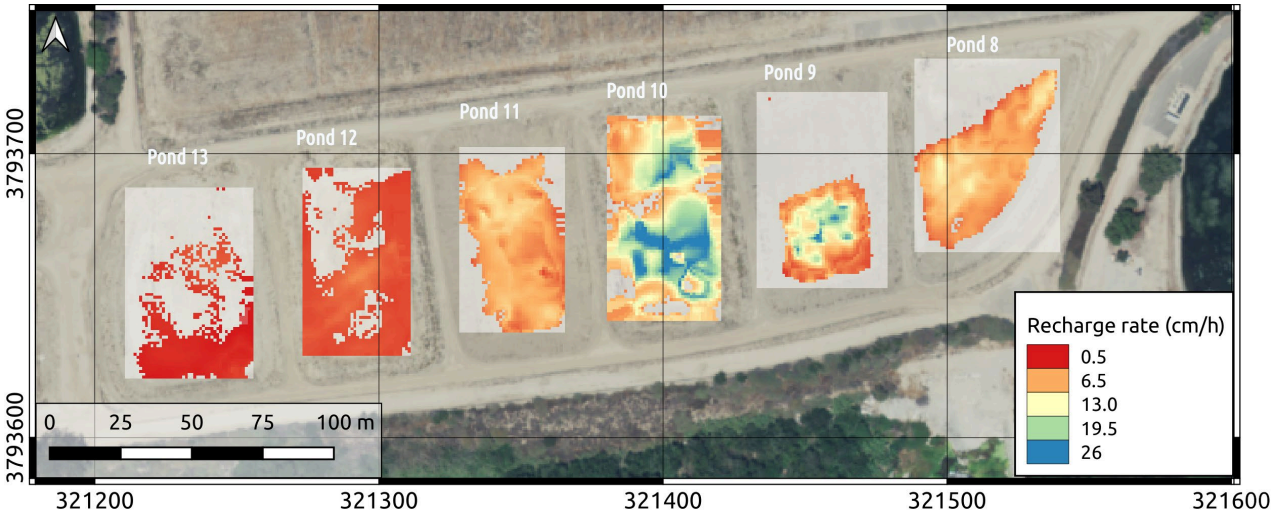

Figure 27. Estimated infiltration rates based on groundwater recharge modeling (Hydrus 1D) for 1 m ×1 m grid cells within each pond, using the K_{sat} distribution estimated from the EMI data.

3.3 Min3P 3D Infiltration Rates

Infiltration rates within a 3D volume were modeled for Pond 9 using a modified workflow developed on a previous LBL MAR project that simulated the K_{sat} field from the ERT data. The K_{sat} field was incorporated into the MIN3P numerical flow and reactive transport code for variably saturated media. We modified this workflow because we were able to collect valuable data that was missed in the last study, for instance K_{sat} was measured with the permeameter at a number of different sites with different soil types across Ponds 8 – 13, and K_{sat} was derived by developing a relationship between the K_{sat} measurement and the associated soil type that produced a certain response in the EMI/ERT data. This relationship was then used to interpolate the EMI/ERT 3D data into 3D K_{sat} distributions foregoing the need for heavy computing power to estimate K_{sat}. The data was interpolated onto an unstructured model finite difference mesh with 1.17M model nodes for Pond 9 alone. The water level data from the METER sensors was used to establish a pressure head across Pond 9 to develop a modeled pressure field induced by ponding. The 3D model boundary conditions were then set and tested iteratively for fine tuning. A single iterative run took 6 hours with every step to fine tune the boundary conditions which represent regional groundwater levels on the sides, and deep recharge at the bottom boundary. The model was then allowed to run over 3 days to simulate transient infiltration rates across Pond 9, and transient recharge rates to the deep groundwater aquifer. The same workflow would have been repeated for Pond 10, but one

water level sensor was never flooded in the northeast corner and the second sensor failed near the beginning of the experiment.

Results in Figure 28 from the 3D infiltration modeling in Pond 9 are shown as cross-sections in the north-south direction at 6, 12, 18, 24 and 36 hours after flooding. The north zone beneath the surficial silty clayey soil shows little infiltration with a saturation around 5% compared to the southern end of the pond where deep sandy soils convey the recharged water deep into the subsurface. The saturation front (blue colors) show the soils progressively saturate up to 40%. The high resolution of these results even captures that the southwest corner of Pond 9 (Fig. 28 red dashed box) infiltrates more water than the southeast corner.

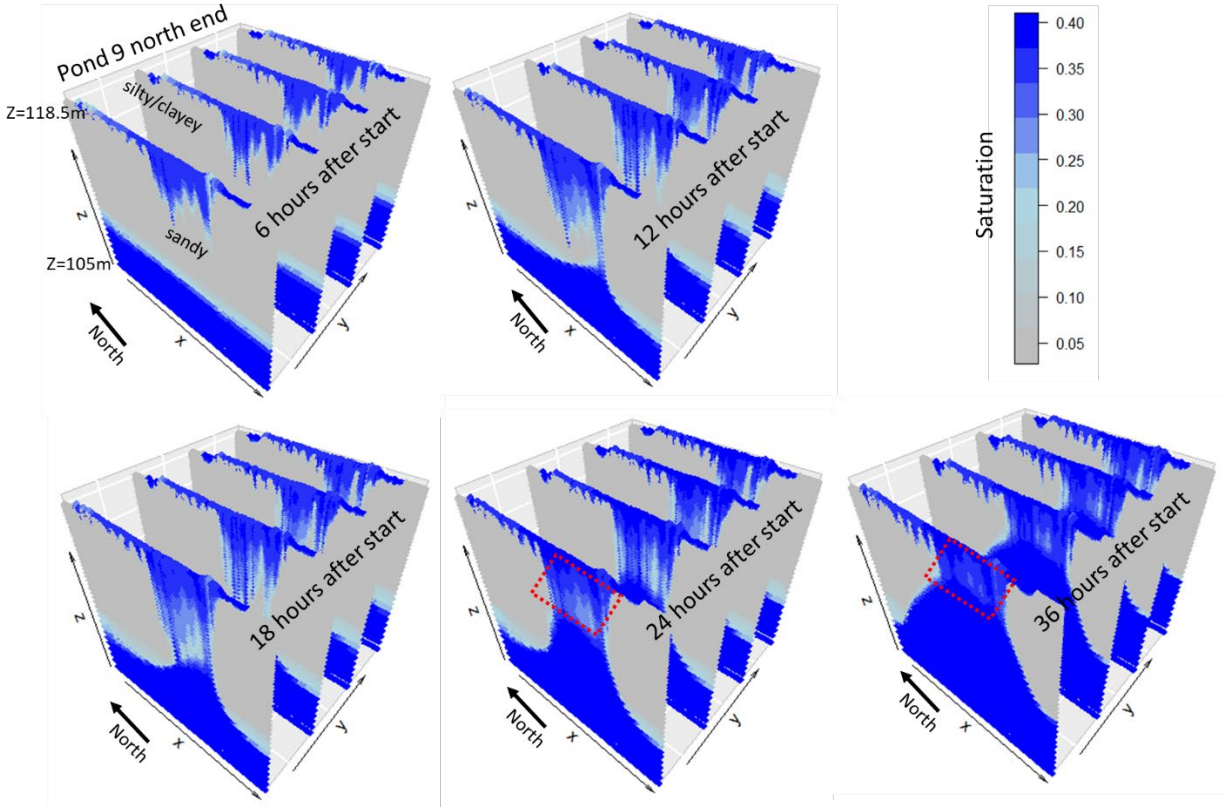

Figure 28. Pond 9 simulated infiltration over 36 hours shown in north-south cross sections. The majority of the infiltration happens at the south end of the Pond 9 through the sandy soils. Saturation below the north end of the pond are 5% or less. Red dashed box shows the southwest corner infiltrates more water than the southeast corner.

Infiltration rates were then calculated for the 3D volume and two planar view planes were extracted at the 117 m and 110 m elevation depths (pond bottom is at 118 m). The infiltration rates 1 m below the bottom of Pond 9 (Figure 29A, 117 m) shows the distribution of infiltration rates with the low permeability soils in the north (0.42 cm/h or 26.3 gal/day) infiltrating much lower than the sandy soils in the south (16 cm/h or 1014 gal/day). Deeper in the subsurface at 110 m elevation the infiltration rates increase by an order of magnitude, 0.42 cm/h (117 m) to 4.1 cm/h (110 m). The southern end of Pond 9 stays relatively the same with depth increasing in some areas and

decreasing a little in others (Figs 29 A and B).

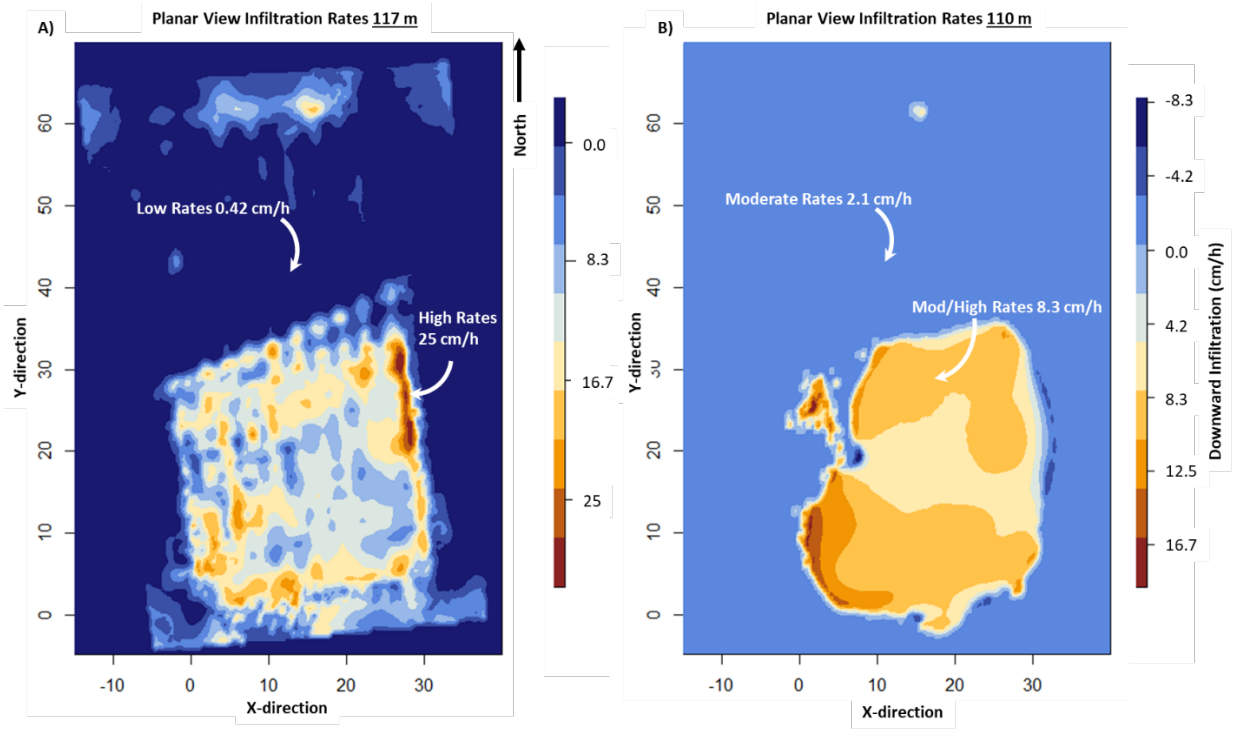

Figure 29. Pond 9 estimated infiltration rate distributions from 3D modeling at elevation 117 m (A) and 110 m (B). Note the pond bottom is at 118 m). Downward infiltration rates (positive) in the north end of the pond increase with depth (B) and stay relatively the same on the south end with depth.

4.0 *Discussion*

The main challenge during the performance of this project was the COVID-19 restrictions and the associated travel restrictions as the pandemic cases increased and decreased around the state. Only when cases were low would travel restrictions be lifted and work could be done at the facility. This caused large gaps in time between phases and extended the project beyond the original project timeline but did not affect the overall quality of the project or the goals.

The study goals were as follows:

1. Develop an approach using geophysical methods and other sensors to characterize the subsurface soils and quantify recharge in selected percolation ponds during controlled recharge events.
2. Identify the potential to improve recharge in the selected ponds.
3. Determine if water was leaking ("leakage") or lost from the ponds directly into the adjacent Arroyo or recharging the aquifer.
4. Determine if this approach is transferable to any other location within Metropolitan's service area.

The approach used to meet the goals of this project were very successful. Fast reconnaissance EMI quickly identified the soil spatial variability across Ponds 8 - 13 (Fig. 6). Highlighting the ponds (9 and 10) that were the best candidates for contrasting potential infiltration and candidates for further characterization of deeper soil spatial variability (Fig. 7) and hydrological properties (Fig. 11, K_{sat}). The EMI and ERT geophysical models were strategic in soil boring placement to confirm soil types to develop the geological model before performing the recharge phase. Deploying the EMI and ERT first, reduced the drilling costs by limiting the number of borings to four for characterization compared to drilling 'blind' to characterize the subsurface which would have resulted in numerous boreholes installed in a grid pattern that had the potential of misrepresenting the boundaries of the soil types and spatial distribution of the soils for later recommended engineering alteration for improved infiltration. The strength of this approach is combining the methods in the right order to optimize our knowledge of the subsurface and reduce the cost.

Results from the characterization phase highlighted the lateral and vertical soil distributions within Ponds 8 – 13 and the recharge phase highlighted the importance of **preferential fast flow path control on infiltration**. The southern end of Pond 9 infiltrated all of the applied water deep into the subsurface compared to the silty clayey soils on the north end of the pond. The borings in Pond 10 indicated similar sandy soils throughout the pond, but even Pond 10 had preferential flow paths in fairly uniform soils (Fig. 22). Understanding the soil distributions is paramount for optimizing the recharge capabilities of recharge basins.

The streamside ERT (Fig. 26) confirmed *no short-circuiting back into the adjacent arroyo*, but instead **deep infiltration and recharge into the unconfined aquifer**. Time-lapse ERT is a useful tool when using water as a tracer for movement in the subsurface.

Developing an empirical relationship between EMI or ERT with permeameter measurements at selected locations allowed us to transform the EMI data into a spatial 3D dataset of Ksat which was then incorporated into two modeling approaches: 1D Hydrus and 3D Min3P simulators. Each model was able to estimate the infiltration rates within all the ponds using Hydrus and Pond 9 (3D) using Min3P. Both offer a different approach to capturing infiltration rates but where they differ is the Hydrus model used a synthetic scenario to understand the infiltration potential of each pond in the shallow subsurface using the EMI data and Min3P used the recharge event data and timelines. The Hydrus approach was used as a way to quickly assess the potential of the ponds as the simulations took about 1 – 2 hours for each pond. The Min3P approach was used to more accurately quantify and represent the subsurface flow conditions during a recharge event which could later be used to feed a hydrological model for operation and maintenance plans and reporting purposes. Since the Min3P model is a 3D model it has considerably more setup and run time because it includes saturation and other data, and simulations took 2 – 3 days on average. But ultimately, what approach is used depends on what information is needed.

A simple approach to monitor infiltration rates over time is using the DTPs or a vertical array of temperature sensors. This approach proved effective at capturing the infiltration rates in the top 1.5 m of soil over time, but estimates could be improved through longer multiday recharge events versus 24 hours in this study. This approach has implications for monitoring when the next application of water should occur as the data could be telemetered real-time to a server running VFLUX or some other script. These sensors are very low cost and is a simple method for monitoring vertical recharge rates. All three approaches (VFLUX, Hydrus, and Min3P) estimated similar infiltration rates in the same portions of Pond 9.

Basin Modification Recommendations

One of the main goals of the project was to develop recommendations, if possible, to improve the infiltration rates of the ponds through modification. A simple, cost effective approach to understand infiltration potential of the soils was showcased by collecting strategic information from EMI on all ponds (~2 hours, all ponds), soil permeability (~4-5 hours, all ponds) and soil borings (1 day) strategically placed. Then, develop the data relationships to estimate K_{sat} across a site and estimate infiltration rate distributions using Hydrus 1D. Figures 8 and 26 highlight the soil and infiltration rate spatial variability. For instance, the low permeability soils on the north end of Pond 9 are underlain by sandy soils (Fig. 30, 3D orange colors) and the low permeability soils above it (blue colors, 2D slices) is approximately 1 m thick. The surficial low permeability soils have infiltration rates <0.5 cm/h. This layer is thin and could easily be removed exposing the more permeable sands below (Fig. 30, 3D layer). A simulation of this modification in Hydrus 1D would increase the infiltration rates from <0.5 cm/h up to as high as 7.9 cm/h, more than an order of magnitude increase. Putting this in volumetric terms, for a 24 h recharge event this would *improve an infiltration volume from 2186 m^3 (1.77 AF) to 6224 m^3 (5.04 AF)!* That's a **185% increase** in volume.

Compare this to Pond 10 which infiltrated 8590 m^3 in 24 h but never completely filled. A simple modification to Pond 9 could improve its recharge capacity (25% to 72%) of Pond 10 capacity. In contrast, Figure 8 shows Ponds 12 and 13 have a low permeability zone a depth starting at 1 m depth with a potential recharge of 1278 m^3 and 354 m^3, respectively. Potential recommendations for these ponds could be to use them as settling ponds to avoid clogging better recharge ponds or install dry wells/trenches with coarse sediments into the sandier soils below the low permeability layer. Overall, the characterization phase approach took four days to collect the data with a two-person crew but offers insights much more valuable than the cost of collection.

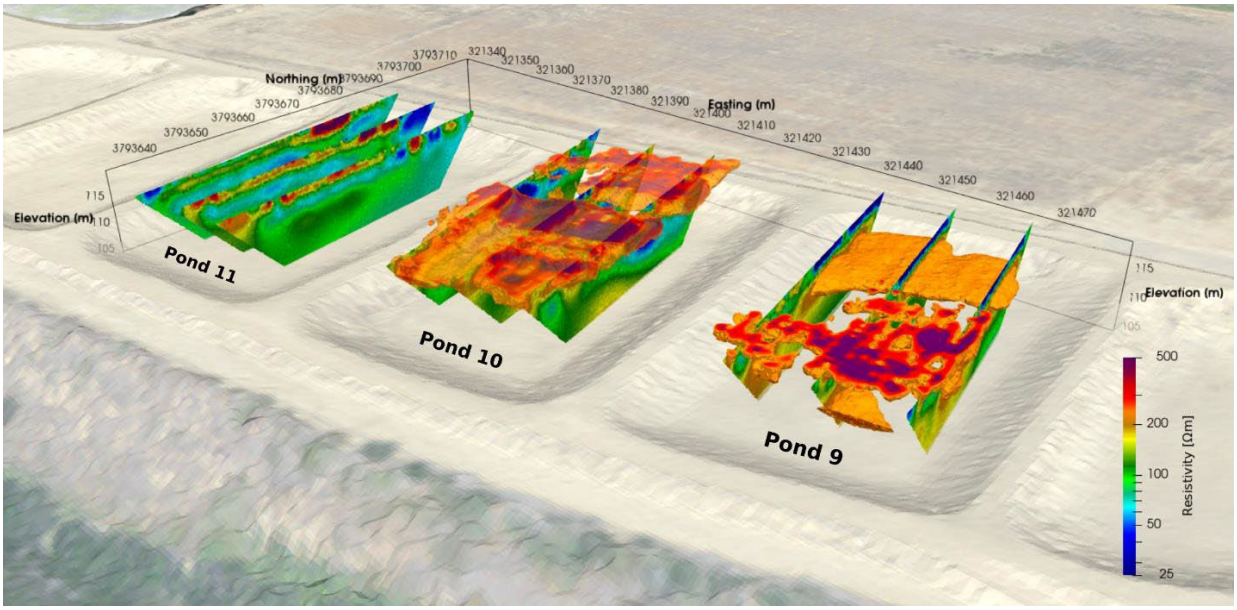

Figure 30. Electrical resistivity models obtained from the EMI and ERT. Shown are slices through the 3D models for ponds 9 and 10, and the 2D transects that were acquired in pond 11. For ponds 9 and 10, resistivities > 200 Ωm is shown, which represent the sandy layers. Note that at the

northern part of pond 9, this layer is overlain by a ~1m thick layer of low resistivity (blue colors).

5.0 Conclusions

This study showcases the importance and effectiveness of using basins as a managed aquifer recharge technology to help mitigate aquifer drawdown due to increased groundwater extraction and extended drought periods in a changing climate. Approaches to quantify recharge under new regulations to satisfy reporting requirements and to effectively manage water resources is lacking. In this study, we introduced an approach or workflow that is dynamic in deployment and integrates electrical geophysics with direct and indirect measurements of hydrogeological properties. This approach with these technologies can be adapted to any site considered for recharge (e.g. basins, bioswales, drywells, etc.) depending on water managers goals. Importantly, the approach can be used to locate prime recharge sites or, as shown in this study, potential modifications to existing structures to greatly improve existing recharge. Modifications for Pond 9 have the potential to improve recharge by 185% which results in 3.2 AF (0.87 Mgal) recharged per day in one pond! That's roughly 96 AF (26 Mgal) in a single month.

Here we presented three ways to model infiltration rates depending on need and budget. If the goal is to inform a hydrological model to perform forecast simulations for long-term operations the 3D MIN3P model can provide that data, but if the budget is smaller and the target is to optimize the infiltration capability of the site the scenario described in Section 4.0.1 using Hydrus 1D could offer the solution. This approach would identify the preferential flow paths so they could be exploited.

This study has shown how this approach not only characterizes the subsurface in great detail and can provide valuable information for further recharge study design, but it has also visualized how water migrates through the subsurface via preferential flow paths to deep aquifer recharge without flowing back into the river after infiltration. Furthermore, the results have shown that this strategic approach of data integration such as soil moisture, K_{sat}, amount of applied water, soil temperature and texture provide a number of physical and hydrological parameters that can be used in simple to complex models to quantify recharge in 1D, 2D, and 3D.

This approach is a valuable toolbox for water resource management into the future, during an uncertain water stressed future. In addition to understanding recharge at a single site, this pilot study also provides a cookbook (Figure 31) approach that can provide valuable data to the region, and the state at large, on recharge performance in floodplain settings within certain soil types. These datasets can be very valuable when performing large scale basin forecasting because they provide ground-truthed data.

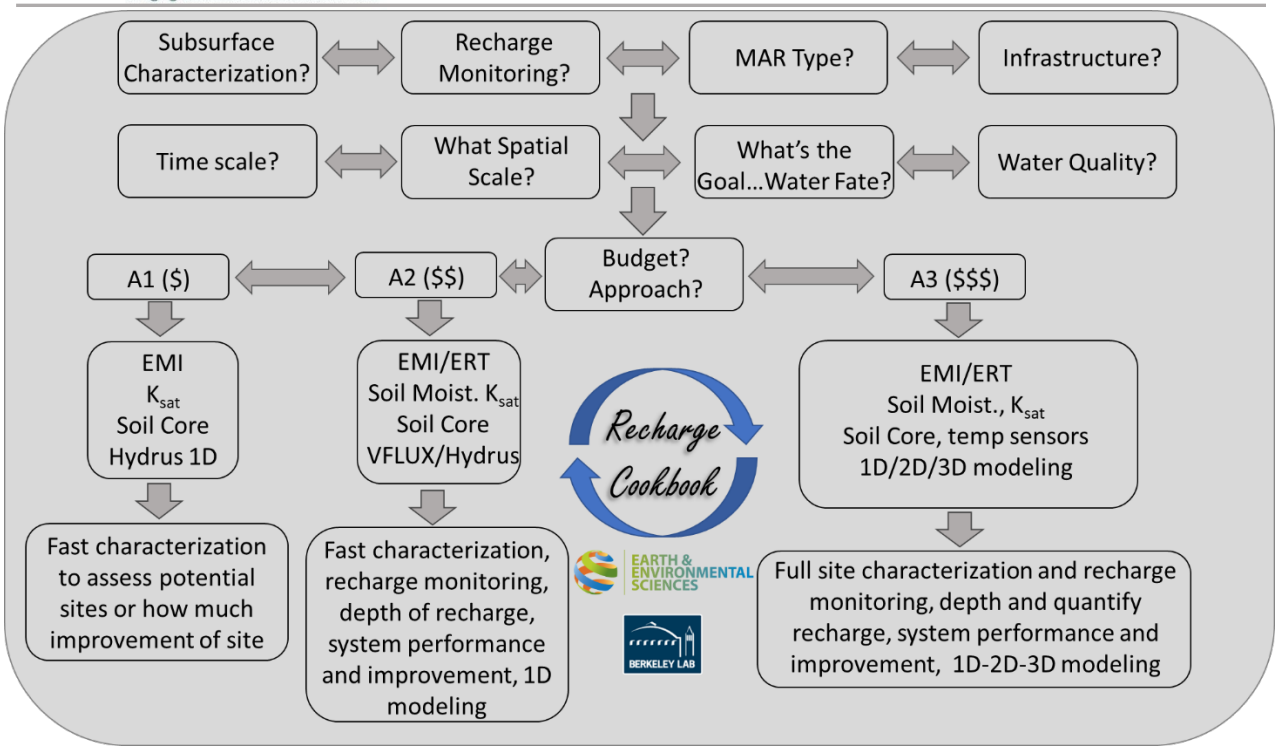

Figure 31. LBNL Recharge Cookbook guidance document for planning groundwater recharge site development, monitoring, improvement, etc. based on goals and budget.

Appendix A

EMI Calibration and Inversion Images

EM Data Inversion - P8

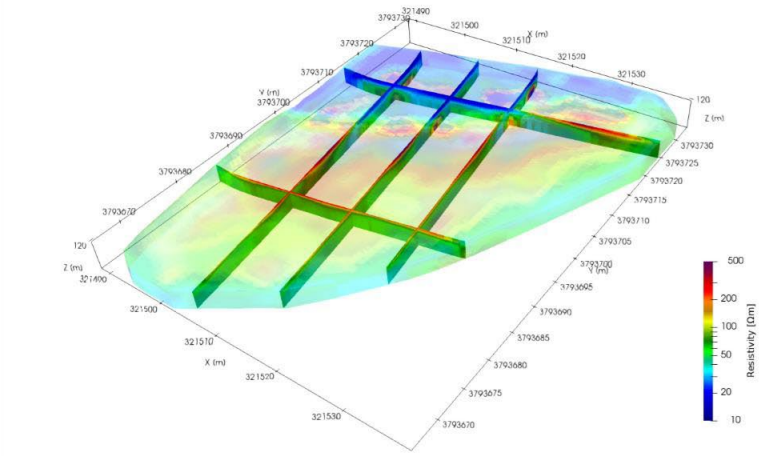

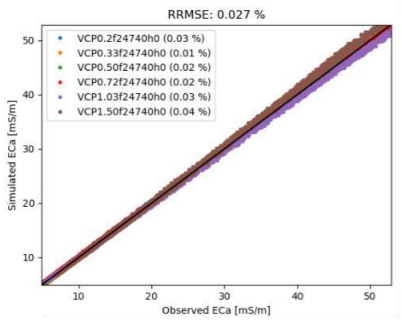

EM Data Inversion - P9

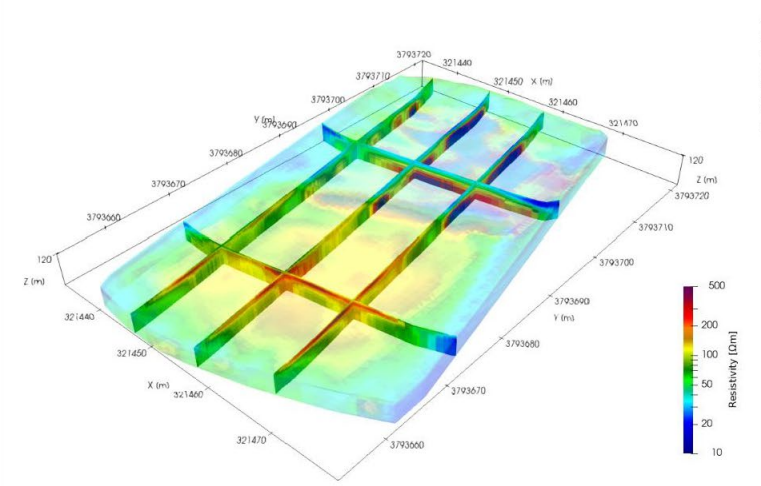

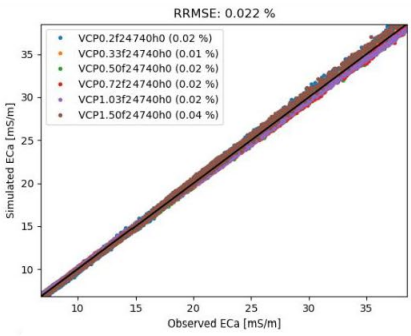

EM Data Inversion - P10

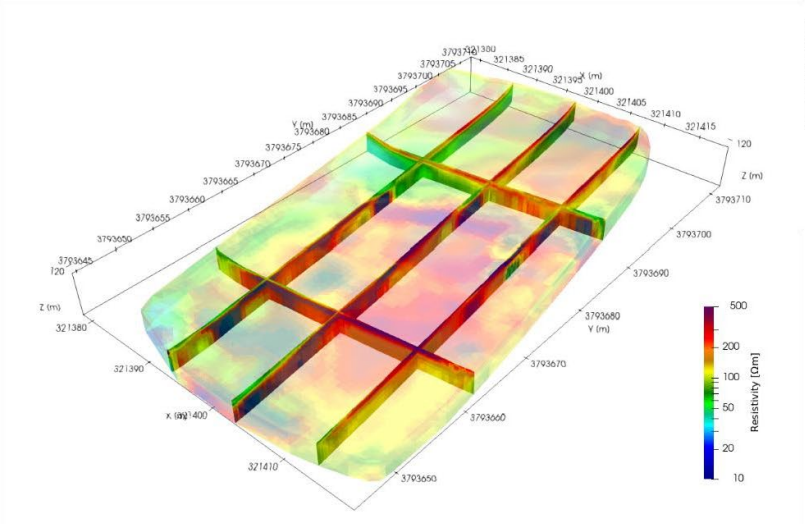

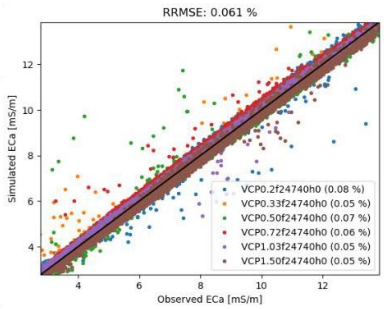

EM Data Inversion - P11

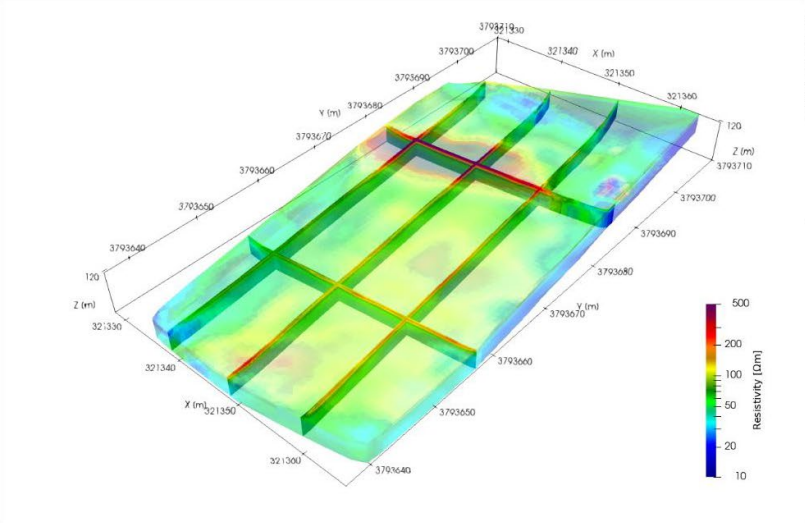

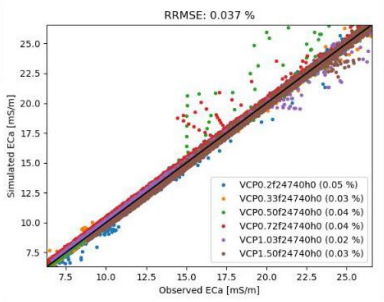

EM Data Inversion - P12

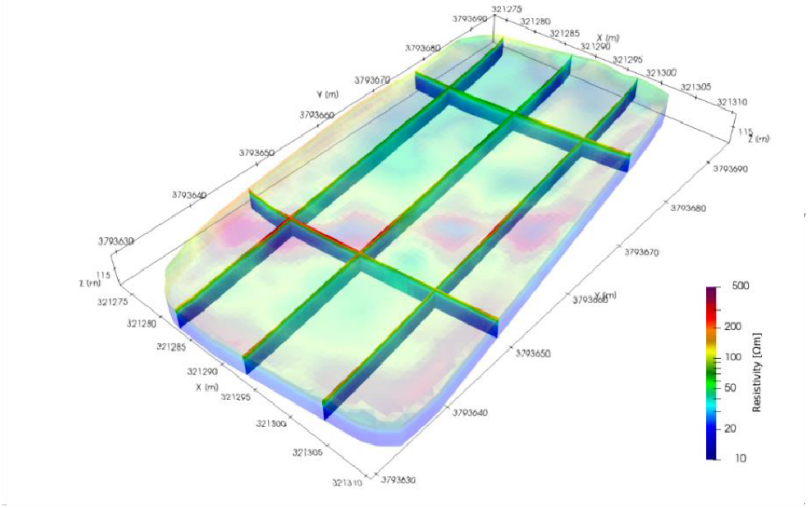

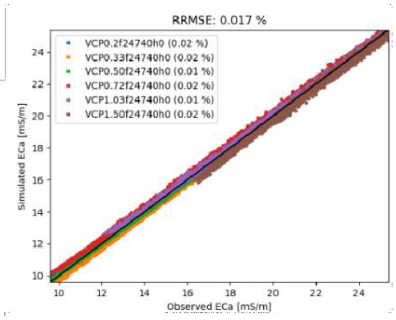

EM Data Inversion - P13

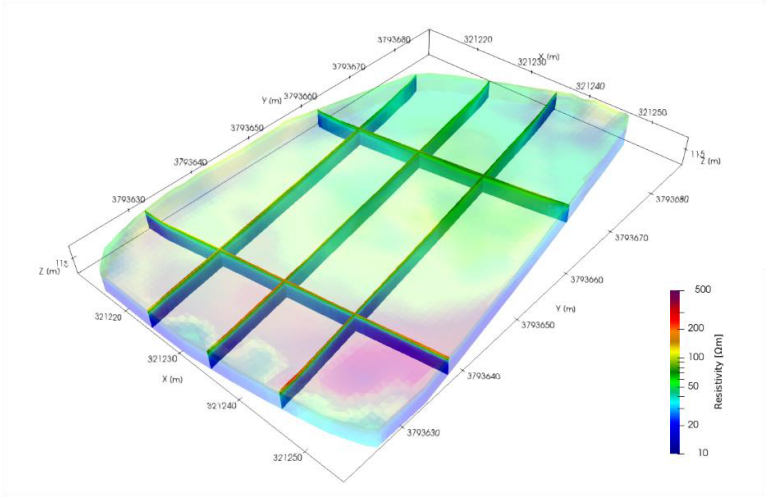

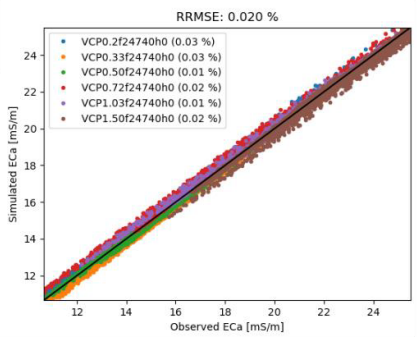

Appendix B: DTP Images

Pond 9

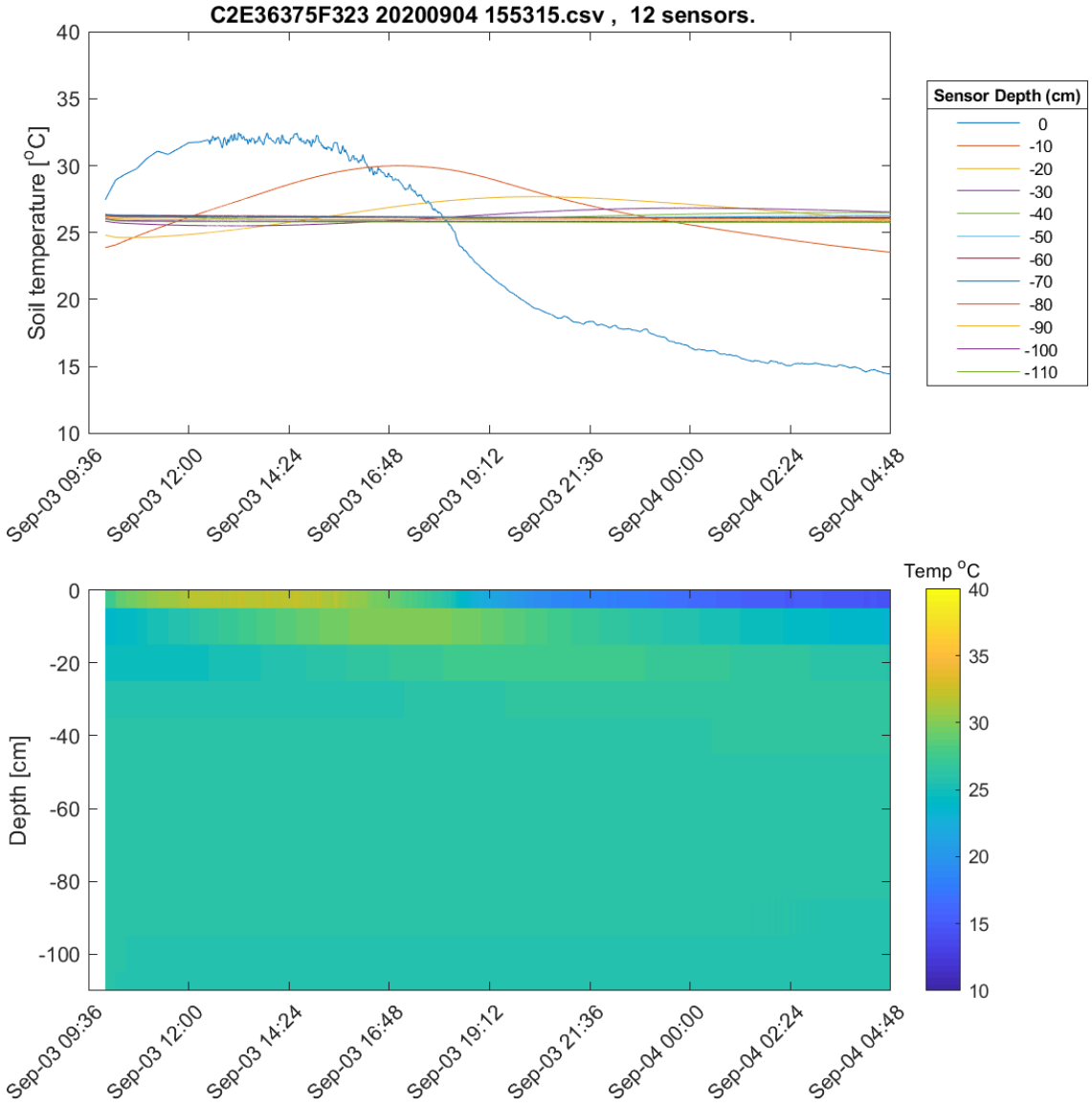
C2E36375F323 20200904 155315.csv , 12 sensors.
Soil temperature [°C]
Sensor Depth (cm)
0
-10
-20
-30
-40
-50
-60
-70
-80
-90
-100
-110
Depth [cm]
Temp °C
Sep-03 09:36
Sep-03 12:00
Sep-03 14:24
Sep-03 16:48
Sep-03 19:12
Sep-03 21:36
Sep-04 00:00
Sep-04 02:24
Sep-04 04:48

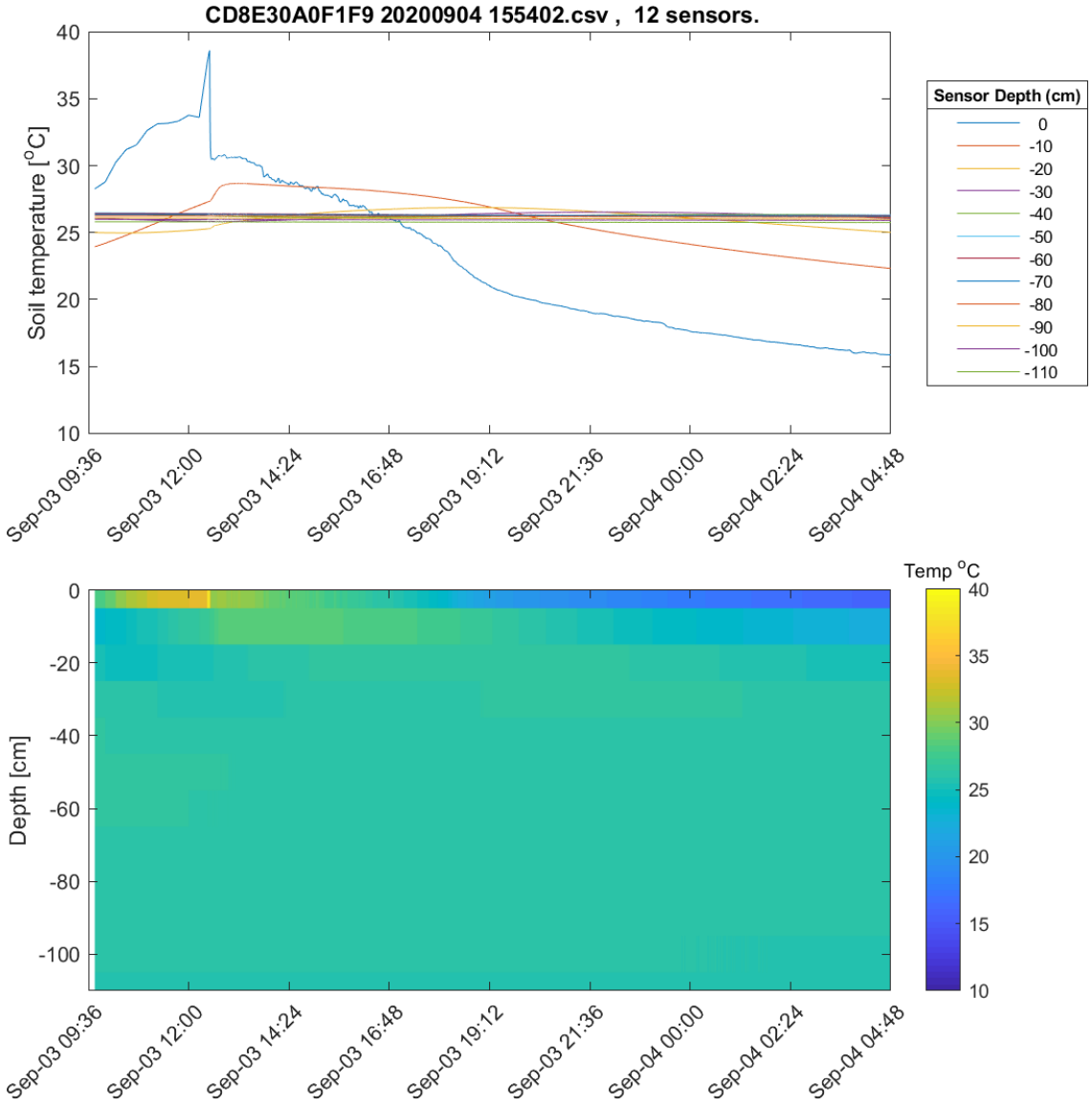
CD8E30A0F1F9 20200904 155402.csv , 12 sensors.
Soil temperature [°C]
Sensor Depth (cm)
0
-10
-20
-30
-40
-50
-60
-70
-80
-90
-100
-110
Depth [cm]
Temp °C
Sep-03 09:36
Sep-03 12:00
Sep-03 14:24
Sep-03 16:48
Sep-03 19:12
Sep-03 21:36
Sep-04 00:00
Sep-04 02:24
Sep-04 04:48

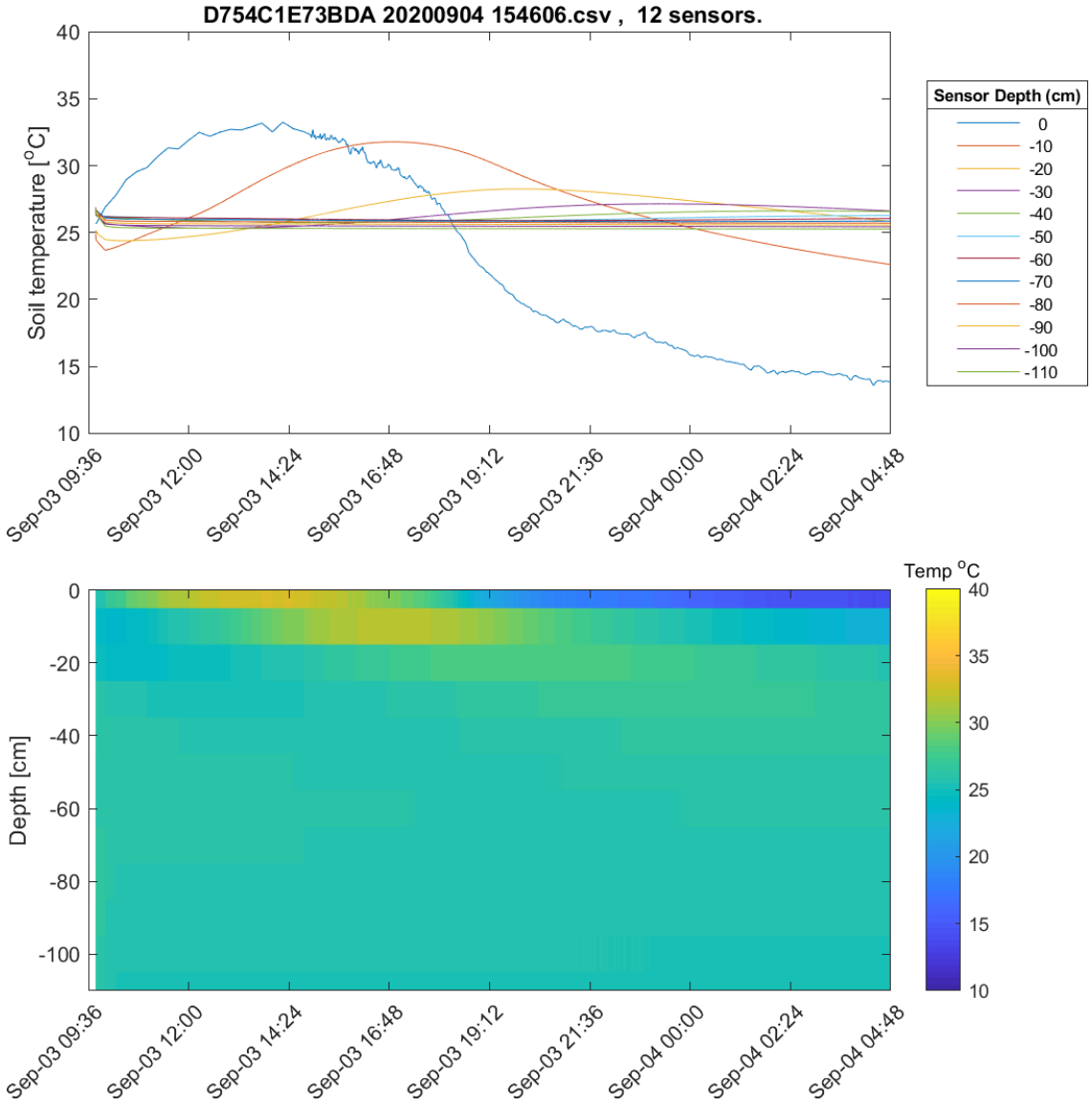
D754C1E73BDA 20200904 154606.csv , 12 sensors.
Soil temperature [°C]
Sensor Depth (cm)
0
-10
-20
-30
-40
-50
-60
-70
-80
-90
-100
-110
Depth [cm]
Temp °C
Sep-03 09:36
Sep-03 12:00
Sep-03 14:24
Sep-03 16:48
Sep-03 19:12
Sep-03 21:36
Sep-04 00:00
Sep-04 02:24
Sep-04 04:48

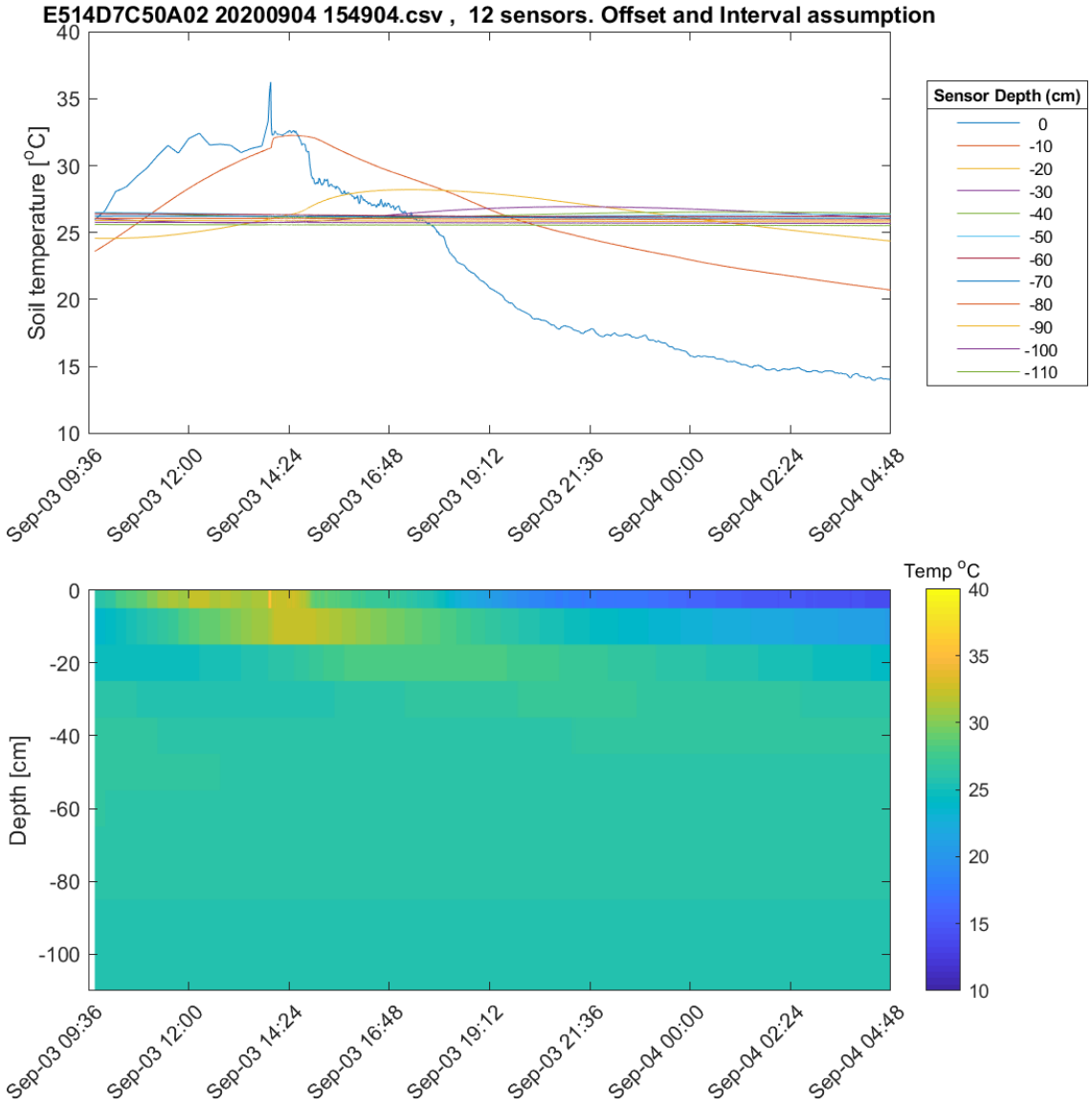
E514D7C50A02 20200904 154904.csv , 12 sensors. Offset and Interval assumption
Soil temperature [°C]
Sensor Depth (cm)
0
-10
-20
-30
-40
-50
-60
-70
-80
-90
-100
-110
Sep-03 09:36
Sep-03 12:00
Sep-03 14:24
Sep-03 16:48
Sep-03 19:12
Sep-03 21:36
Sep-04 00:00
Sep-04 02:24
Sep-04 04:48
Depth [cm]
Temp °C

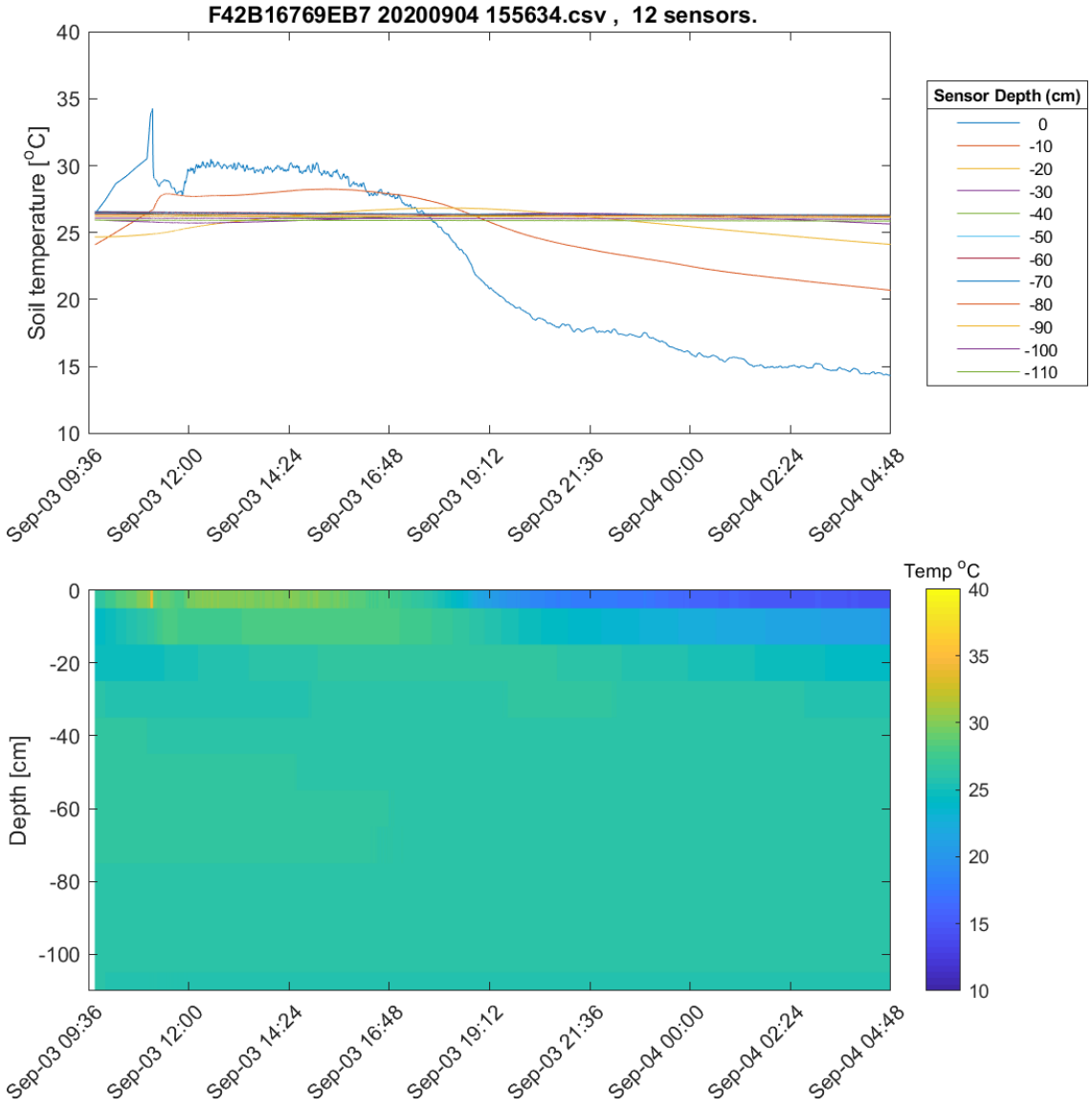
F42B16769EB7 20200904 155634.csv , 12 sensors.
Soil temperature [°C]
Sensor Depth (cm)
0
-10
-20
-30
-40
-50
-60
-70
-80
-90
-100
-110
Depth [cm]
Temp °C
Sep-03 09:36
Sep-03 12:00
Sep-03 14:24
Sep-03 16:48
Sep-03 19:12
Sep-03 21:36
Sep-04 00:00
Sep-04 02:24
Sep-04 04:48

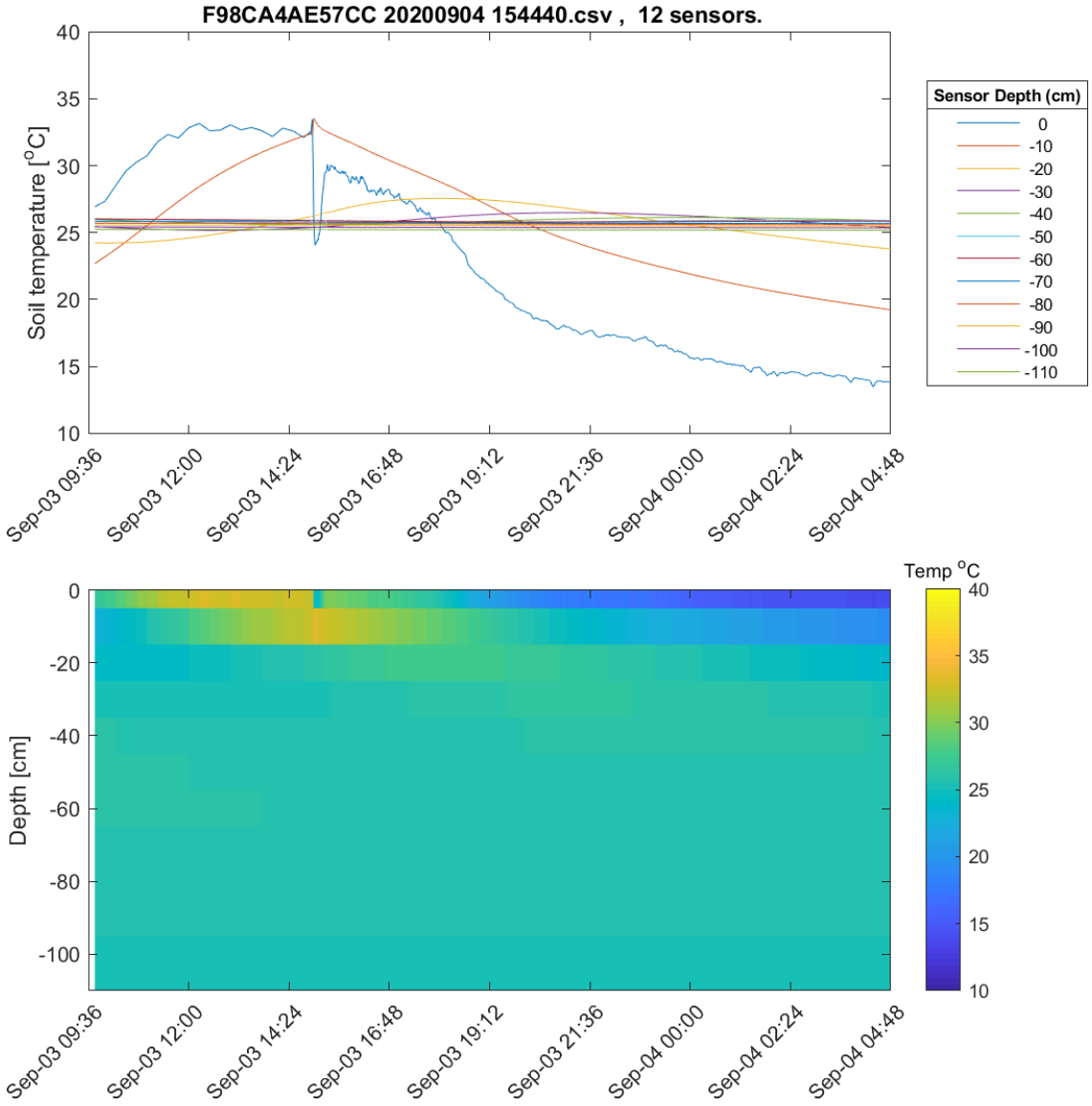
F98CA4AE57CC 20200904 154440.csv , 12 sensors.
Soil temperature [°C]
Sensor Depth (cm)
0
-10
-20
-30
-40
-50
-60
-70
-80
-90
-100
-110
Sep-03 09:36
Sep-03 12:00
Sep-03 14:24
Sep-03 16:48
Sep-03 19:12
Sep-03 21:36
Sep-04 00:00
Sep-04 02:24
Sep-04 04:48
Depth [cm]
Temp °C

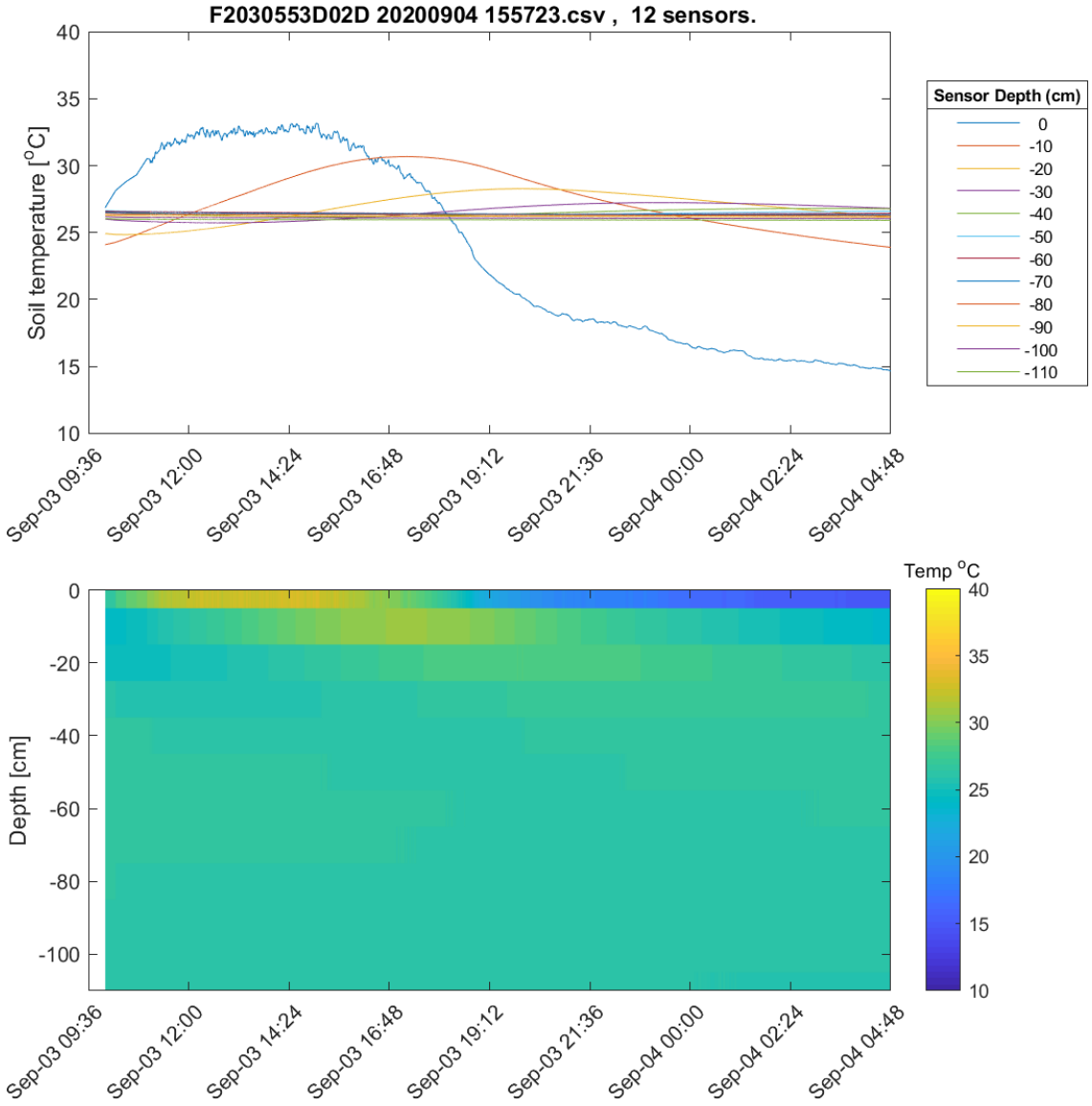
F2030553D02D 20200904 155723.csv , 12 sensors.
Soil temperature [°C]
Sensor Depth (cm)
0
-10
-20
-30
-40
-50
-60
-70
-80
-90
-100
-110
Depth [cm]
Temp °C
Sep-03 09:36
Sep-03 12:00
Sep-03 14:24
Sep-03 16:48
Sep-03 19:12
Sep-03 21:36
Sep-04 00:00
Sep-04 02:24
Sep-04 04:48

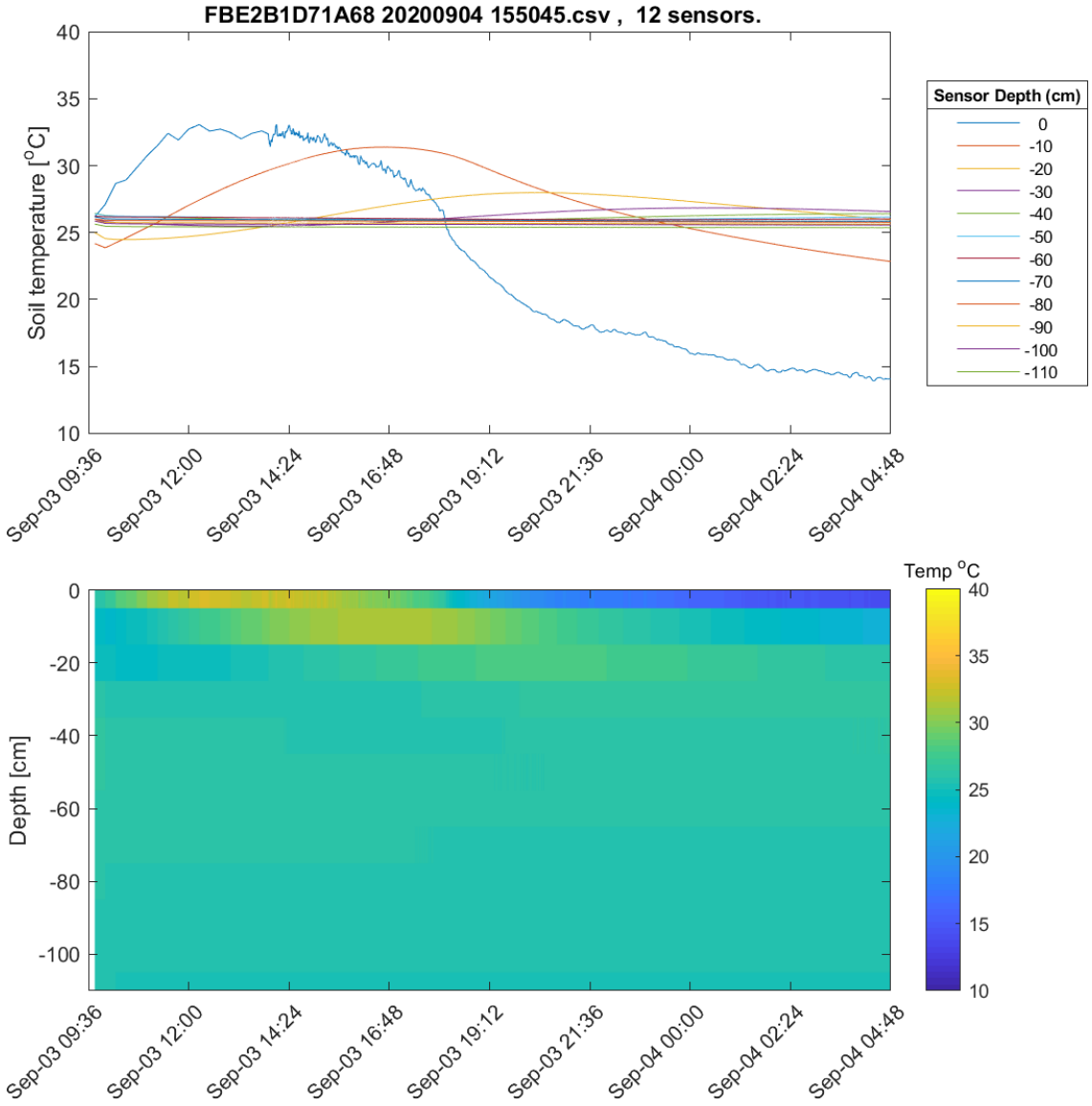
FBE2B1D71A68 20200904 155045.csv , 12 sensors.
Soil temperature [°C]
Sensor Depth (cm)
0
-10
-20
-30
-40
-50
-60
-70
-80
-90
-100
-110
Depth [cm]
Temp °C
Sep-03 09:36
Sep-03 12:00
Sep-03 14:24
Sep-03 16:48
Sep-03 19:12
Sep-03 21:36
Sep-04 00:00
Sep-04 02:24
Sep-04 04:48

Pond 10 DTP

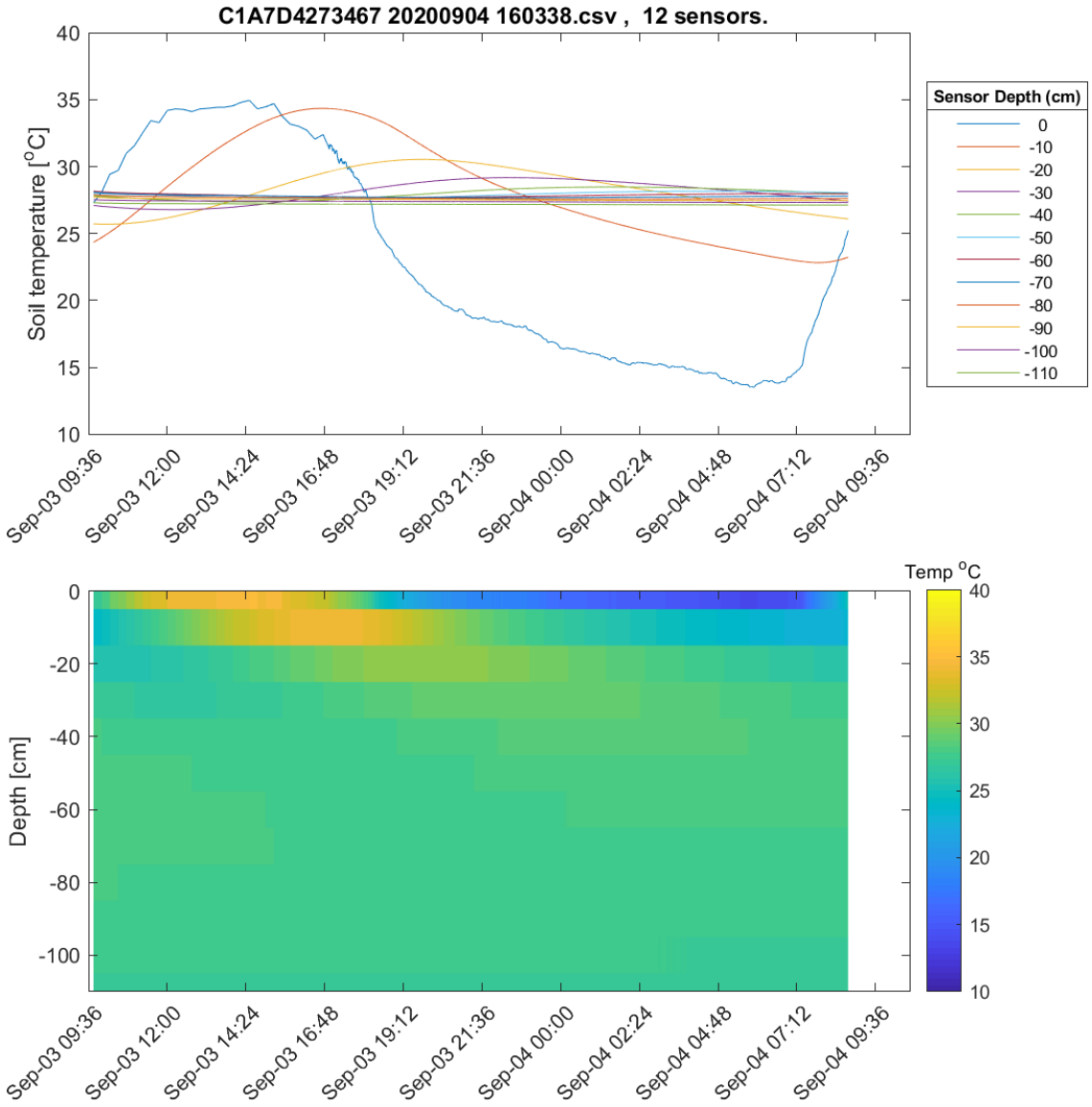
C1A7D4273467 20200904 160338.csv , 12 sensors.
Soil temperature [°C]
Sensor Depth (cm)
0
-10
-20
-30
-40
-50
-60
-70
-80
-90
-100
-110
Depth [cm]
Temp °C
Sep-03 09:36
Sep-03 12:00
Sep-03 14:24
Sep-03 16:48
Sep-03 19:12
Sep-03 21:36
Sep-04 00:00
Sep-04 02:24
Sep-04 04:48
Sep-04 07:12
Sep-04 09:36

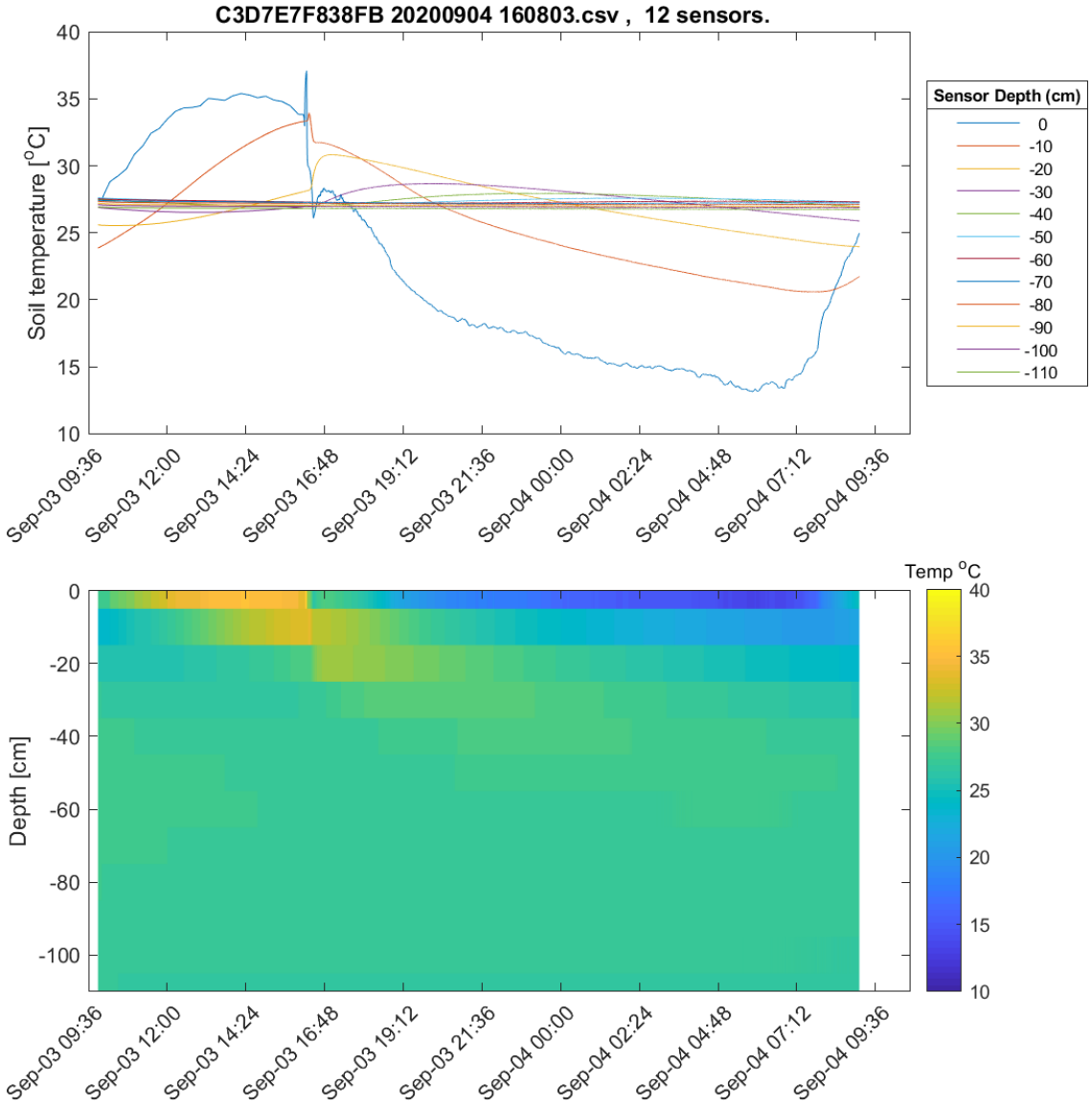
C3D7E7F838FB 20200904 160803.csv , 12 sensors.
Soil temperature [°C]
Sensor Depth (cm)
0
-10
-20
-30
-40
-50
-60
-70
-80
-90
-100
-110
Depth [cm]
Temp °C
Sep-03 09:36
Sep-03 12:00
Sep-03 14:24
Sep-03 16:48
Sep-03 19:12
Sep-03 21:36
Sep-04 00:00
Sep-04 02:24
Sep-04 04:48
Sep-04 07:12
Sep-04 09:36

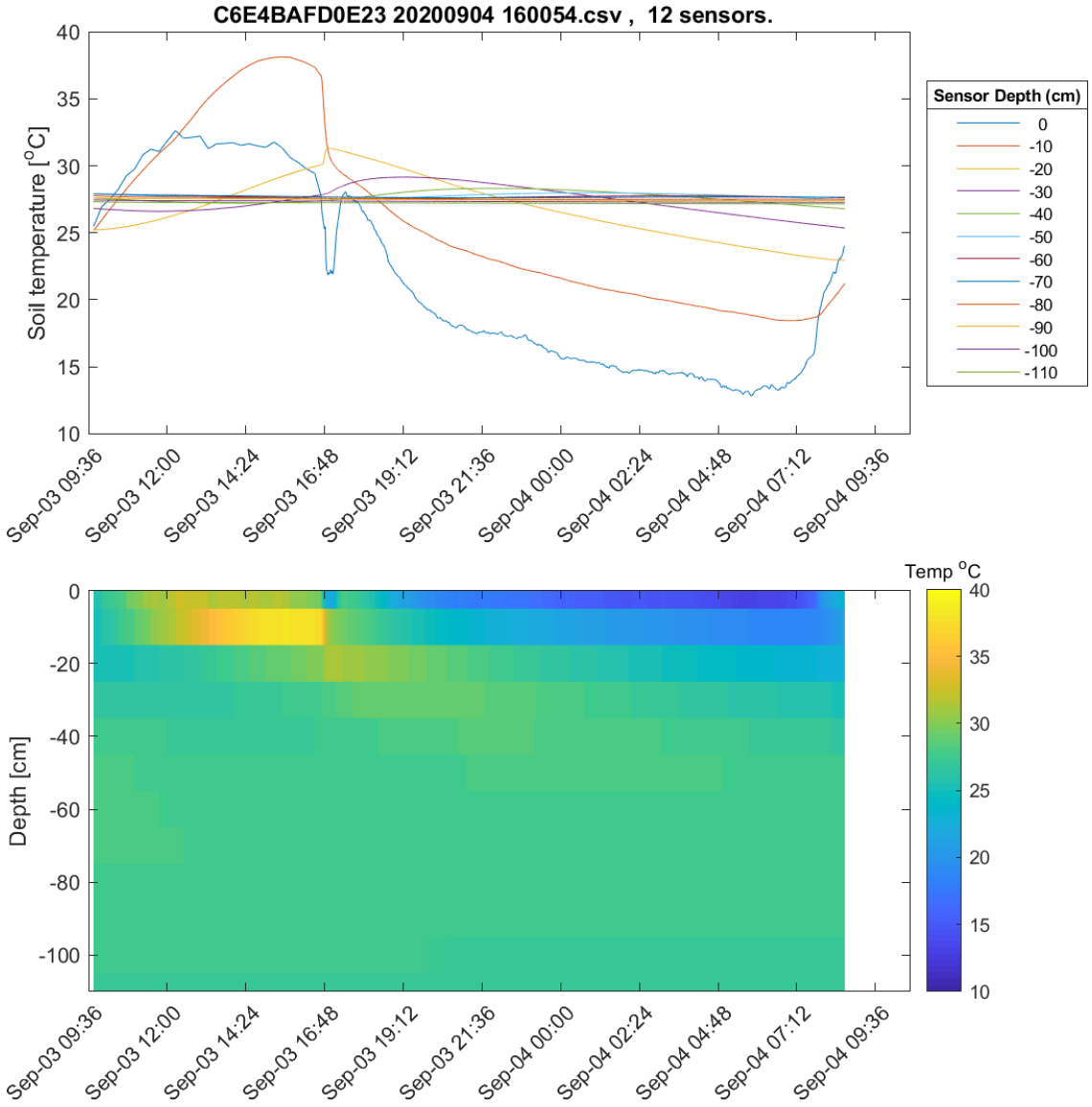
C6E4BAFD0E23 20200904 160054.csv , 12 sensors.
Soil temperature [°C]
Sensor Depth (cm)
0
-10
-20
-30
-40
-50
-60
-70
-80
-90
-100
-110
Depth [cm]
Temp °C
Sep-03 09:36
Sep-03 12:00
Sep-03 14:24
Sep-03 16:48
Sep-03 19:12
Sep-03 21:36
Sep-04 00:00
Sep-04 02:24
Sep-04 04:48
Sep-04 07:12
Sep-04 09:36

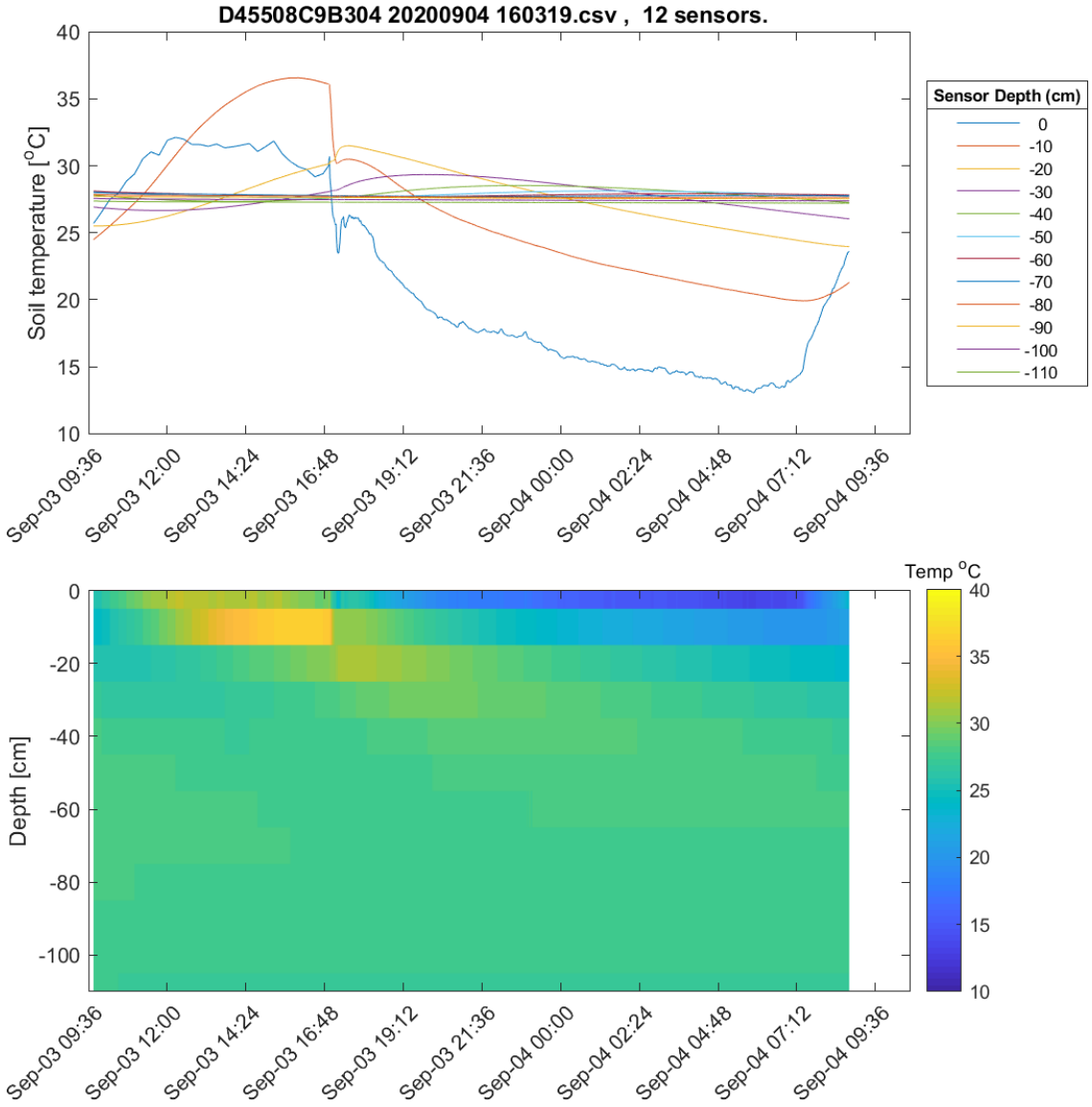
D45508C9B304 20200904 160319.csv , 12 sensors.
Soil temperature [°C]
Sensor Depth (cm)
0
-10
-20
-30
-40
-50
-60
-70
-80
-90
-100
-110
Sep-03 09:36
Sep-03 12:00
Sep-03 14:24
Sep-03 16:48
Sep-03 19:12
Sep-03 21:36
Sep-04 00:00
Sep-04 02:24
Sep-04 04:48
Sep-04 07:12
Sep-04 09:36
Depth [cm]
Temp °C

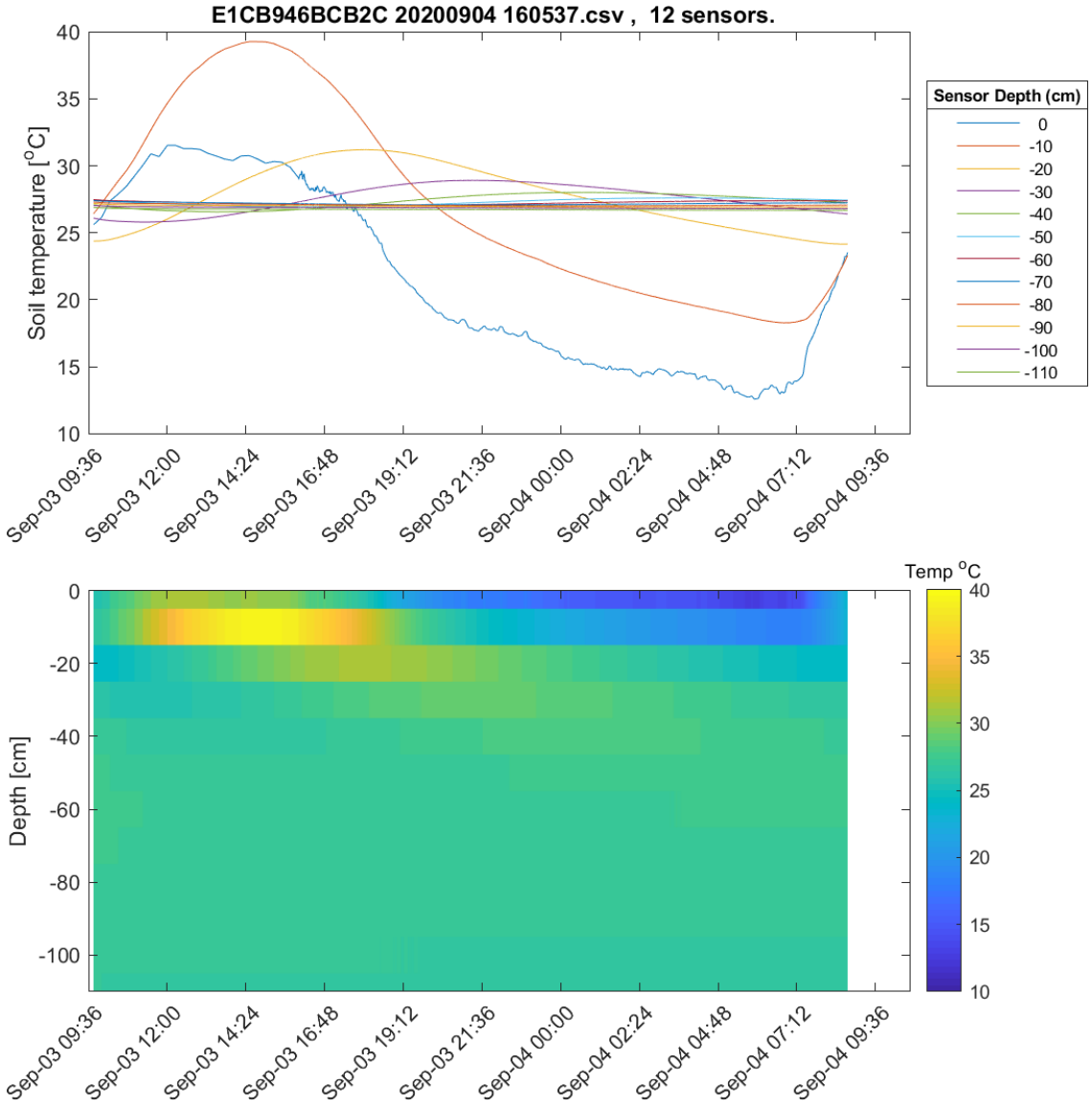
E1CB946BCB2C 20200904 160537.csv , 12 sensors.
Soil temperature [°C]
Sensor Depth (cm)
0
-10
-20
-30
-40
-50
-60
-70
-80
-90
-100
-110
Depth [cm]
Temp °C
Sep-03 09:36
Sep-03 12:00
Sep-03 14:24
Sep-03 16:48
Sep-03 19:12
Sep-03 21:36
Sep-04 00:00
Sep-04 02:24
Sep-04 04:48
Sep-04 07:12
Sep-04 09:36

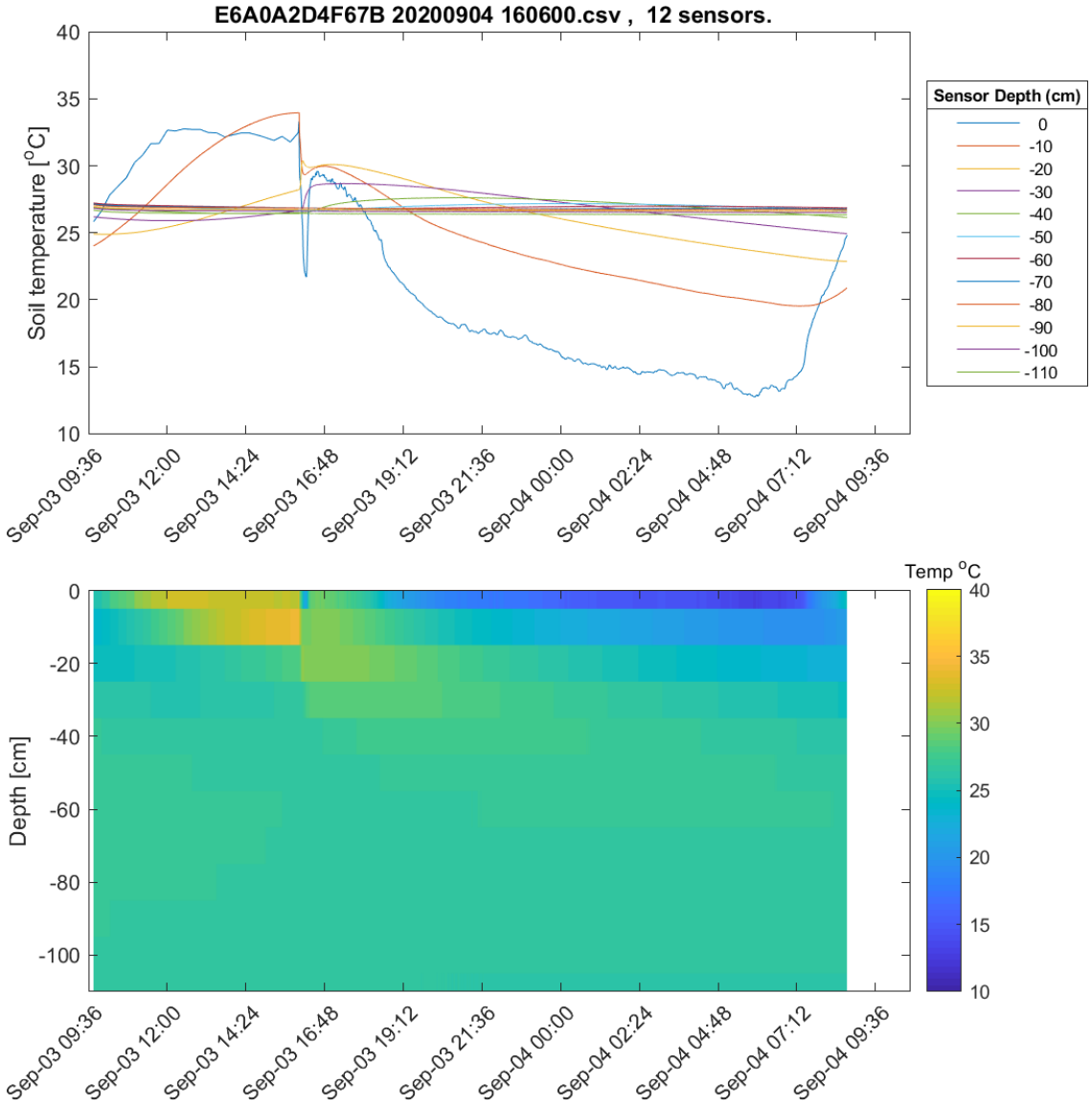
E6A0A2D4F67B 20200904 160600.csv , 12 sensors.
Soil temperature [°C]
Sensor Depth (cm)
0
-10
-20
-30
-40
-50
-60
-70
-80
-90
-100
-110
Depth [cm]
Temp °C
Sep-03 09:36
Sep-03 12:00
Sep-03 14:24
Sep-03 16:48
Sep-03 19:12
Sep-03 21:36
Sep-04 00:00
Sep-04 02:24
Sep-04 04:48
Sep-04 07:12
Sep-04 09:36

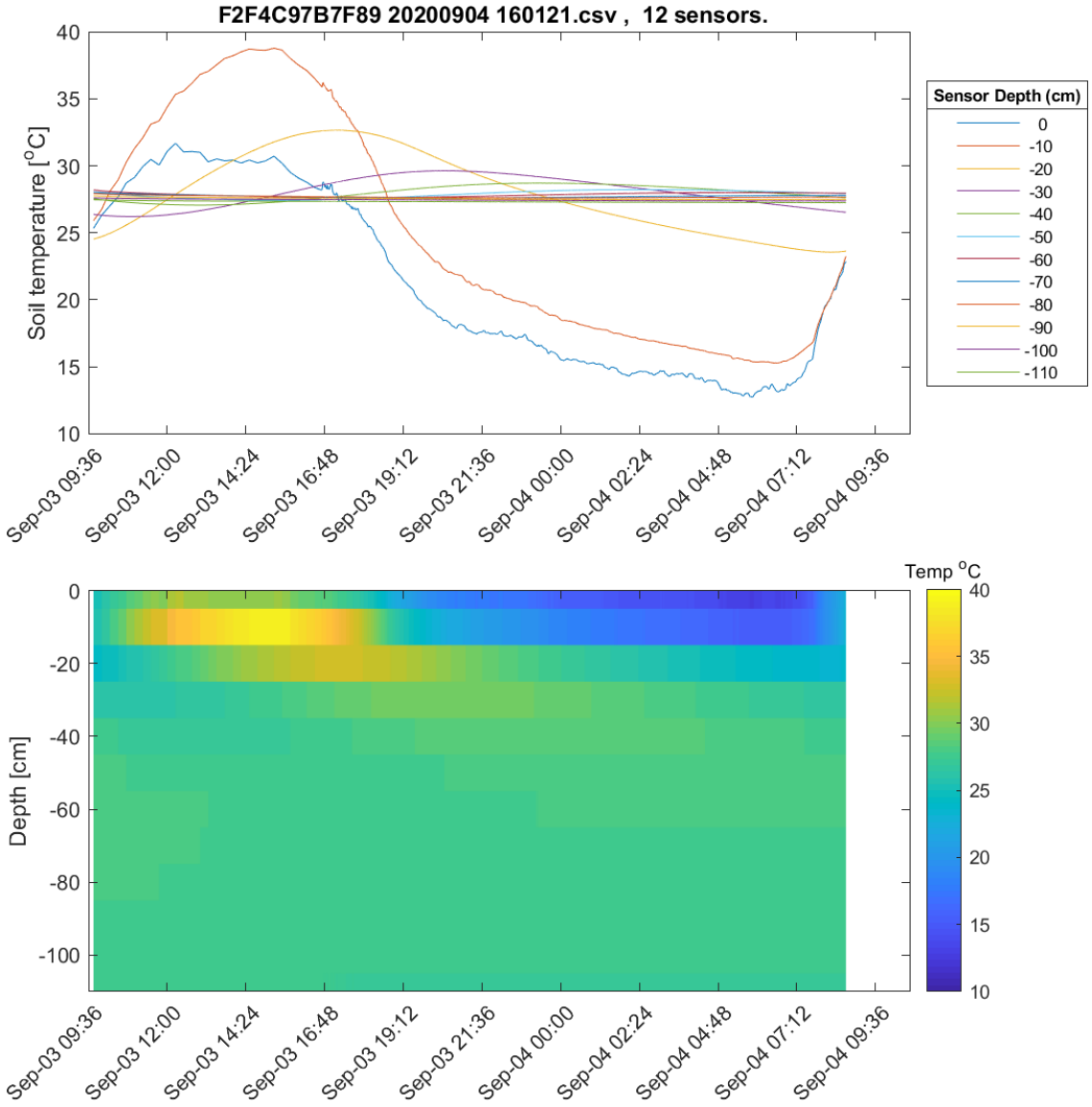
F2F4C97B7F89 20200904 160121.csv , 12 sensors.
Soil temperature [°C]
Sensor Depth (cm)
0
-10
-20
-30
-40
-50
-60
-70
-80
-90
-100
-110
Depth [cm]
Temp °C
Sep-03 09:36
Sep-03 12:00
Sep-03 14:24
Sep-03 16:48
Sep-03 19:12
Sep-03 21:36
Sep-04 00:00
Sep-04 02:24
Sep-04 04:48
Sep-04 07:12
Sep-04 09:36

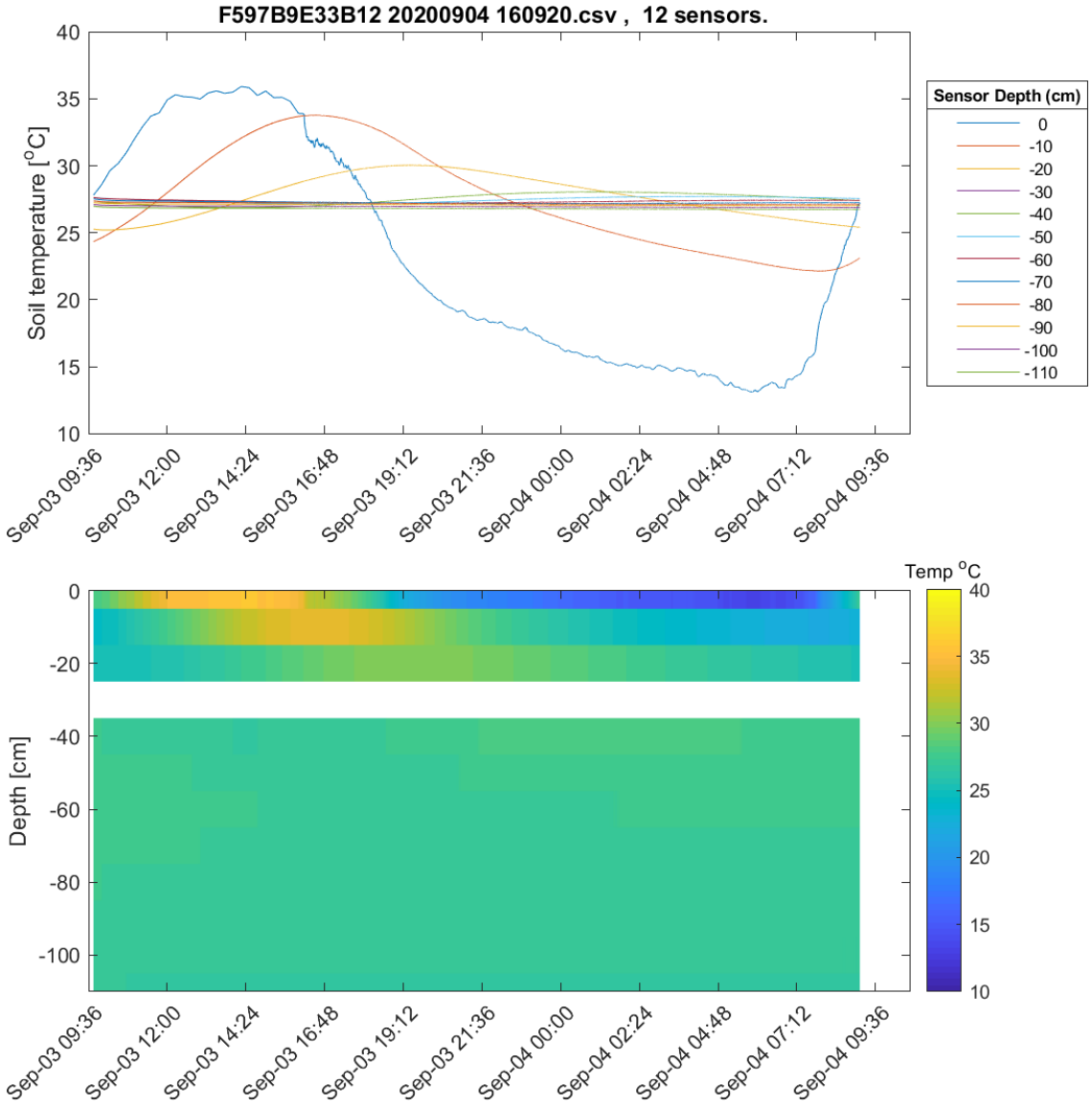
F597B9E33B12 20200904 160920.csv , 12 sensors.
Soil temperature [°C]
Sensor Depth (cm)
0
-10
-20
-30
-40
-50
-60
-70
-80
-90
-100
-110
Depth [cm]
Temp °C
Sep-03 09:36
Sep-03 12:00
Sep-03 14:24
Sep-03 16:48
Sep-03 19:12
Sep-03 21:36
Sep-04 00:00
Sep-04 02:24
Sep-04 04:48
Sep-04 07:12
Sep-04 09:36

Recharge Phase – DTP

Pond 9

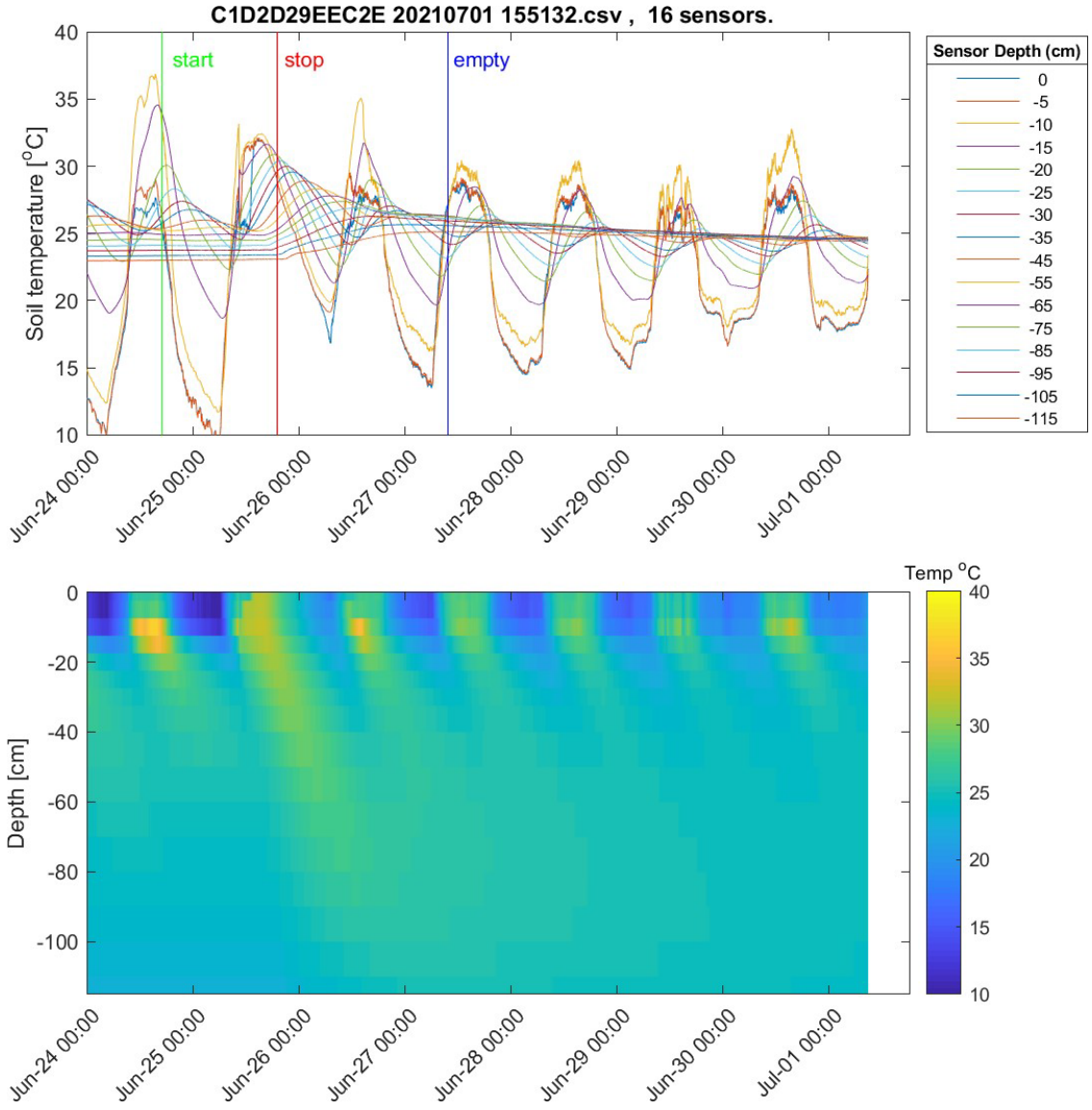
C1D2D29EEC2E 20210701 155132.csv , 16 sensors.
start
stop
empty
Soil temperature [°C]
Sensor Depth (cm)
0
-5
-10
-15
-20
-25
-30
-35
-45
-55
-65
-75
-85
-95
-105
-115
Jun-24 00:00
Jun-25 00:00
Jun-26 00:00
Jun-27 00:00
Jun-28 00:00
Jun-29 00:00
Jun-30 00:00
Jul-01 00:00
Depth [cm]
Temp °C

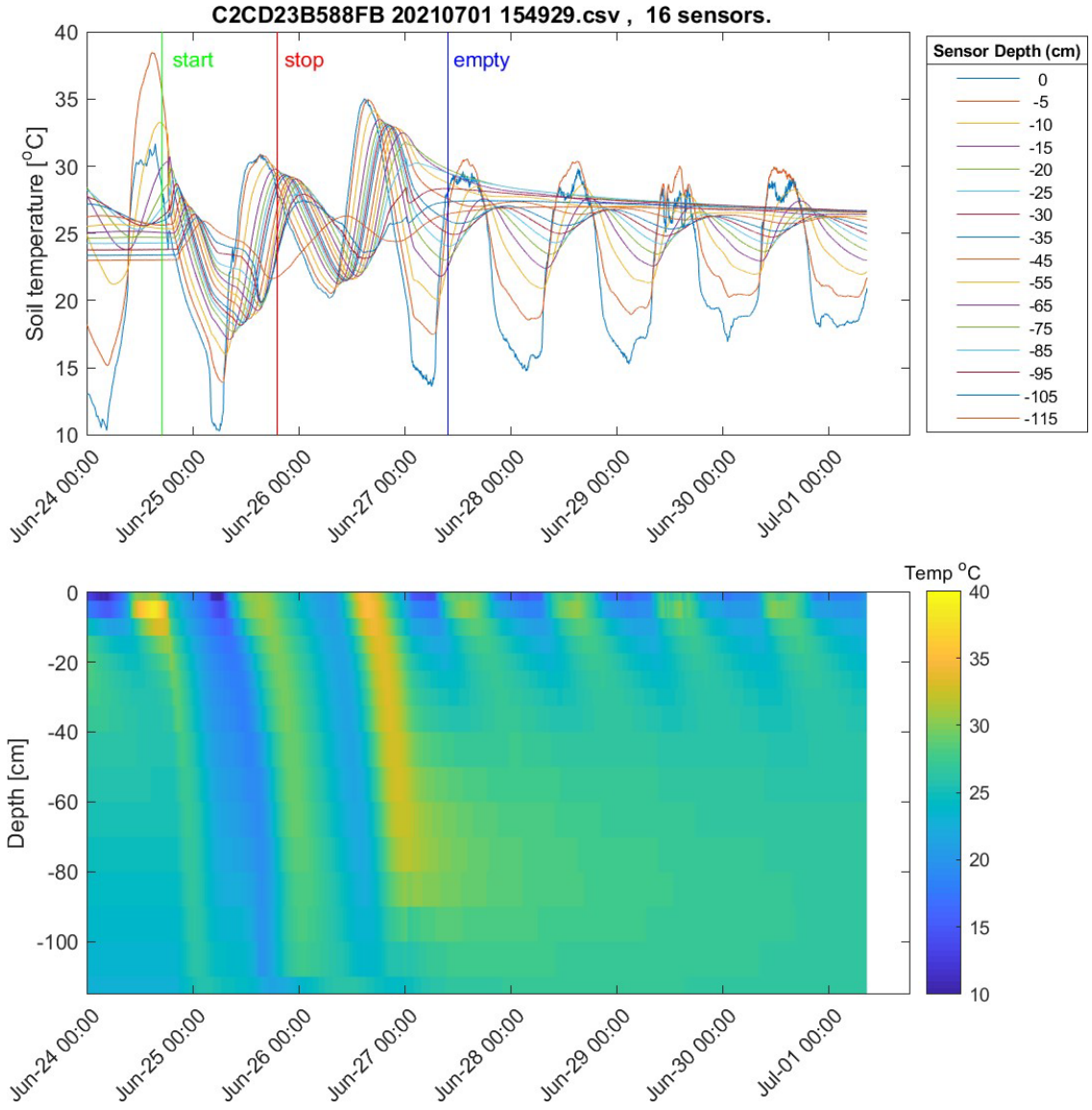
C2CD23B588FB 20210701 154929.csv , 16 sensors.
start
stop
empty
Soil temperature [°C]
Sensor Depth (cm)
0
-5
-10
-15
-20
-25
-30
-35
-45
-55
-65
-75
-85
-95
-105
-115
Jun-24 00:00
Jun-25 00:00
Jun-26 00:00
Jun-27 00:00
Jun-28 00:00
Jun-29 00:00
Jun-30 00:00
Jul-01 00:00
Temp °C
Depth [cm]

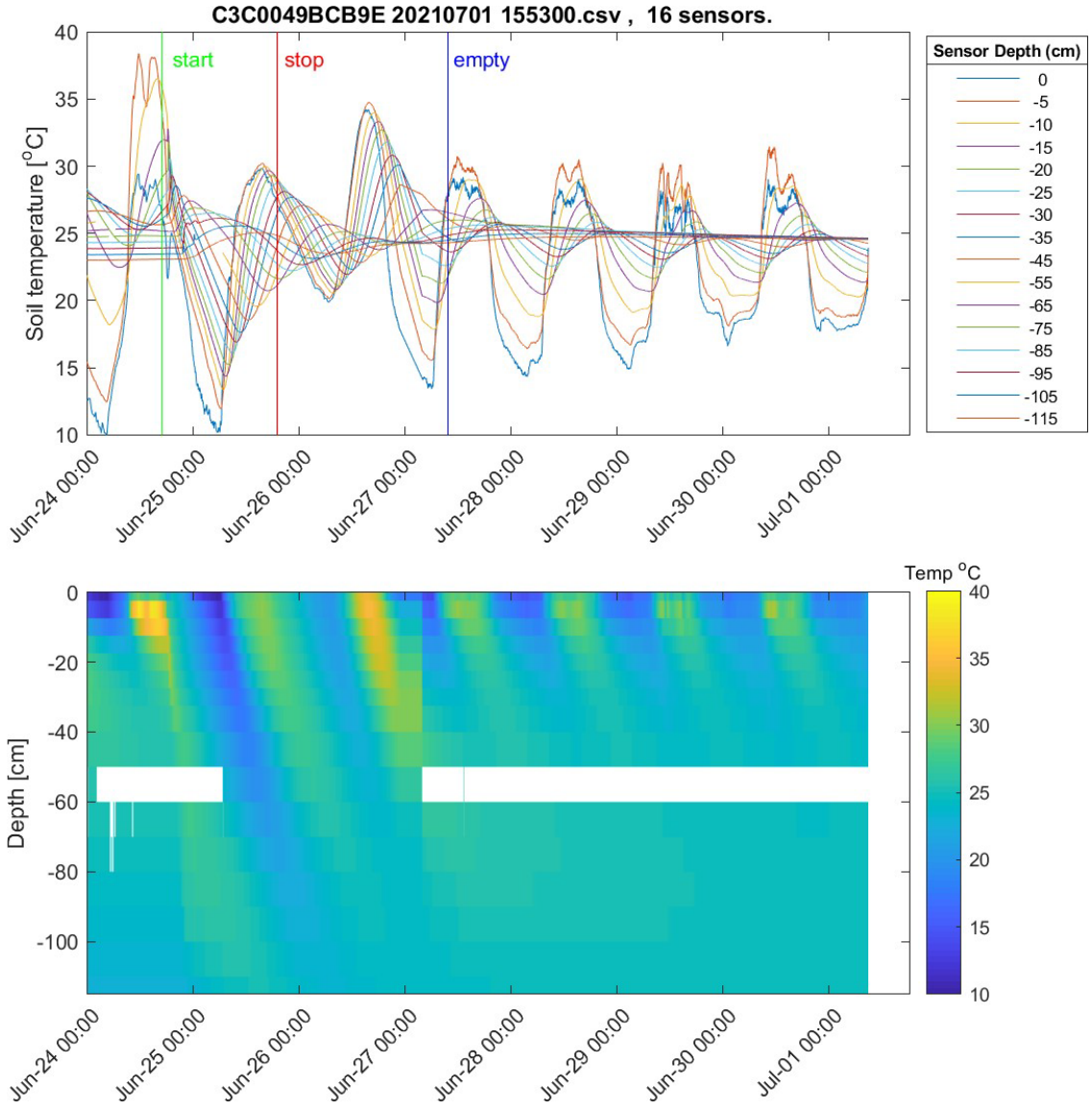
C3C0049BCB9E 20210701 155300.csv , 16 sensors.
start
stop
empty
Soil temperature [°C]
Sensor Depth (cm)
0
-5
-10
-15
-20
-25
-30
-35
-45
-55
-65
-75
-85
-95
-105
-115
Jun-24 00:00
Jun-25 00:00
Jun-26 00:00
Jun-27 00:00
Jun-28 00:00
Jun-29 00:00
Jun-30 00:00
Jul-01 00:00
Depth [cm]
Temp °C

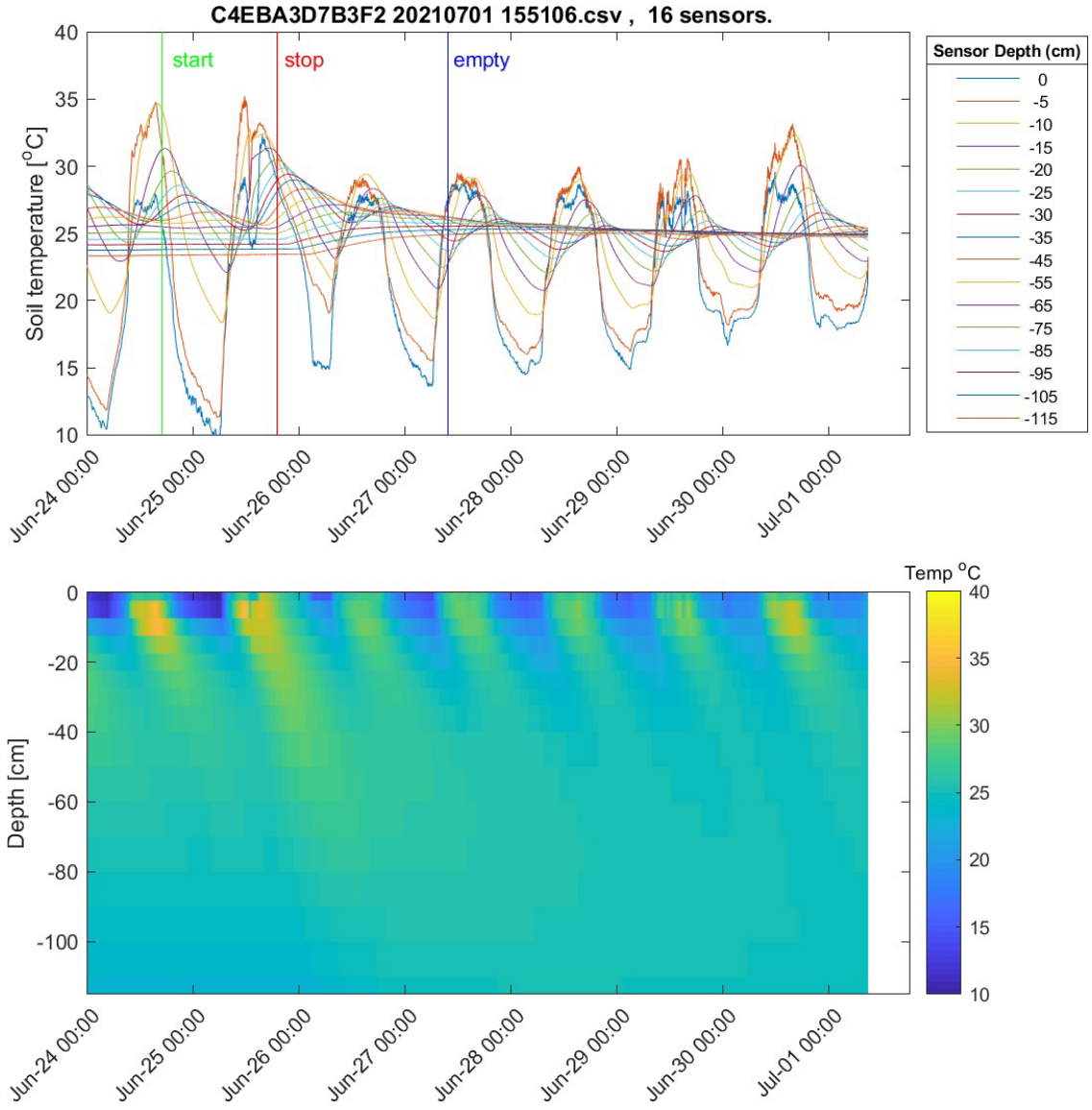
C4EBA3D7B3F2 20210701 155106.csv , 16 sensors.
start
stop
empty
Soil temperature [°C]
Sensor Depth (cm)
0
-5
-10
-15
-20
-25
-30
-35
-45
-55
-65
-75
-85
-95
-105
-115
Jun-24 00:00
Jun-25 00:00
Jun-26 00:00
Jun-27 00:00
Jun-28 00:00
Jun-29 00:00
Jun-30 00:00
Jul-01 00:00
Depth [cm]
Temp °C

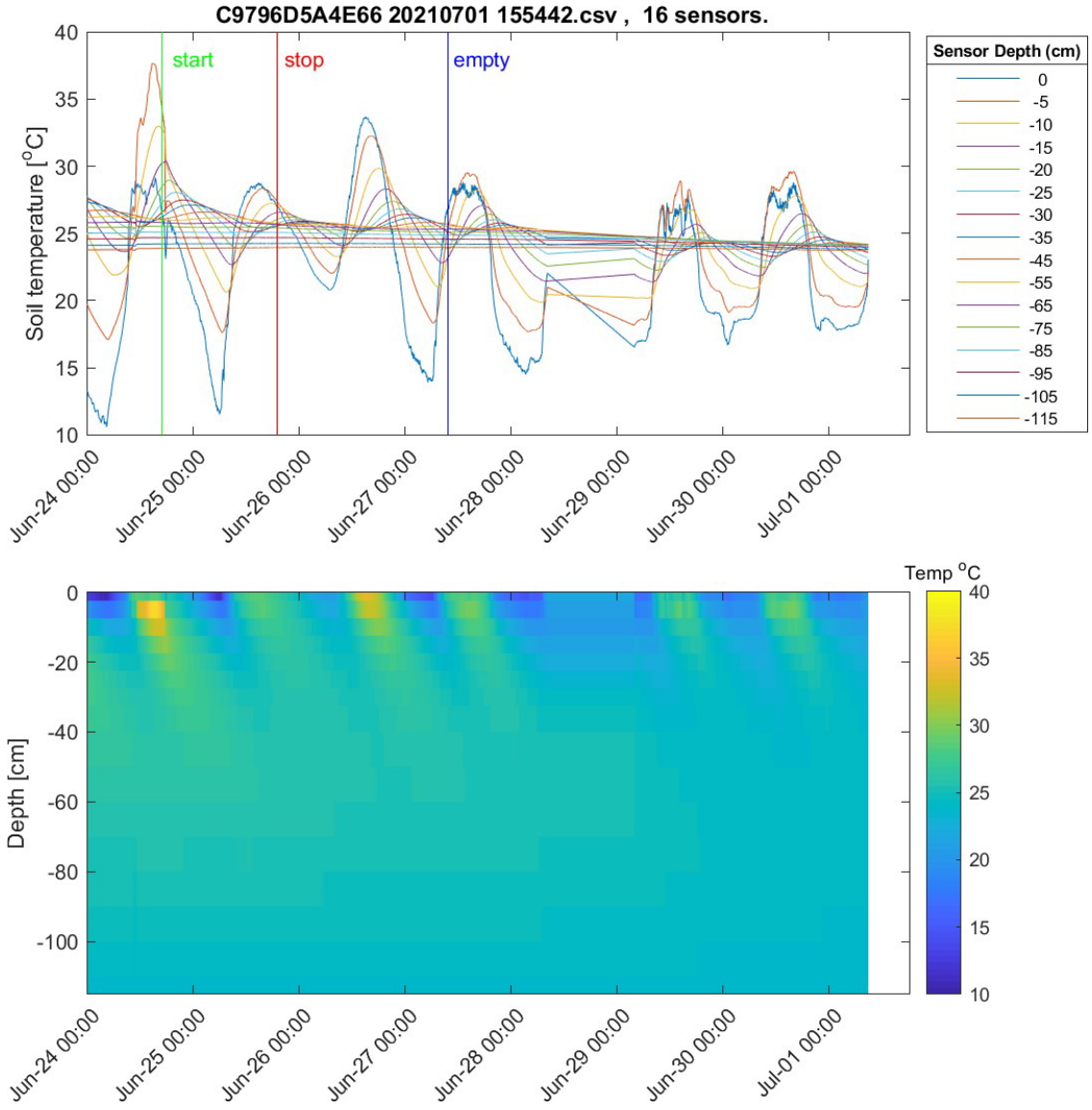
C9796D5A4E66 20210701 155442.csv , 16 sensors.
start
stop
empty
Soil temperature [°C]
Sensor Depth (cm)
0
-5
-10
-15
-20
-25
-30
-35
-45
-55
-65
-75
-85
-95
-105
-115
Jun-24 00:00
Jun-25 00:00
Jun-26 00:00
Jun-27 00:00
Jun-28 00:00
Jun-29 00:00
Jun-30 00:00
Jul-01 00:00
Temp °C
Depth [cm]

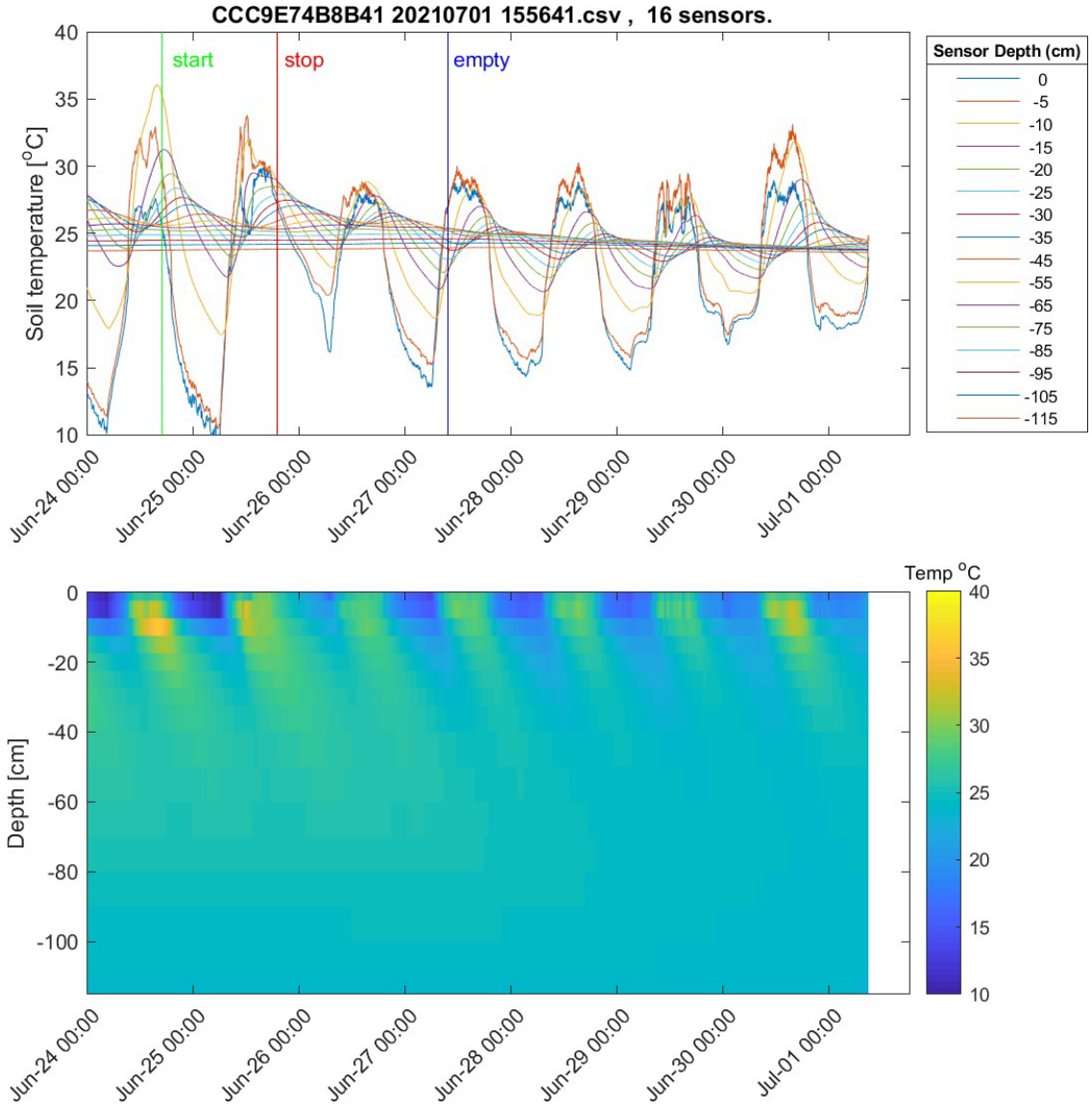
CCC9E74B8B41 20210701 155641.csv , 16 sensors.
start
stop
empty
Soil temperature [°C]
Sensor Depth (cm)
0
-5
-10
-15
-20
-25
-30
-35
-45
-55
-65
-75
-85
-95
-105
-115
Jun-24 00:00
Jun-25 00:00
Jun-26 00:00
Jun-27 00:00
Jun-28 00:00
Jun-29 00:00
Jun-30 00:00
Jul-01 00:00
Temp °C
Depth [cm]

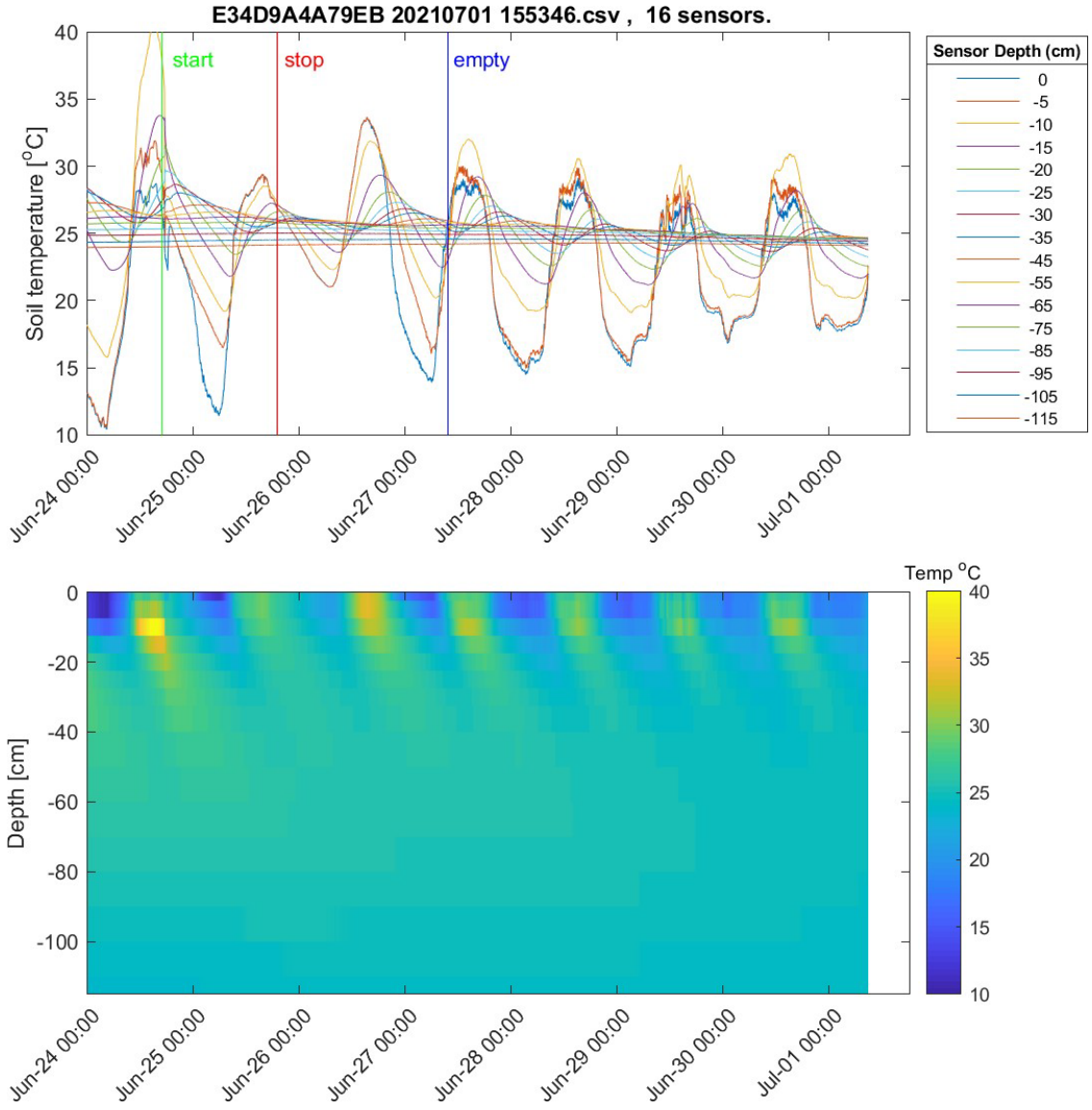
E34D9A4A79EB 20210701 155346.csv , 16 sensors.
start
stop
empty
Soil temperature [°C]
Sensor Depth (cm)
0
-5
-10
-15
-20
-25
-30
-35
-45
-55
-65
-75
-85
-95
-105
-115
Jun-24 00:00
Jun-25 00:00
Jun-26 00:00
Jun-27 00:00
Jun-28 00:00
Jun-29 00:00
Jun-30 00:00
Jul-01 00:00
Temp °C
Depth [cm]

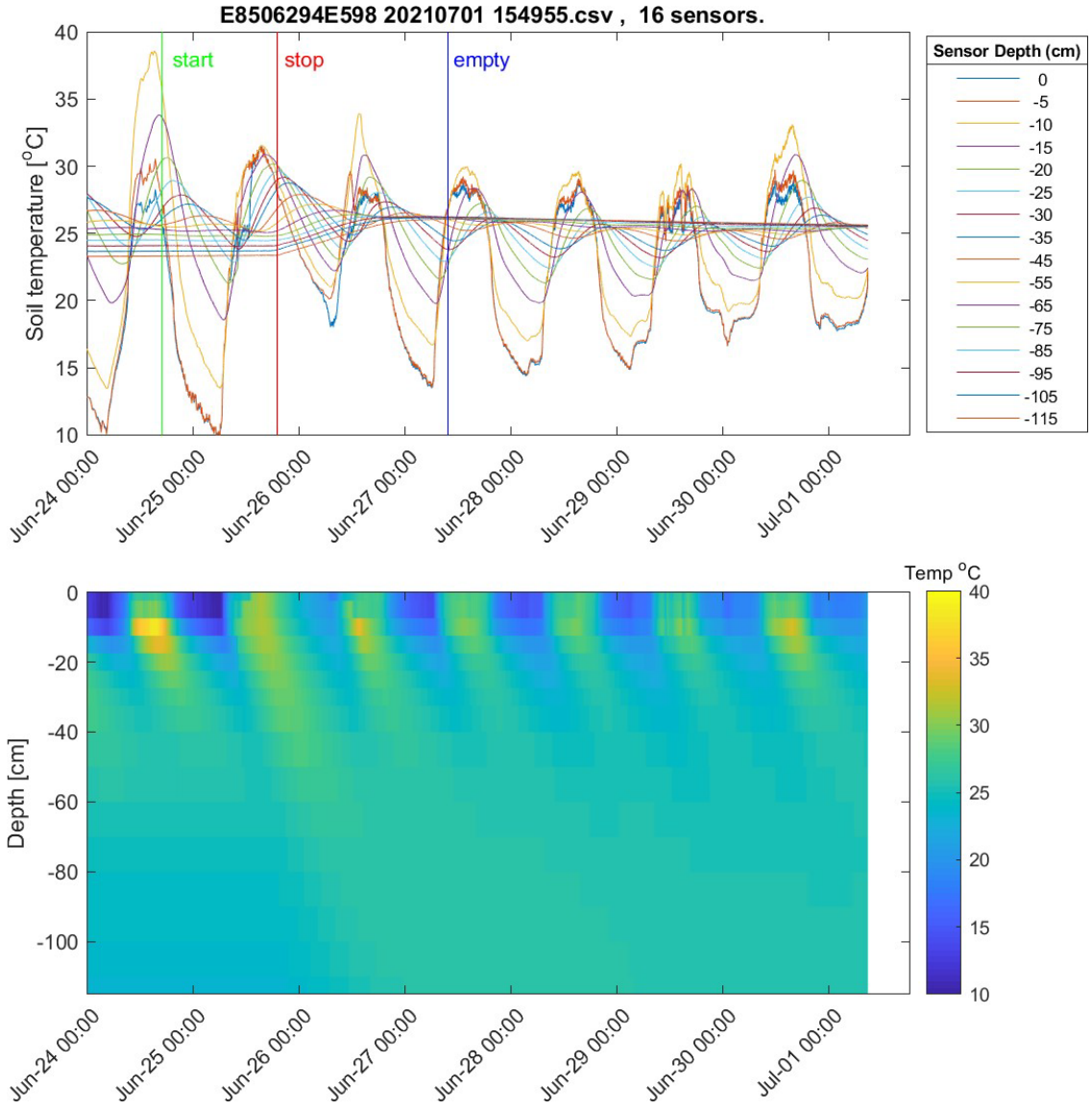
E8506294E598 20210701 154955.csv , 16 sensors.
start
stop
empty
Soil temperature [°C]
Sensor Depth (cm)
0
-5
-10
-15
-20
-25
-30
-35
-45
-55
-65
-75
-85
-95
-105
-115
Jun-24 00:00
Jun-25 00:00
Jun-26 00:00
Jun-27 00:00
Jun-28 00:00
Jun-29 00:00
Jun-30 00:00
Jul-01 00:00
Temp °C
Depth [cm]

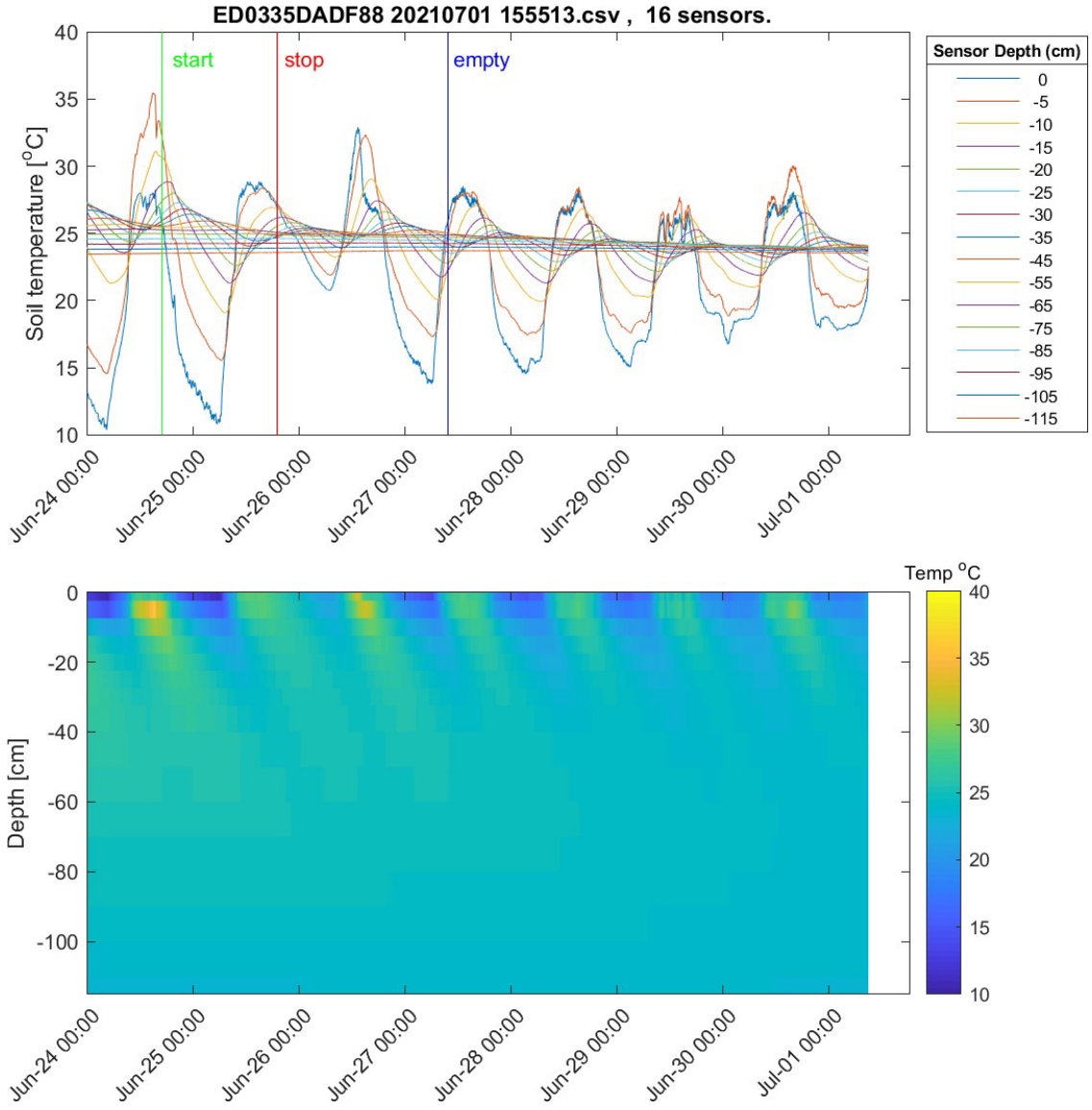
ED0335DADF88 20210701 155513.csv , 16 sensors.
start
stop
empty
Soil temperature [°C]
Sensor Depth (cm)
0
-5
-10
-15
-20
-25
-30
-35
-45
-55
-65
-75
-85
-95
-105
-115
Jun-24 00:00
Jun-25 00:00
Jun-26 00:00
Jun-27 00:00
Jun-28 00:00
Jun-29 00:00
Jun-30 00:00
Jul-01 00:00
Temp °C
Depth [cm]

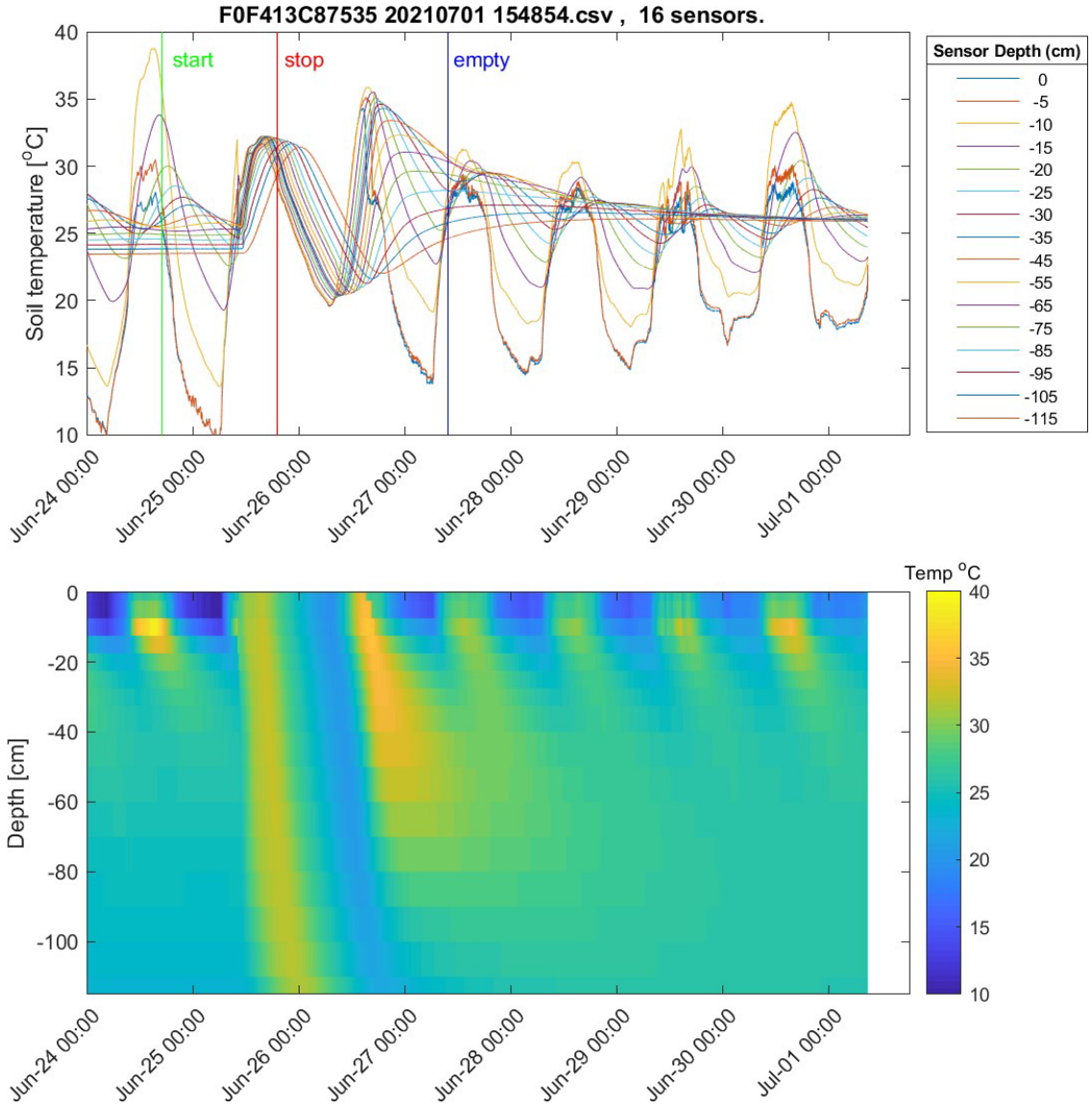
F0F413C87535 20210701 154854.csv , 16 sensors.
start
stop
empty
Soil temperature [°C]
Sensor Depth (cm)
0
-5
-10
-15
-20
-25
-30
-35
-45
-55
-65
-75
-85
-95
-105
-115
Jun-24 00:00
Jun-25 00:00
Jun-26 00:00
Jun-27 00:00
Jun-28 00:00
Jun-29 00:00
Jun-30 00:00
Jul-01 00:00
Temp °C
Depth [cm]

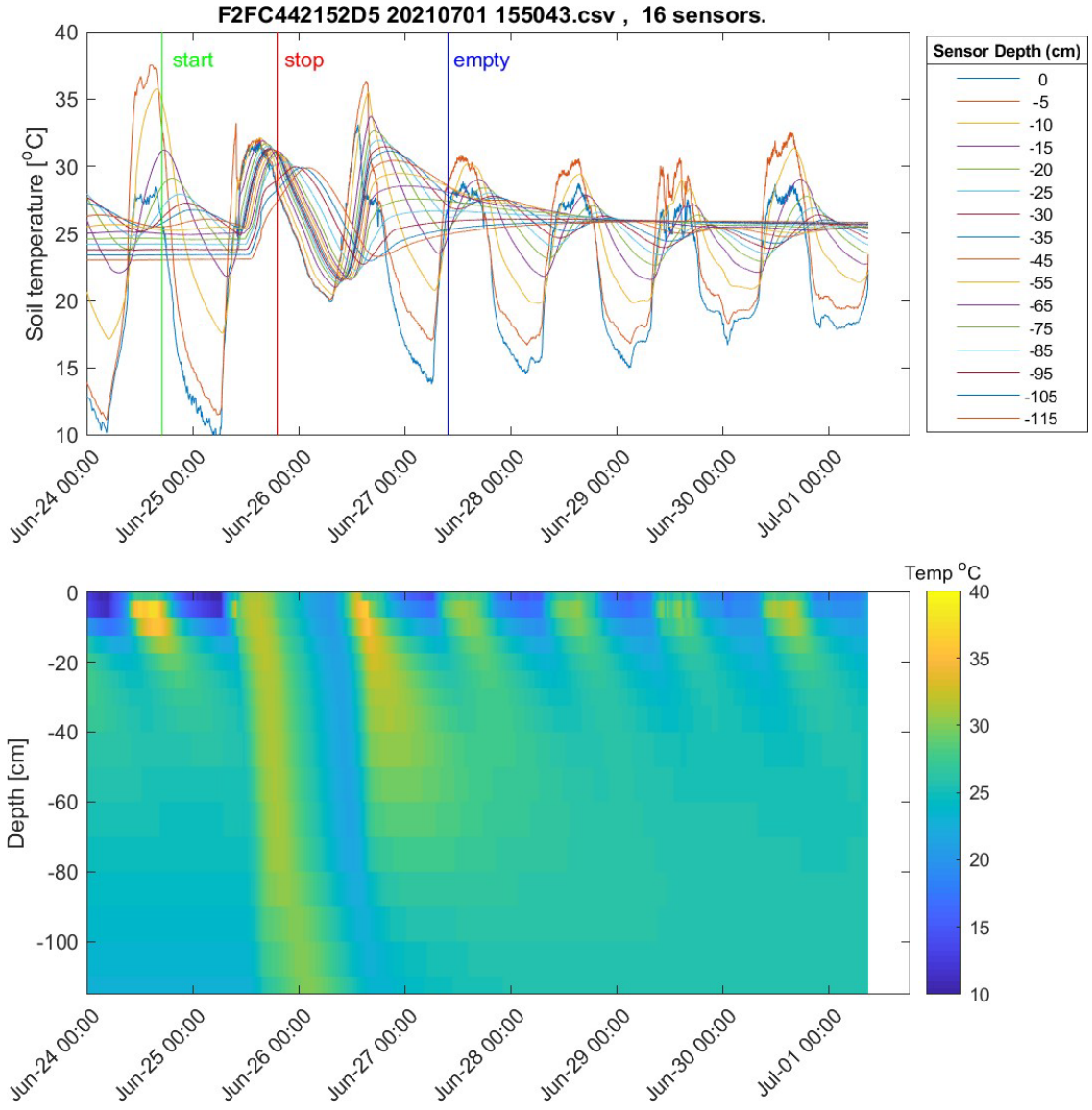
F2FC442152D5 20210701 155043.csv , 16 sensors.
start
stop
empty
Soil temperature [°C]
Sensor Depth (cm)
0
-5
-10
-15
-20
-25
-30
-35
-45
-55
-65
-75
-85
-95
-105
-115
Jun-24 00:00
Jun-25 00:00
Jun-26 00:00
Jun-27 00:00
Jun-28 00:00
Jun-29 00:00
Jun-30 00:00
Jul-01 00:00
Temp °C
Depth [cm]

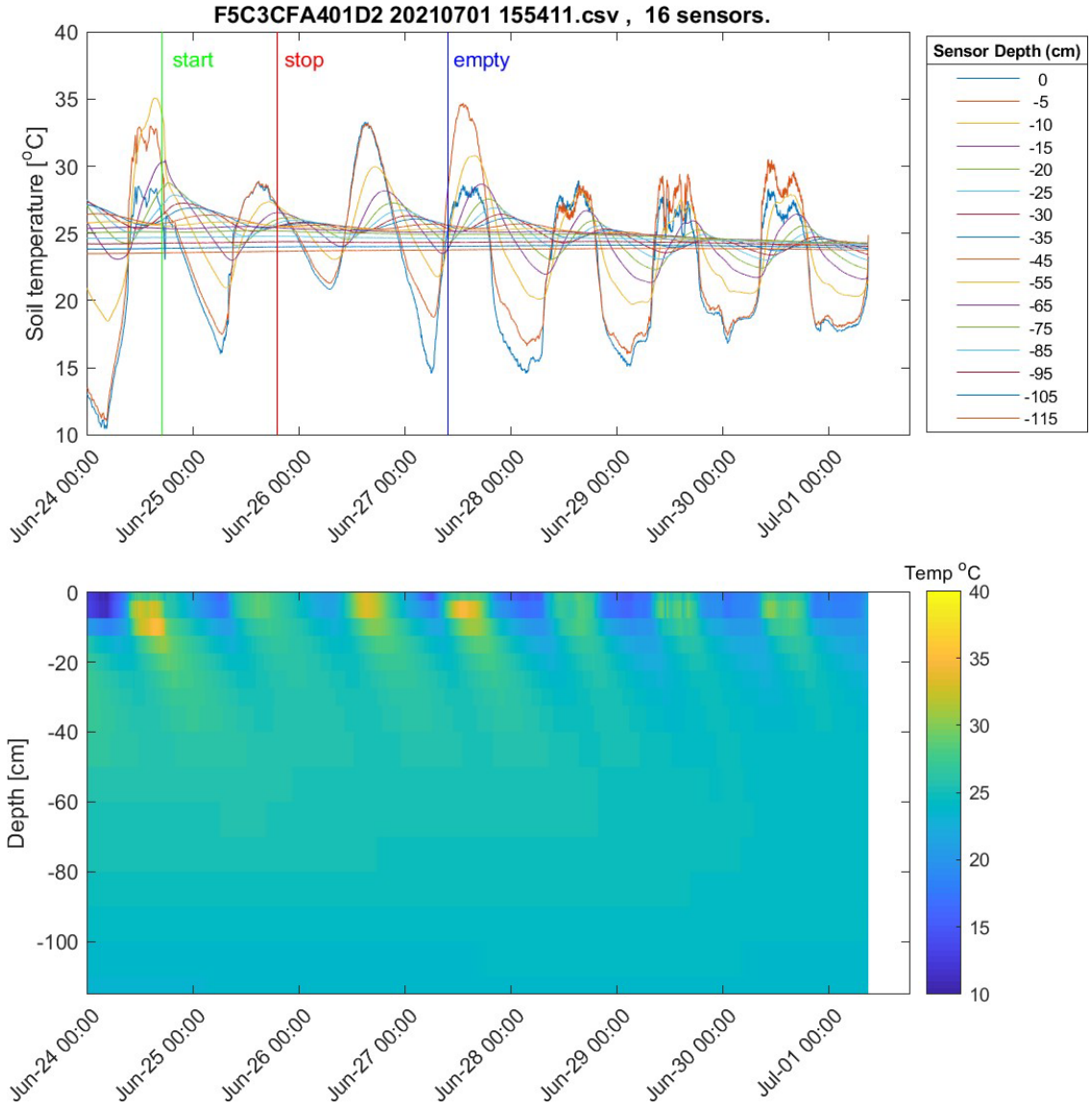
F5C3CFA401D2 20210701 155411.csv , 16 sensors.
start
stop
empty
Soil temperature [°C]
Sensor Depth (cm)
0
-5
-10
-15
-20
-25
-30
-35
-45
-55
-65
-75
-85
-95
-105
-115
Jun-24 00:00
Jun-25 00:00
Jun-26 00:00
Jun-27 00:00
Jun-28 00:00
Jun-29 00:00
Jun-30 00:00
Jul-01 00:00
Depth [cm]
Temp °C

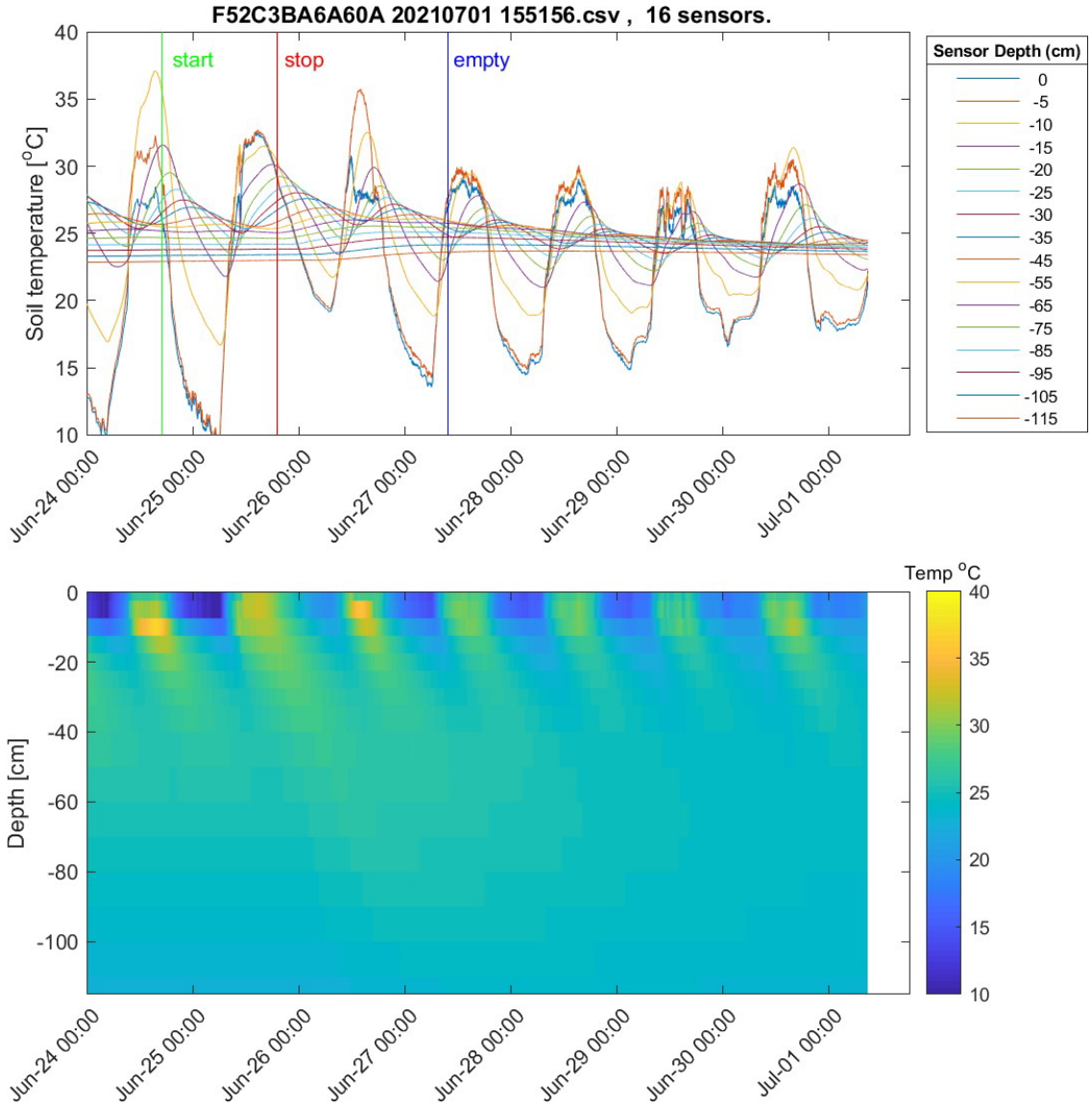
F52C3BA6A60A 20210701 155156.csv , 16 sensors.
start
stop
empty
Soil temperature [°C]
Sensor Depth (cm)
0
-5
-10
-15
-20
-25
-30
-35
-45
-55
-65
-75
-85
-95
-105
-115
Jun-24 00:00
Jun-25 00:00
Jun-26 00:00
Jun-27 00:00
Jun-28 00:00
Jun-29 00:00
Jun-30 00:00
Jul-01 00:00
Temp °C
Depth [cm]

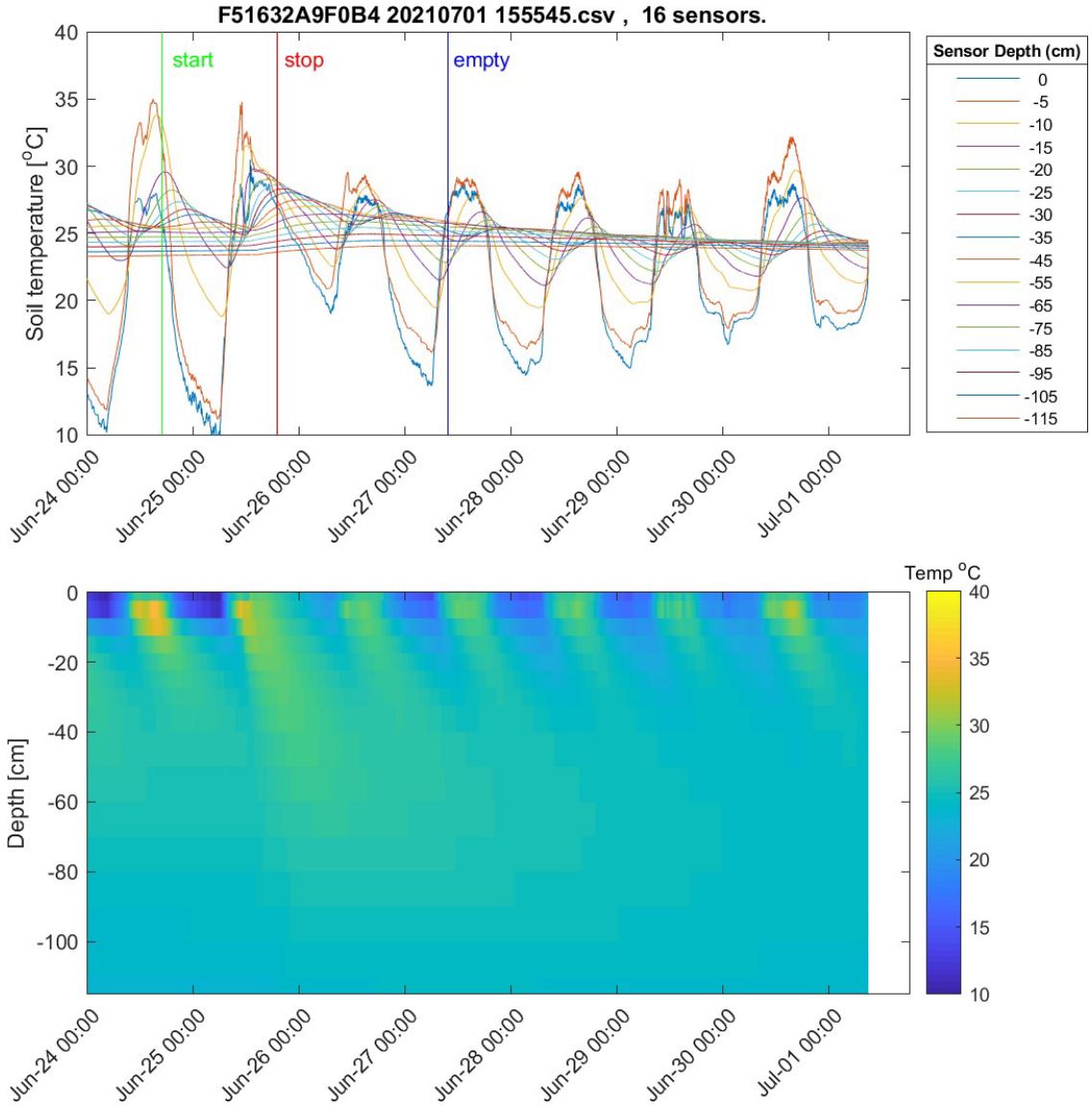
F51632A9F0B4 20210701 155545.csv , 16 sensors.
start
stop
empty
Soil temperature [°C]
Sensor Depth (cm)
0
-5
-10
-15
-20
-25
-30
-35
-45
-55
-65
-75
-85
-95
-105
-115
Jun-24 00:00
Jun-25 00:00
Jun-26 00:00
Jun-27 00:00
Jun-28 00:00
Jun-29 00:00
Jun-30 00:00
Jul-01 00:00
Temp °C
Depth [cm]

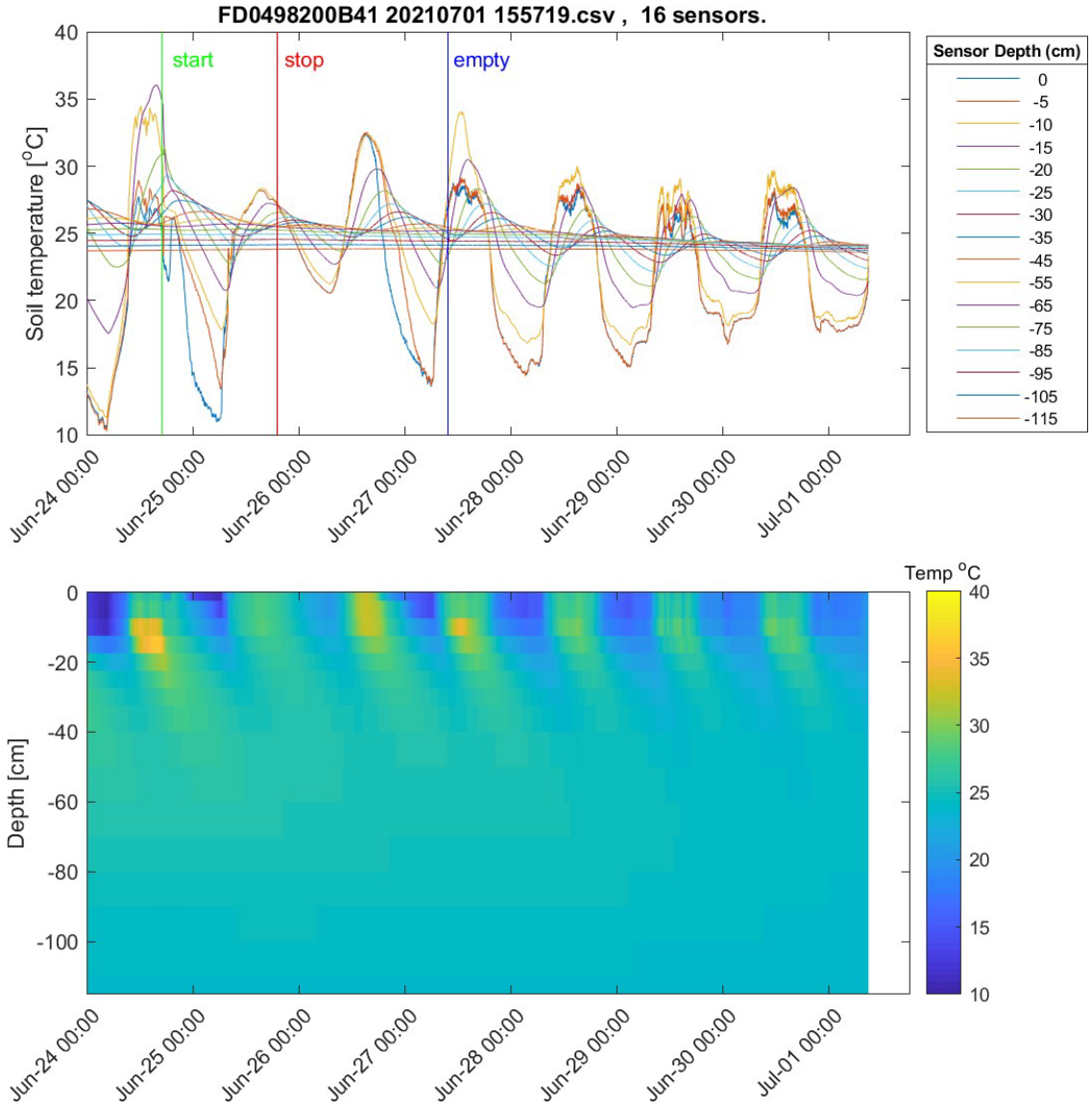
FD0498200B41 20210701 155719.csv , 16 sensors.
start
stop
empty
Soil temperature [°C]
Sensor Depth (cm)
0
-5
-10
-15
-20
-25
-30
-35
-45
-55
-65
-75
-85
-95
-105
-115
Jun-24 00:00
Jun-25 00:00
Jun-26 00:00
Jun-27 00:00
Jun-28 00:00
Jun-29 00:00
Jun-30 00:00
Jul-01 00:00
Temp °C
Depth [cm]

Recharge Phase DTP
Pond 10

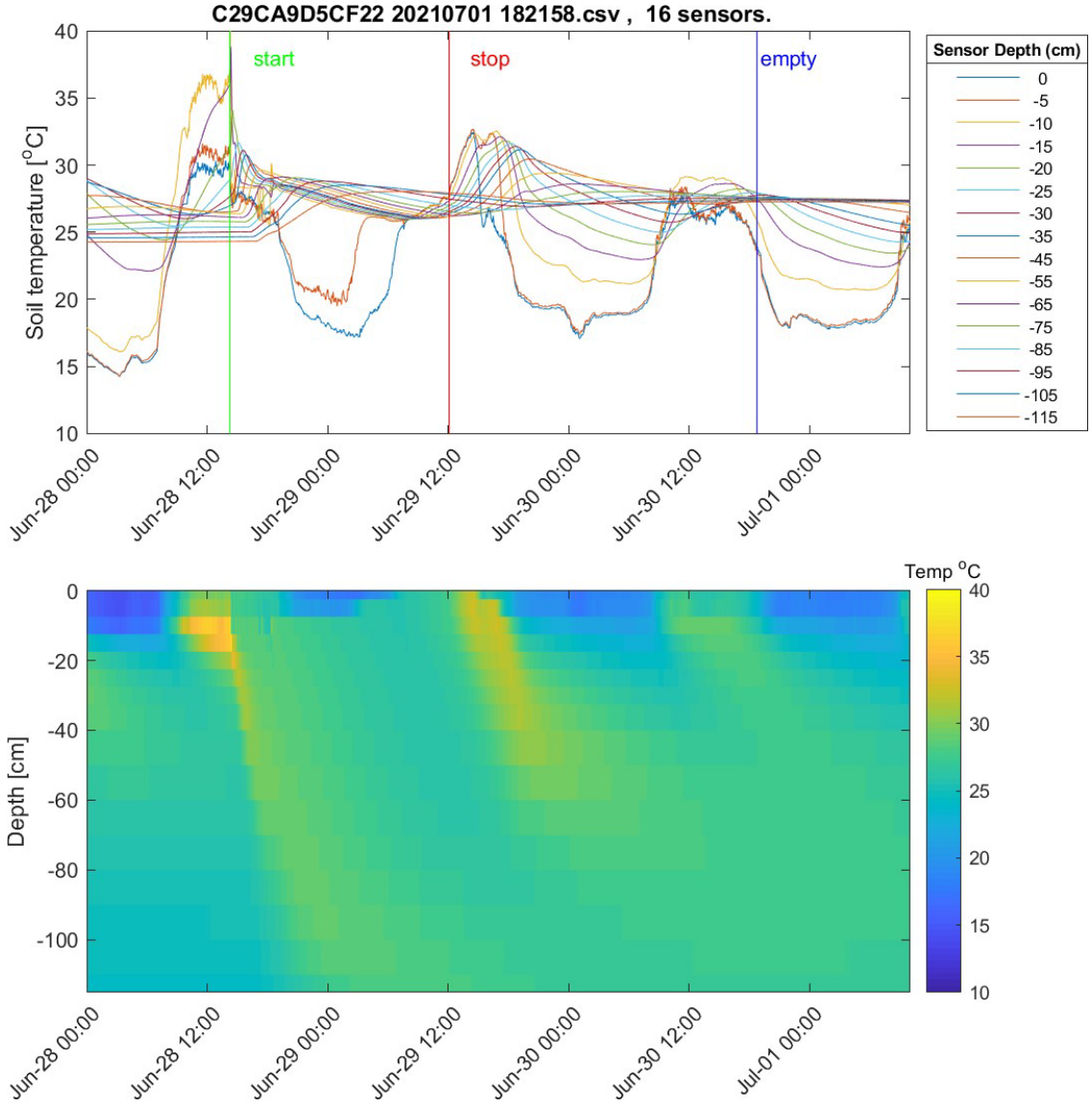
C29CA9D5CF22 20210701 182158.csv , 16 sensors.
start
stop
empty
Soil temperature [°C]
Sensor Depth (cm)
0
-5
-10
-15
-20
-25
-30
-35
-45
-55
-65
-75
-85
-95
-105
-115
Jun-28 00:00
Jun-28 12:00
Jun-29 00:00
Jun-29 12:00
Jun-30 00:00
Jun-30 12:00
Jul-01 00:00
Depth [cm]
Temp °C

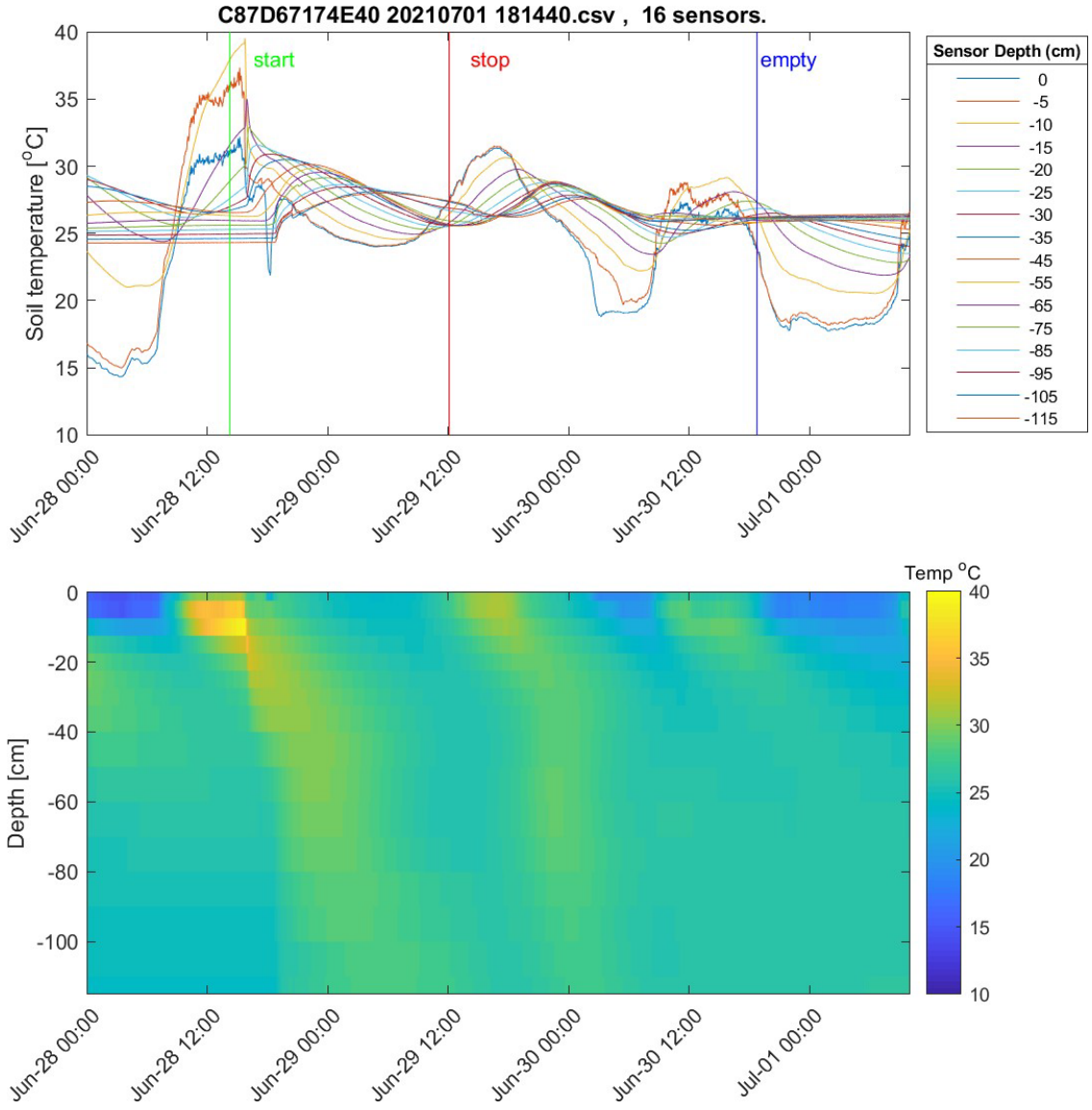
C87D67174E40 20210701 181440.csv , 16 sensors.
start
stop
empty
Soil temperature [°C]
Sensor Depth (cm)
0
-5
-10
-15
-20
-25
-30
-35
-45
-55
-65
-75
-85
-95
-105
-115
Jun-28 00:00
Jun-28 12:00
Jun-29 00:00
Jun-29 12:00
Jun-30 00:00
Jun-30 12:00
Jul-01 00:00
Temp °C
Depth [cm]

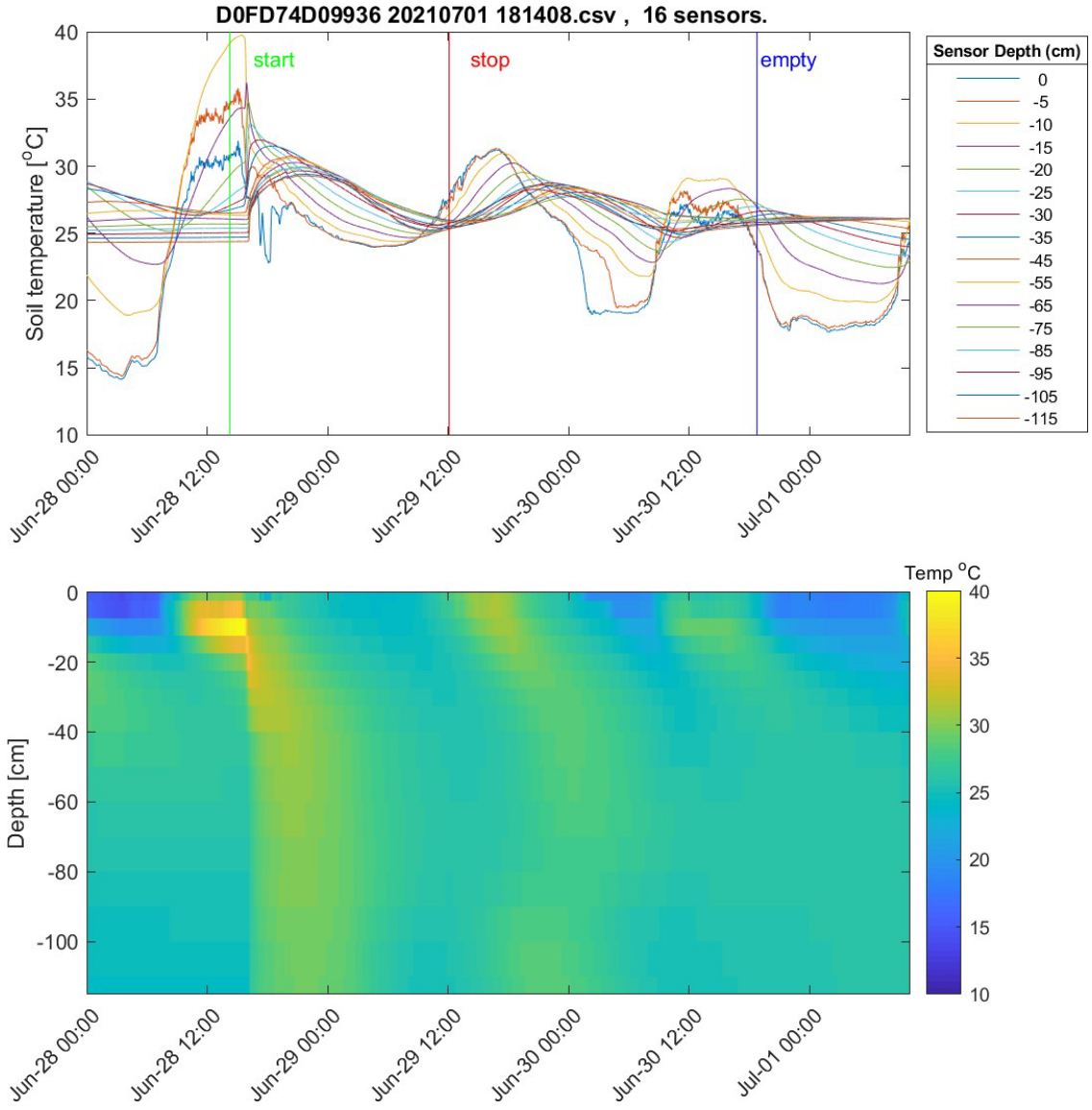
D0FD74D09936 20210701 181408.csv , 16 sensors.
start
stop
empty
Soil temperature [°C]
Sensor Depth (cm)
0
-5
-10
-15
-20
-25
-30
-35
-45
-55
-65
-75
-85
-95
-105
-115
Jun-28 00:00
Jun-28 12:00
Jun-29 00:00
Jun-29 12:00
Jun-30 00:00
Jun-30 12:00
Jul-01 00:00
Temp °C
Depth [cm]

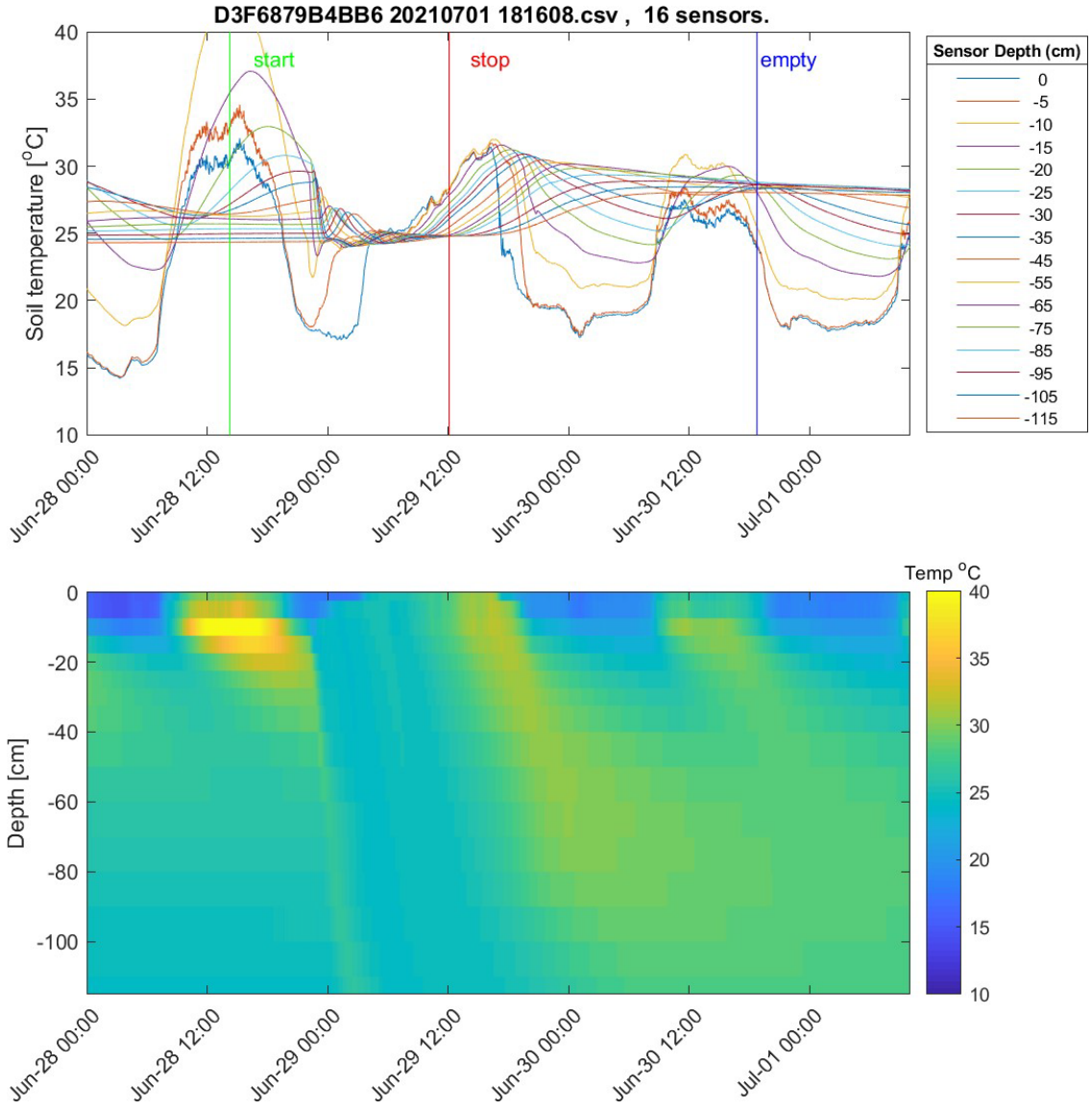
D3F6879B4BB6 20210701 181608.csv , 16 sensors.
start
stop
empty
Soil temperature [°C]
Sensor Depth (cm)
0
-5
-10
-15
-20
-25
-30
-35
-45
-55
-65
-75
-85
-95
-105
-115
Jun-28 00:00
Jun-28 12:00
Jun-29 00:00
Jun-29 12:00
Jun-30 00:00
Jun-30 12:00
Jul-01 00:00
Temp °C
Depth [cm]

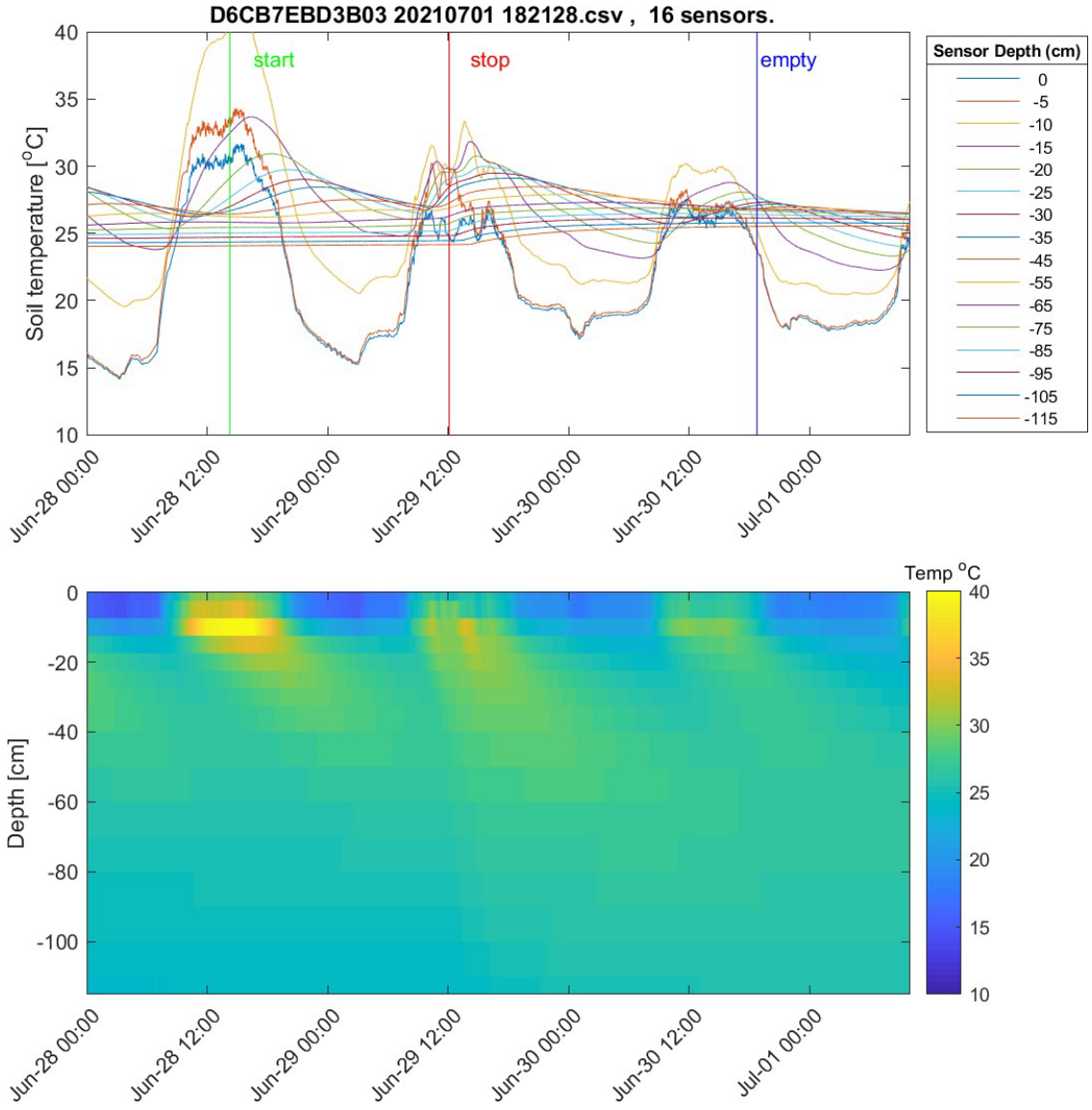
D6CB7EBD3B03 20210701 182128.csv , 16 sensors.
Soil temperature [°C]
start
stop
empty
Sensor Depth (cm)
0
-5
-10
-15
-20
-25
-30
-35
-45
-55
-65
-75
-85
-95
-105
-115
Jun-28 00:00
Jun-28 12:00
Jun-29 00:00
Jun-29 12:00
Jun-30 00:00
Jun-30 12:00
Jul-01 00:00
Temp °C
Depth [cm]

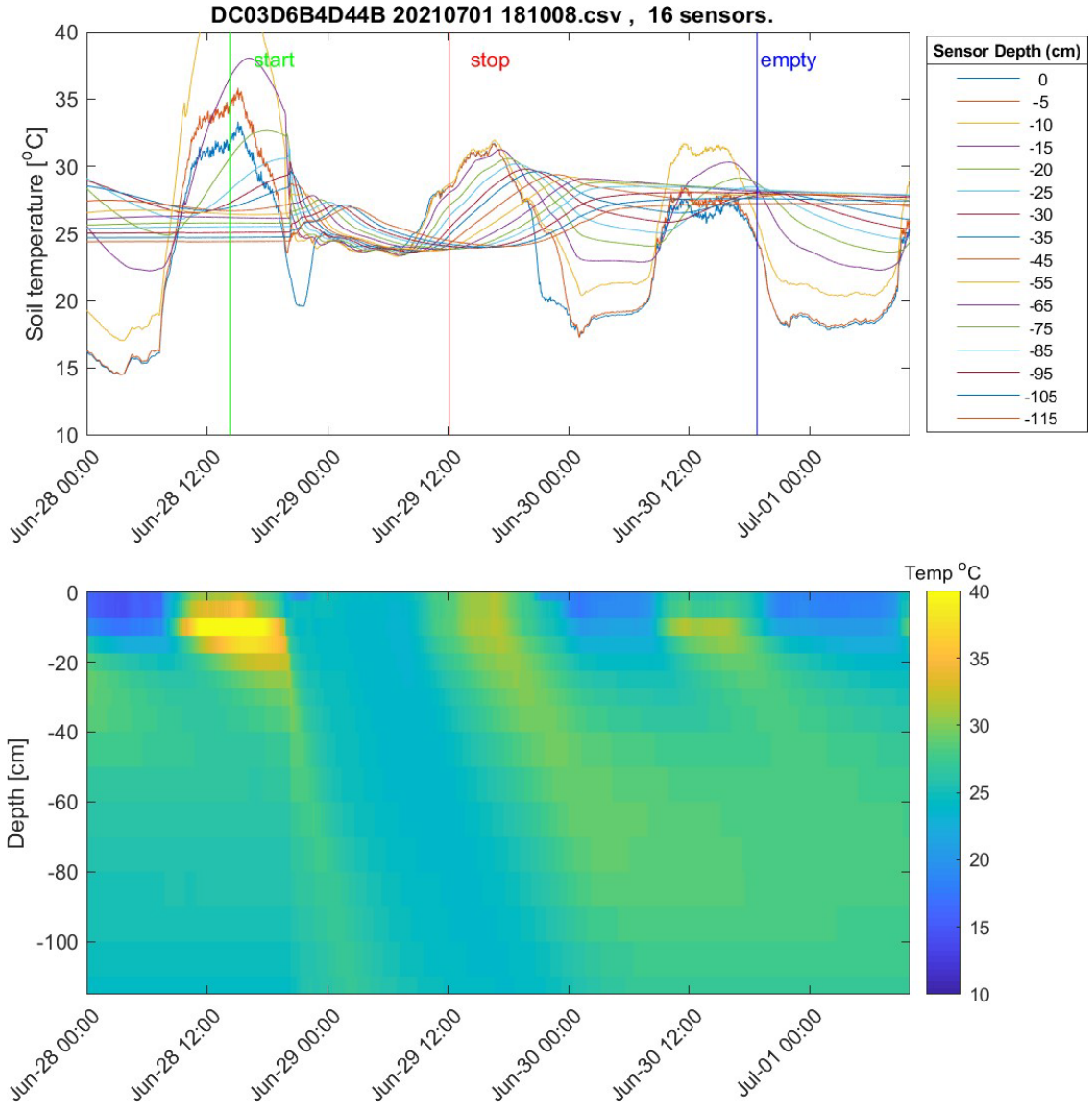
DC03D6B4D44B 20210701 181008.csv , 16 sensors.
start
stop
empty
Soil temperature [°C]
Sensor Depth (cm)
0
-5
-10
-15
-20
-25
-30
-35
-45
-55
-65
-75
-85
-95
-105
-115
Jun-28 00:00
Jun-28 12:00
Jun-29 00:00
Jun-29 12:00
Jun-30 00:00
Jun-30 12:00
Jul-01 00:00
Temp °C
Depth [cm]

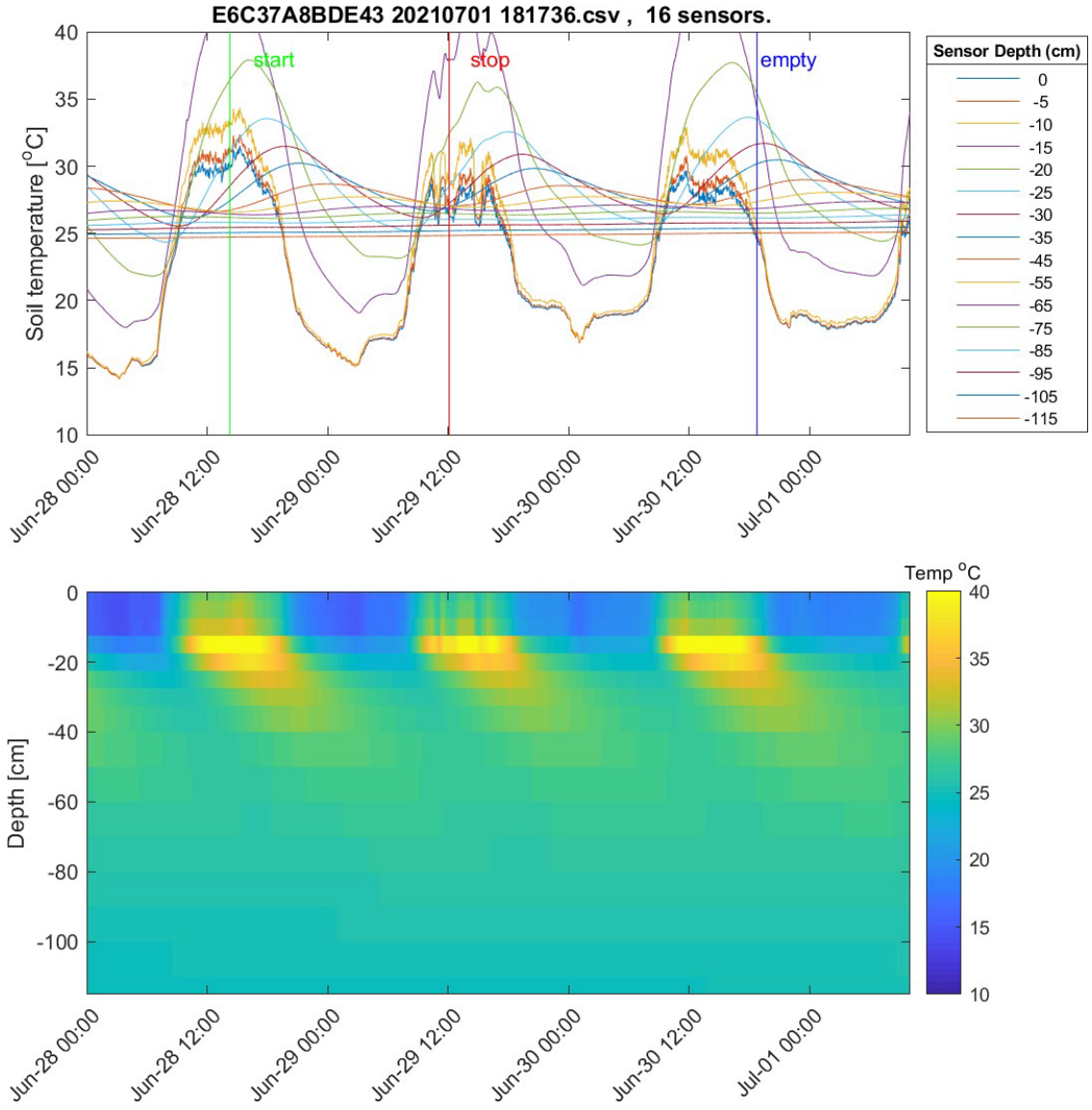
E6C37A8BDE43 20210701 181736.csv , 16 sensors.
start
stop
empty
Soil temperature [°C]
Sensor Depth (cm)
0
-5
-10
-15
-20
-25
-30
-35
-45
-55
-65
-75
-85
-95
-105
-115
Jun-28 00:00
Jun-28 12:00
Jun-29 00:00
Jun-29 12:00
Jun-30 00:00
Jun-30 12:00
Jul-01 00:00
Temp °C
Depth [cm]

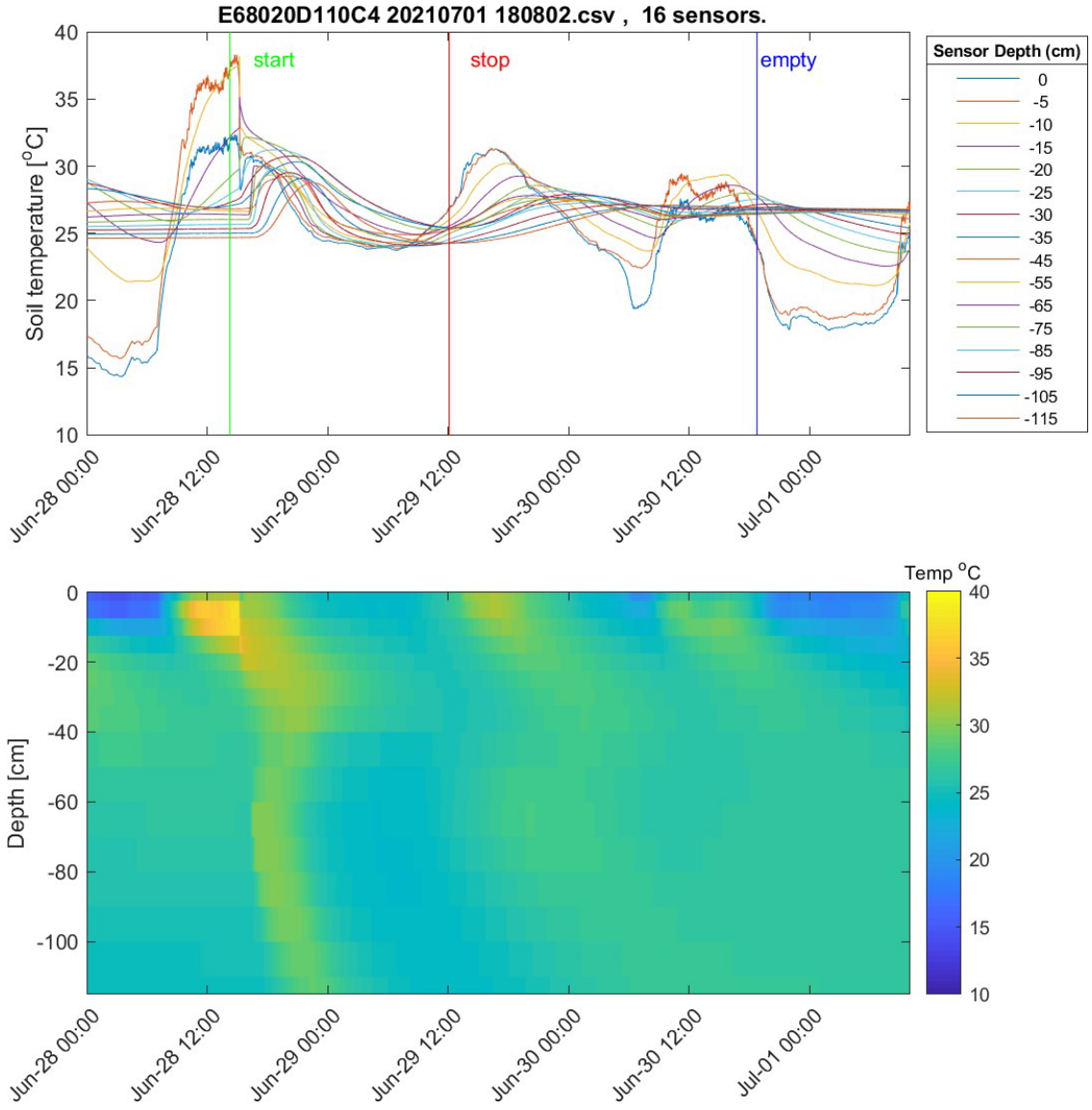
E68020D110C4 20210701 180802.csv , 16 sensors.
start
stop
empty
Soil temperature [°C]
Sensor Depth (cm)
0
-5
-10
-15
-20
-25
-30
-35
-45
-55
-65
-75
-85
-95
-105
-115
Jun-28 00:00
Jun-28 12:00
Jun-29 00:00
Jun-29 12:00
Jun-30 00:00
Jun-30 12:00
Jul-01 00:00
Temp °C
Depth [cm]

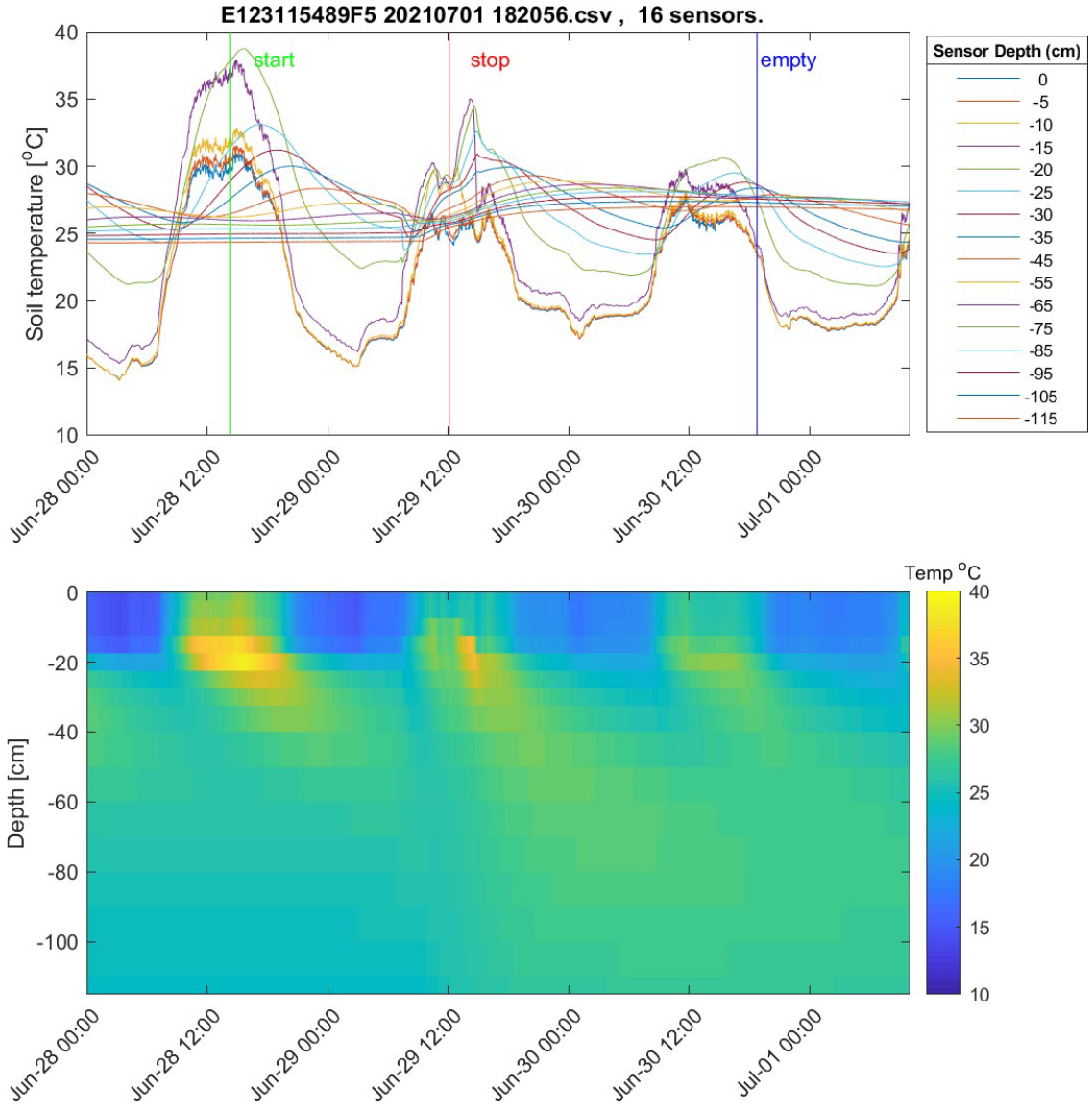
E123115489F5 20210701 182056.csv , 16 sensors.
start
stop
empty
Soil temperature [°C]
Sensor Depth (cm)
0
-5
-10
-15
-20
-25
-30
-35
-45
-55
-65
-75
-85
-95
-105
-115
Jun-28 00:00
Jun-28 12:00
Jun-29 00:00
Jun-29 12:00
Jun-30 00:00
Jun-30 12:00
Jul-01 00:00
Temp °C
Depth [cm]

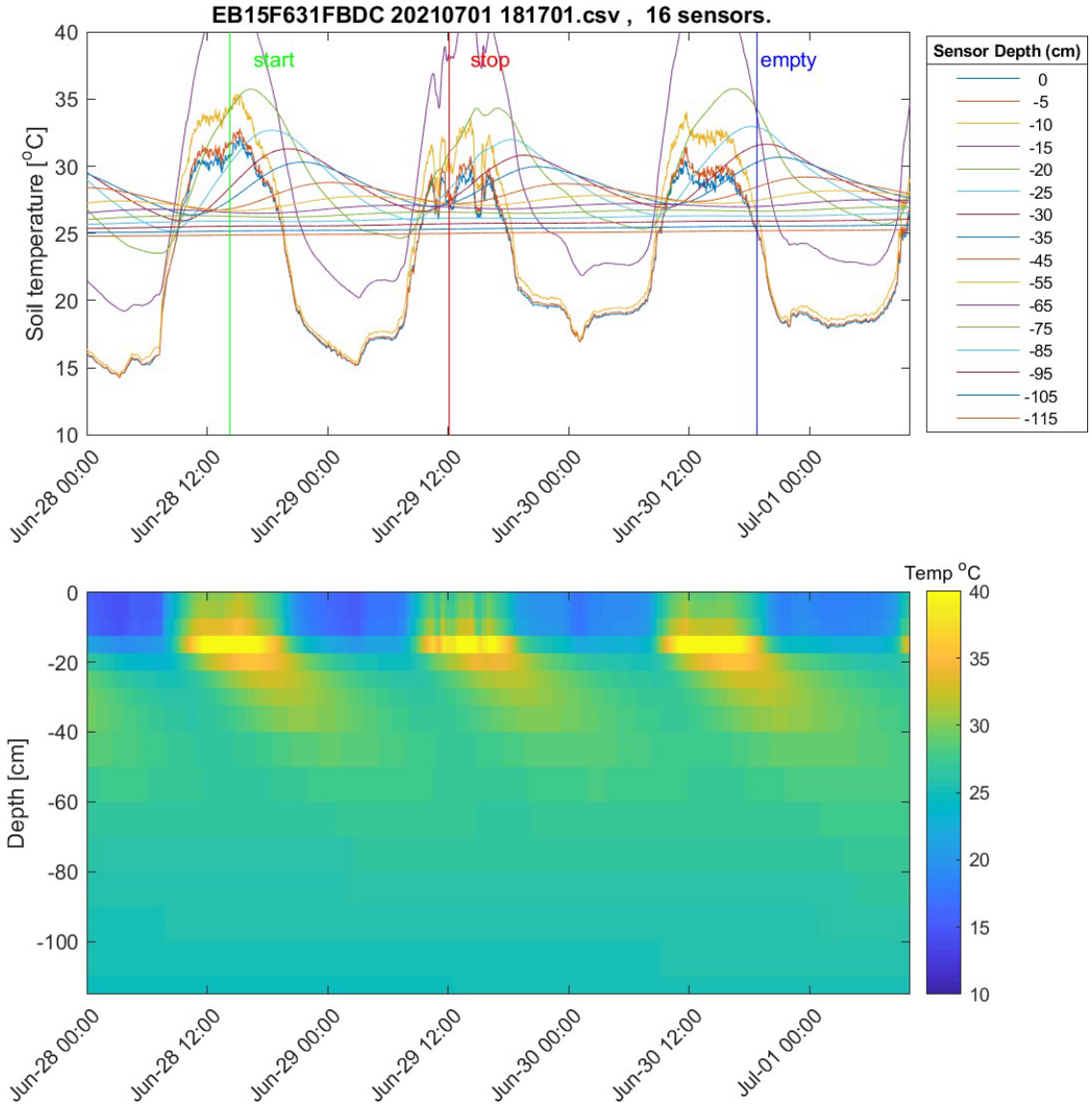
EB15F631FBDC 20210701 181701.csv , 16 sensors.
start
stop
empty
Soil temperature [°C]
Sensor Depth (cm)
0
-5
-10
-15
-20
-25
-30
-35
-45
-55
-65
-75
-85
-95
-105
-115
Jun-28 00:00
Jun-28 12:00
Jun-29 00:00
Jun-29 12:00
Jun-30 00:00
Jun-30 12:00
Jul-01 00:00
Temp °C
Depth [cm]

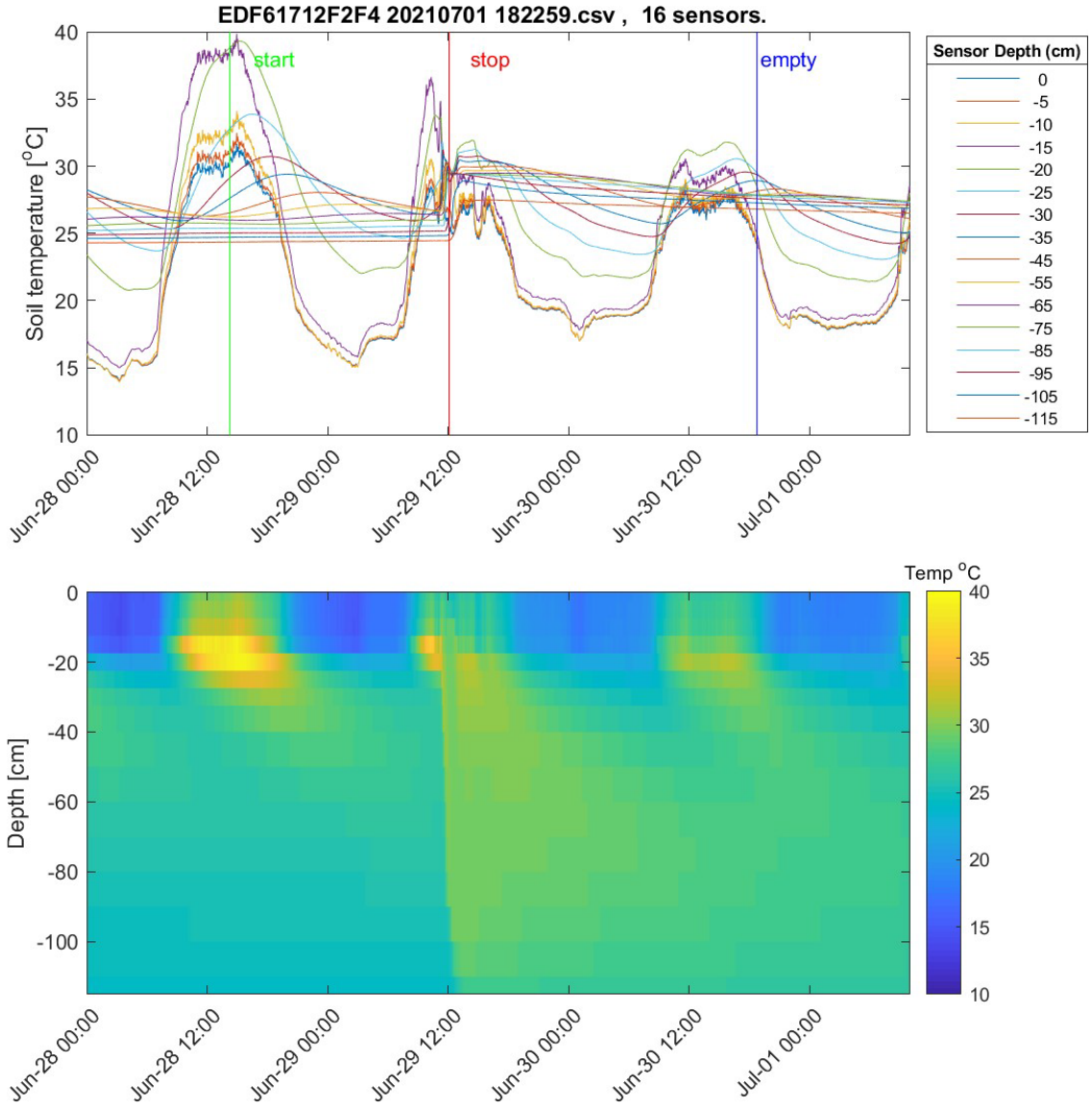
EDF61712F2F4 20210701 182259.csv , 16 sensors.
start
stop
empty
Soil temperature [°C]
Sensor Depth (cm)
0
-5
-10
-15
-20
-25
-30
-35
-45
-55
-65
-75
-85
-95
-105
-115
Jun-28 00:00
Jun-28 12:00
Jun-29 00:00
Jun-29 12:00
Jun-30 00:00
Jun-30 12:00
Jul-01 00:00
Temp °C
Depth [cm]

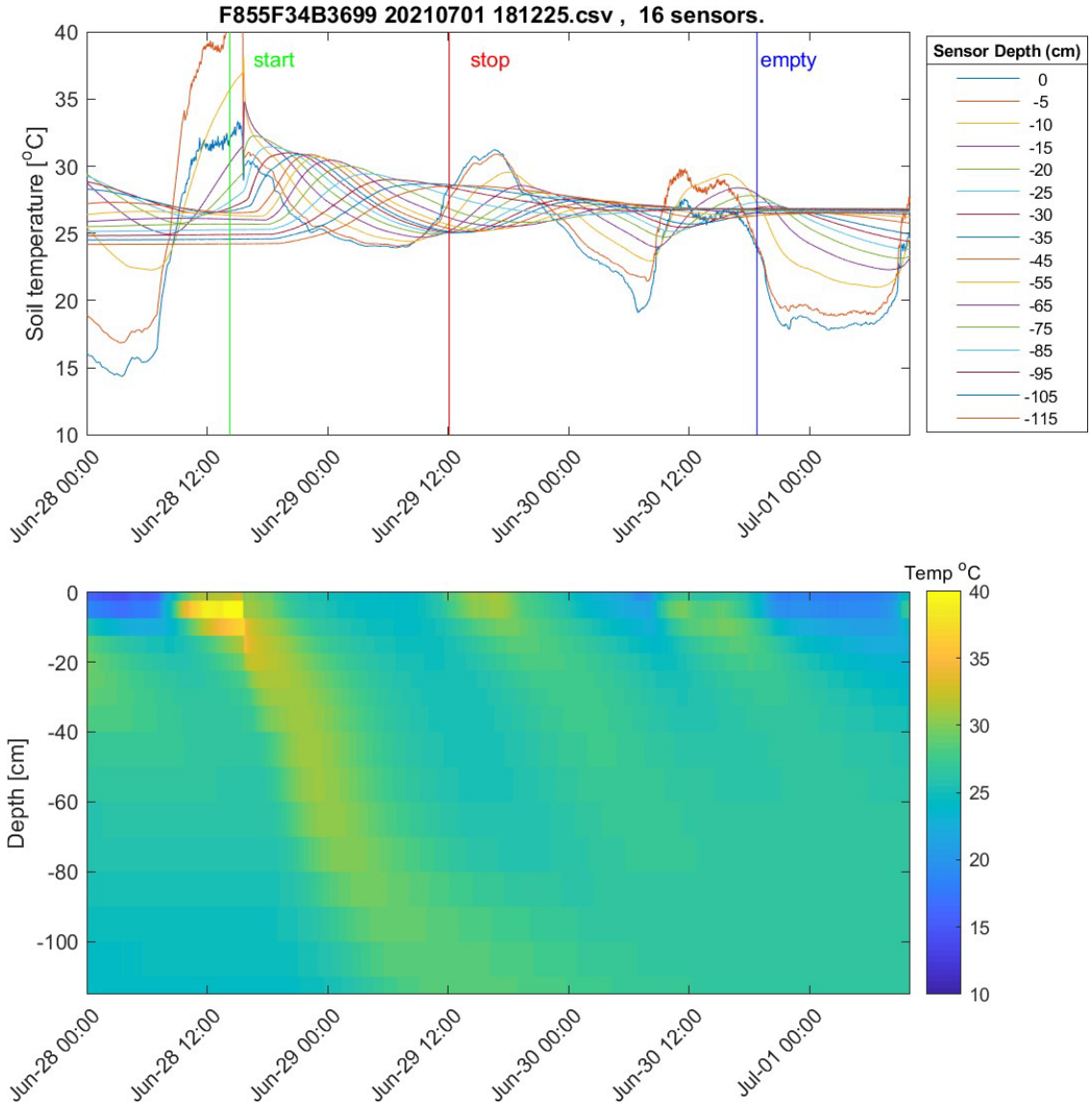
F855F34B3699 20210701 181225.csv , 16 sensors.
start
stop
empty
Soil temperature [°C]
Sensor Depth (cm)
0
-5
-10
-15
-20
-25
-30
-35
-45
-55
-65
-75
-85
-95
-105
-115
Jun-28 00:00
Jun-28 12:00
Jun-29 00:00
Jun-29 12:00
Jun-30 00:00
Jun-30 12:00
Jul-01 00:00
Temp °C
Depth [cm]

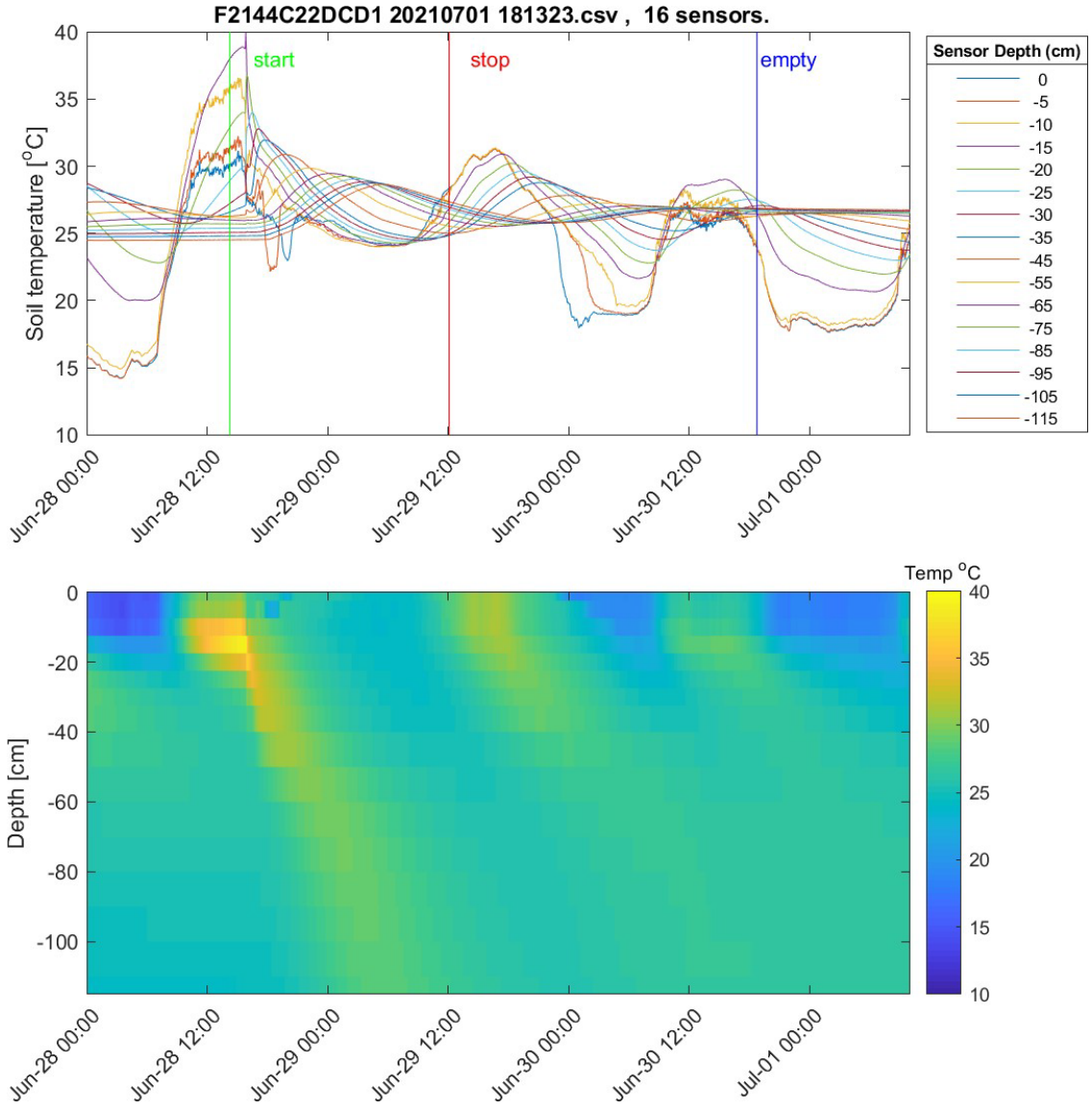
F2144C22DCD1 20210701 181323.csv , 16 sensors.
Soil temperature [°C]
start
stop
empty
Sensor Depth (cm)
0
-5
-10
-15
-20
-25
-30
-35
-45
-55
-65
-75
-85
-95
-105
-115
Jun-28 00:00
Jun-28 12:00
Jun-29 00:00
Jun-29 12:00
Jun-30 00:00
Jun-30 12:00
Jul-01 00:00
Temp °C
Depth [cm]

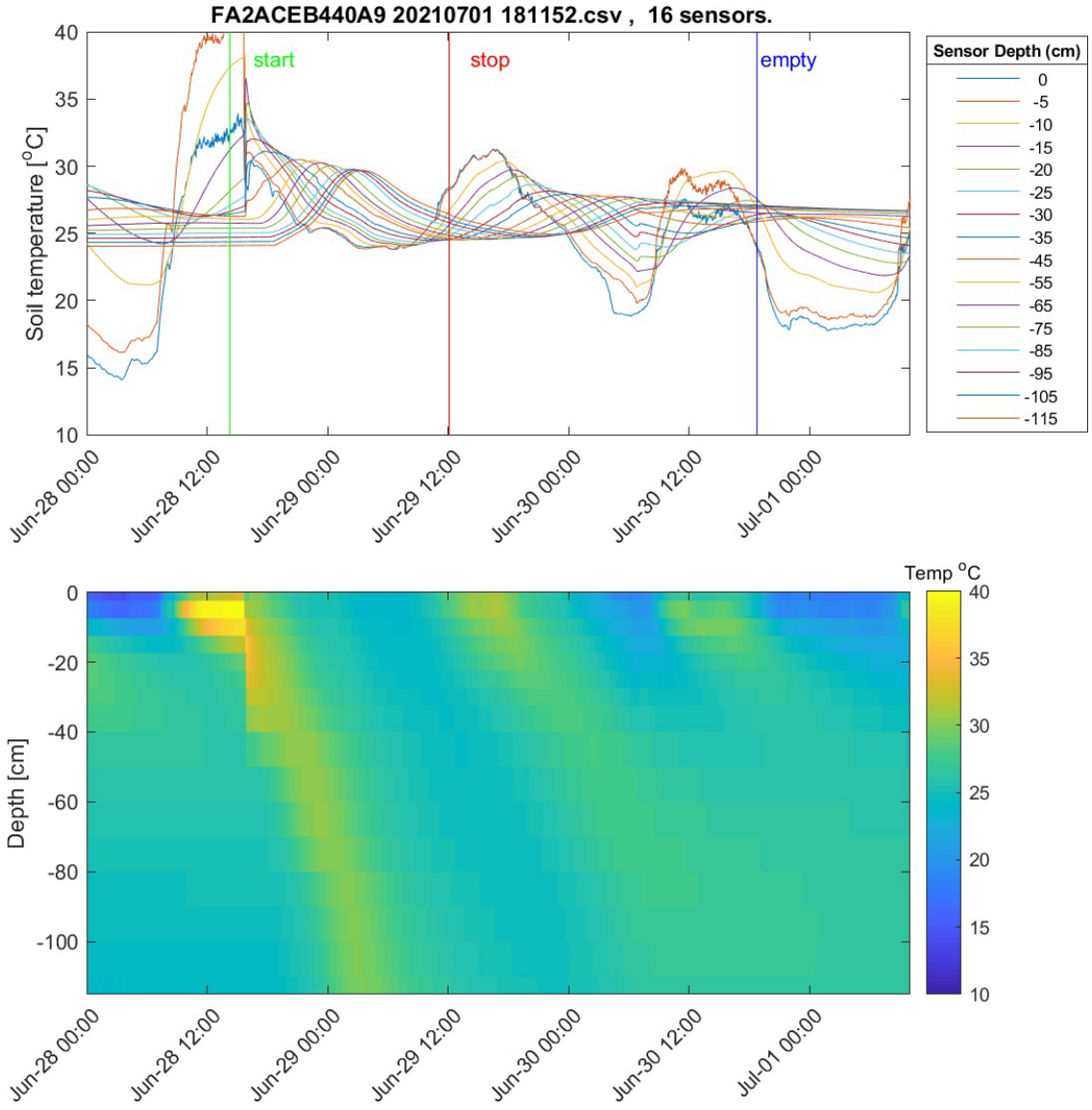
FA2ACEB440A9 20210701 181152.csv , 16 sensors.
Soil temperature [°C]
start
stop
empty
Sensor Depth (cm)
0
-5
-10
-15
-20
-25
-30
-35
-45
-55
-65
-75
-85
-95
-105
-115
Jun-28 00:00
Jun-28 12:00
Jun-29 00:00
Jun-29 12:00
Jun-30 00:00
Jun-30 12:00
Jul-01 00:00
Depth [cm]
Temp °C

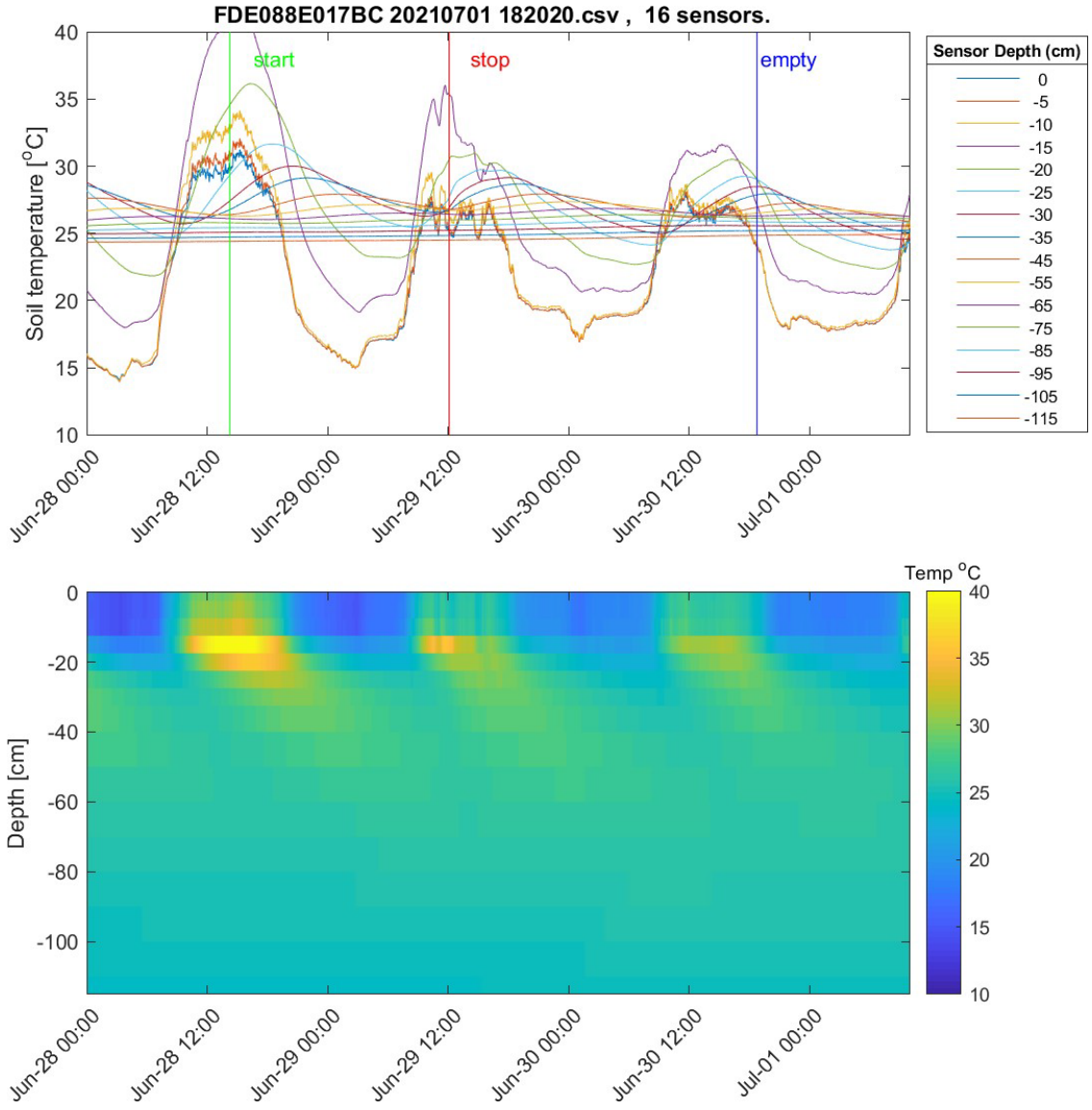
FDE088E017BC 20210701 182020.csv , 16 sensors.
start
stop
empty
Soil temperature [°C]
Sensor Depth (cm)
0
-5
-10
-15
-20
-25
-30
-35
-45
-55
-65
-75
-85
-95
-105
-115
Jun-28 00:00
Jun-28 12:00
Jun-29 00:00
Jun-29 12:00
Jun-30 00:00
Jun-30 12:00
Jul-01 00:00
Temp °C
Depth [cm]

Pond 11

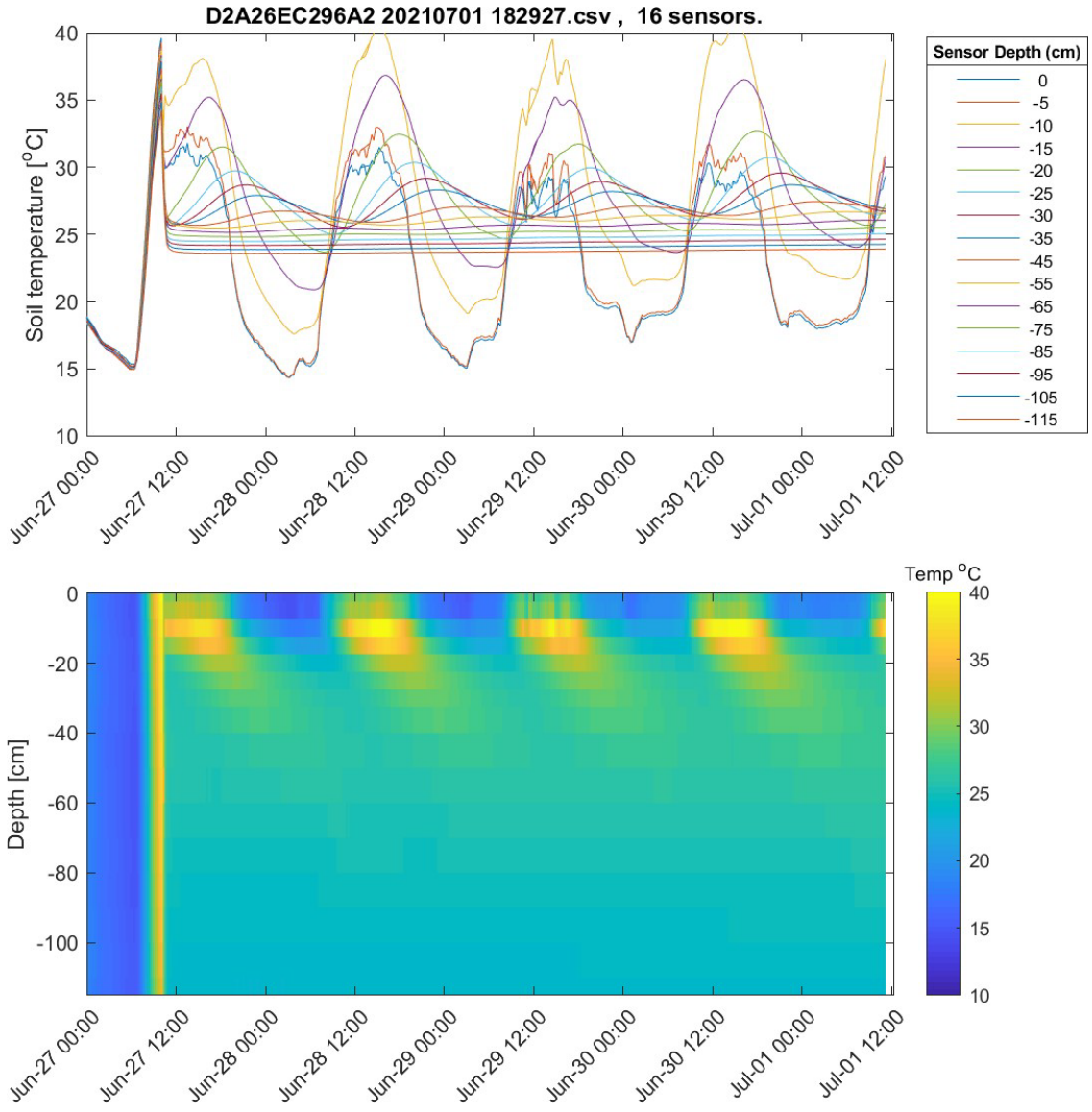
D2A26EC296A2 20210701 182927.csv , 16 sensors.
Soil temperature [°C]
Sensor Depth (cm)
0
-5
-10
-15
-20
-25
-30
-35
-45
-55
-65
-75
-85
-95
-105
-115
Jun-27 00:00
Jun-27 12:00
Jun-28 00:00
Jun-28 12:00
Jun-29 00:00
Jun-29 12:00
Jun-30 00:00
Jun-30 12:00
Jul-01 00:00
Jul-01 12:00
Depth [cm]
Temp °C

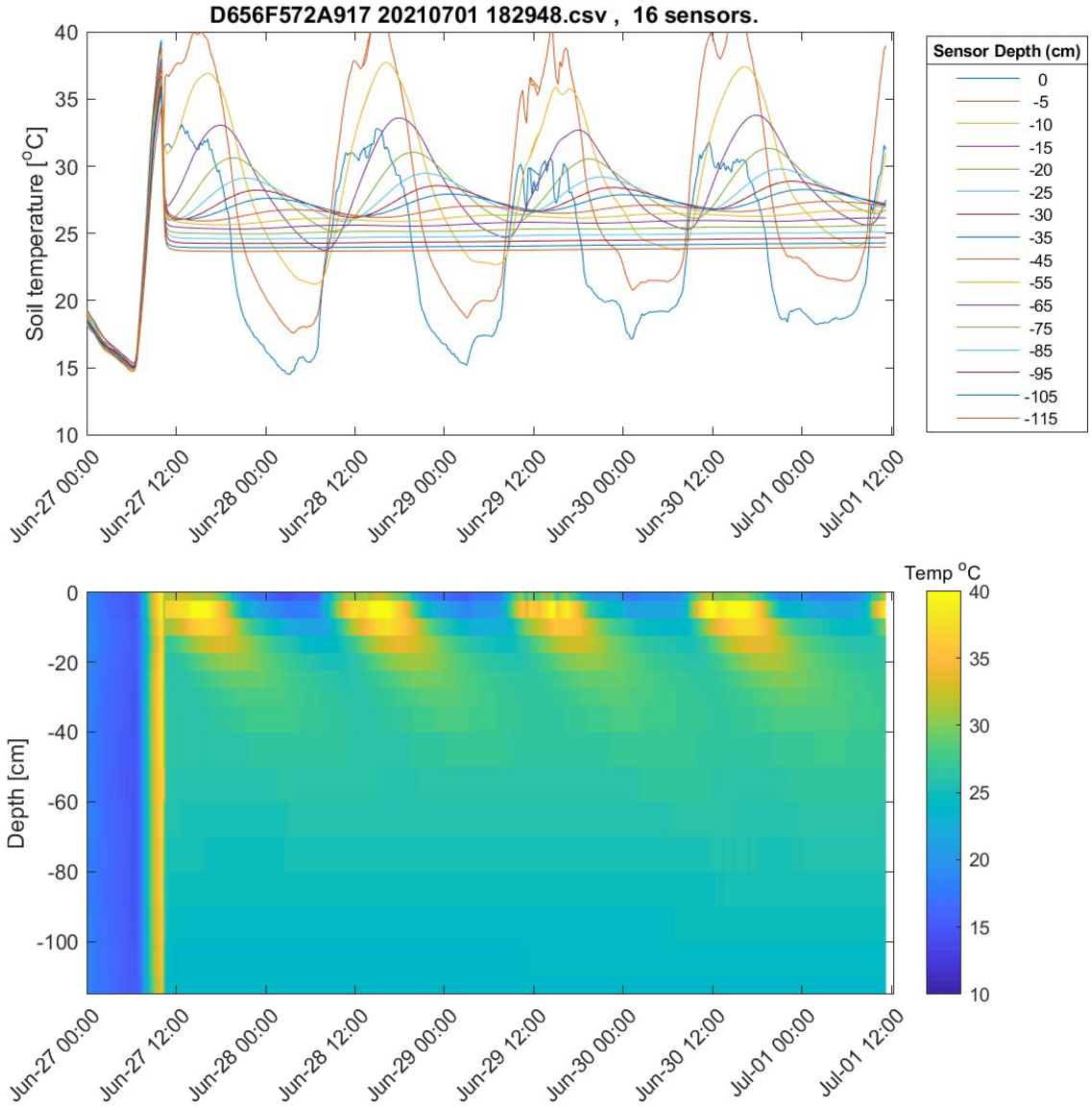
D656F572A917 20210701 182948.csv , 16 sensors.
Soil temperature [°C]
Sensor Depth (cm)
0
-5
-10
-15
-20
-25
-30
-35
-45
-55
-65
-75
-85
-95
-105
-115
Jun-27 00:00
Jun-27 12:00
Jun-28 00:00
Jun-28 12:00
Jun-29 00:00
Jun-29 12:00
Jun-30 00:00
Jun-30 12:00
Jul-01 00:00
Jul-01 12:00
Depth [cm]
Temp °C

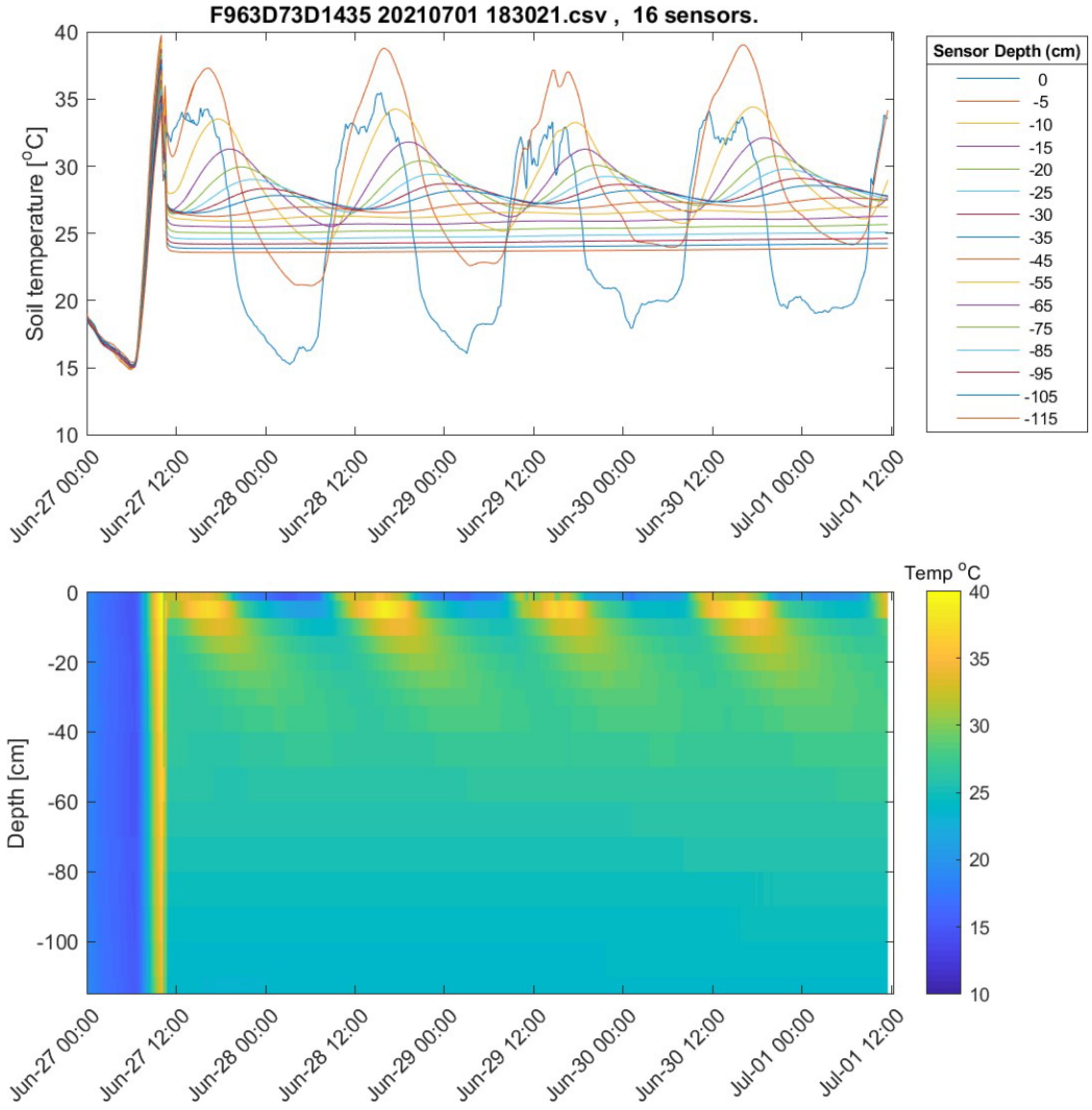
F963D73D1435 20210701 183021.csv , 16 sensors.
Soil temperature [°C]
Sensor Depth (cm)
0
-5
-10
-15
-20
-25
-30
-35
-45
-55
-65
-75
-85
-95
-105
-115
Jun-27 00:00
Jun-27 12:00
Jun-28 00:00
Jun-28 12:00
Jun-29 00:00
Jun-29 12:00
Jun-30 00:00
Jun-30 12:00
Jul-01 00:00
Jul-01 12:00
Depth [cm]
Temp °C

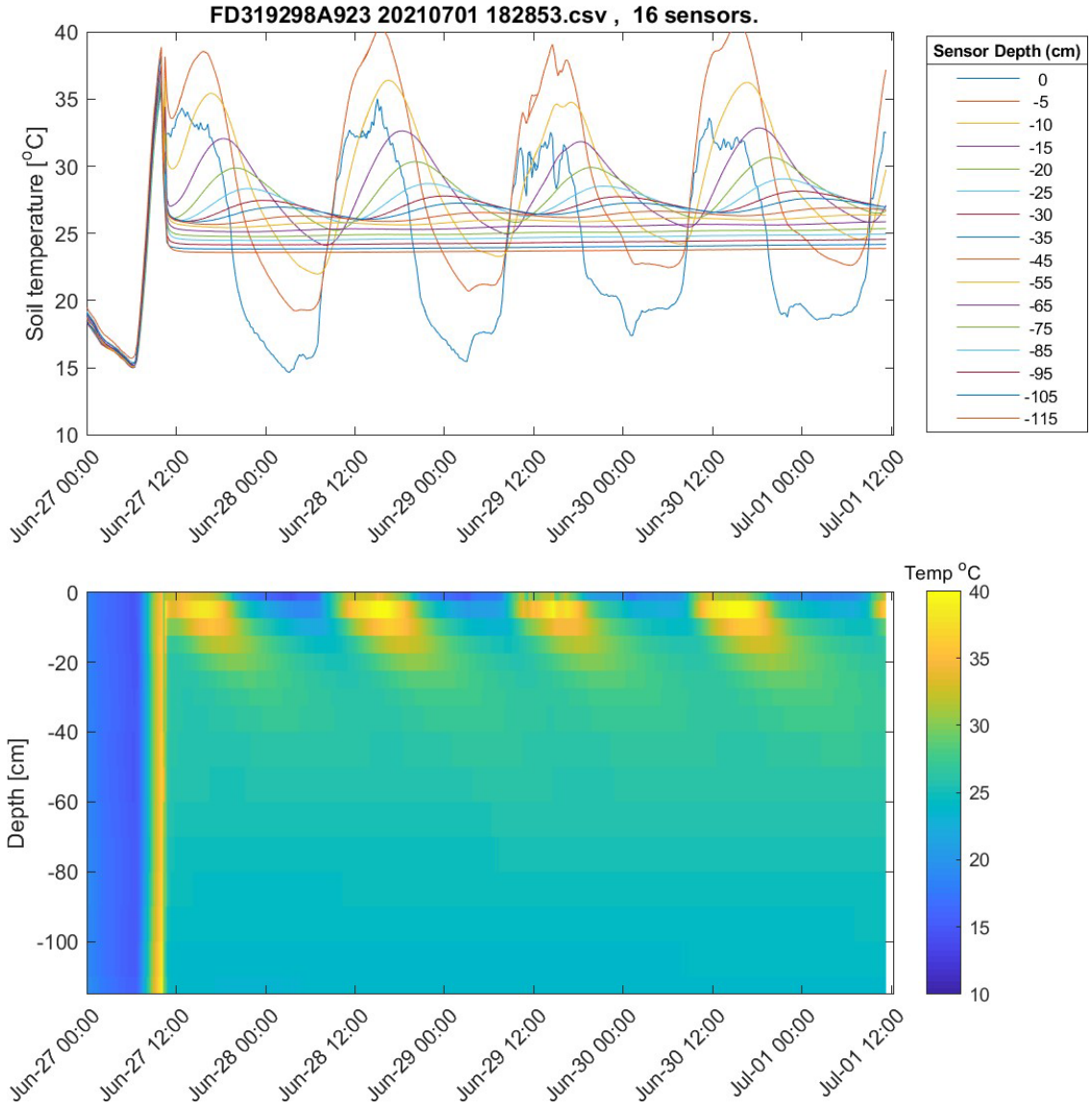
FD319298A923 20210701 182853.csv , 16 sensors.
Soil temperature [°C]
Sensor Depth (cm)
0
-5
-10
-15
-20
-25
-30
-35
-45
-55
-65
-75
-85
-95
-105
-115
Jun-27 00:00
Jun-27 12:00
Jun-28 00:00
Jun-28 12:00
Jun-29 00:00
Jun-29 12:00
Jun-30 00:00
Jun-30 12:00
Jul-01 00:00
Jul-01 12:00
Depth [cm]
Temp °C

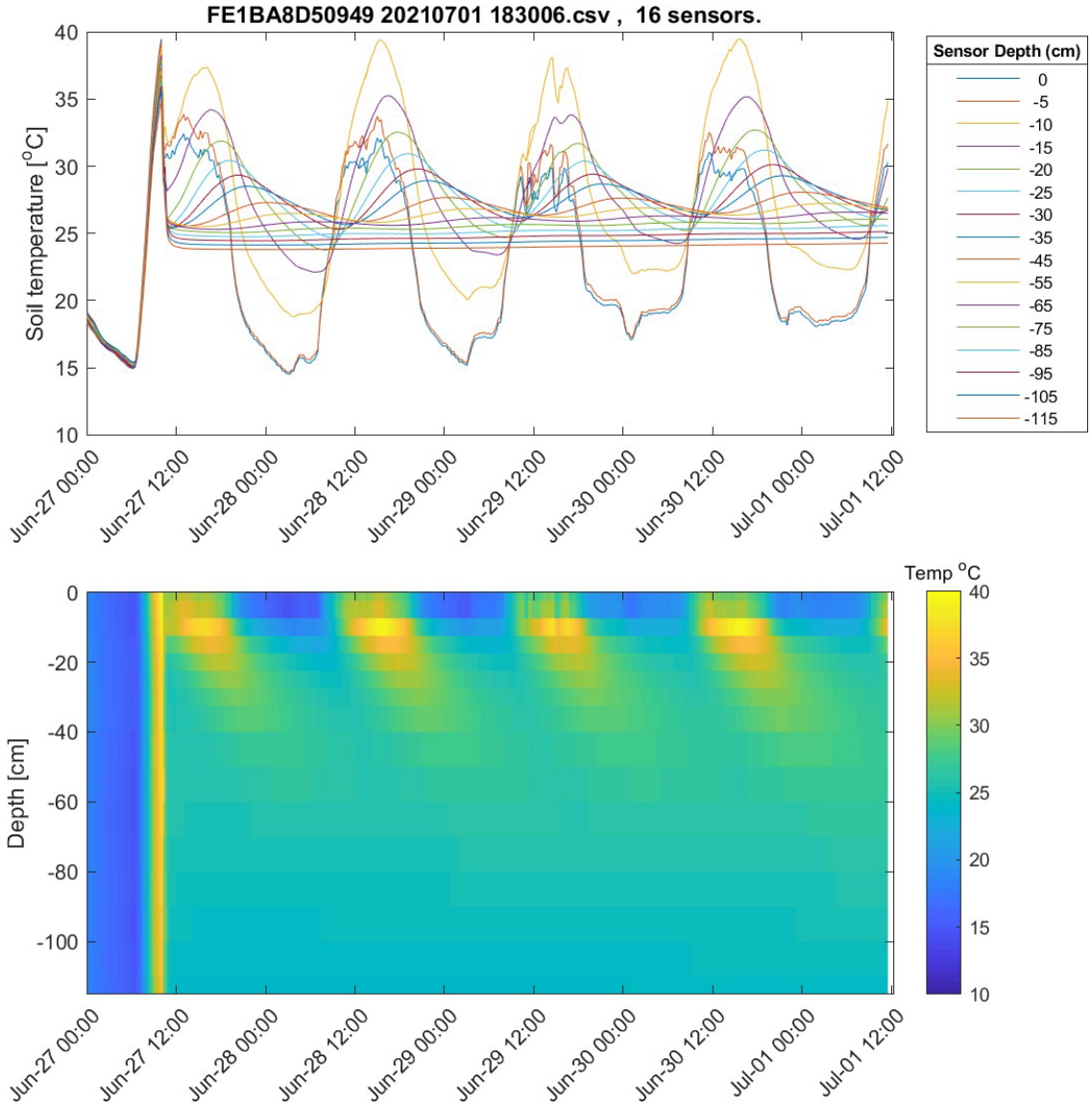
FE1BA8D50949 20210701 183006.csv , 16 sensors.
Soil temperature [°C]
Sensor Depth (cm)
0
-5
-10
-15
-20
-25
-30
-35
-45
-55
-65
-75
-85
-95
-105
-115
Jun-27 00:00
Jun-27 12:00
Jun-28 00:00
Jun-28 12:00
Jun-29 00:00
Jun-29 12:00
Jun-30 00:00
Jun-30 12:00
Jul-01 00:00
Jul-01 12:00
Depth [cm]
Temp °C

Appendix C

Cost and Timeline

The original proposed cost of the project was $240,000.00 that would be split between Metropolitan ($120,000.00) through a funding match under the Future Supply Actions Funding Program. Below is a table outlining the costs of the five listed tasks from Section 6.0 of the FSA Agreement.

6.0 Cost Estimate

Task No.	Task Description	Total Study Cost	Requested Metropolitan Funding Match
4.1	Scoping, Field Design, and Consultation	$20,000	$10,000
4.2	Characterization Campaign	$60,000	$30,000
4.3	Recharge Experiment	$80,000	$40,000
4.4	Data Analysis	$40,000	$20,000
4.5	Data Interpretation / Final Report / Scientific Paper Publication	$40,000	$20,000
	Totals	$240,000.00	$120,000.00

The final cost to project was:

Task No.	Task Description	Total Estimated Costs	Total Billed Costs
4.1	Scoping, Field Design, and Consultation	**$20,000**	**$9,113.92**
4.2	Characterization Campaign	**$60,000**	**$45,310.37**
4.3	Recharge Experiment	**$80,000**	**$51,678.38**
4.4	Data Analysis	**$40,000**	**$54.680.85**
4.5	Data Interpretation / Final Report / Scientific Paper Publication	**$40,000**	**$75,625.72**
NA	Additional funds to manage drilling for Ventura	**$9,500**	**$9,500.00**
	Totals	**$249,500.00**	**$245,909.24**

Schedule timeline Gantt Chart highlighting the progression of the project and when tasks were performed (orange colors) and when COVID-19 delays occurred (red colors).

		Jan-Mar	Apr-Jun	Jul-Sep	Oct-Dec	Jan-Mar	Apr-Jun	Jul-Sep	Oct-Dec
		2020				**2021**			
		Q1	**Q2**	**Q3**	**Q4**	**Q1**	**Q2**	**Q3**	**Q4**
Task	**Task Name**								
4.1	Scoping, Field Design, and Consultation								
4.2	Characterization Campaign								
4.3	Recharge Experiment								
4.4	Data Analysis								
4.5	Data Interpretation / Final Report / Scientific Paper Publication								
		Jan-Mar	Apr-Jun	Jul-Sep	Oct-Dec	Jan-Mar	Apr-Jun	Jul-Sep	Oct-Dec
		2022				**2023**			
		Q1	**Q2**	**Q3**	**Q4**	**Q1**	**Q2**	**Q3**	**Q4**
Task	**Task Name**								
4.1	Scoping, Field Design, and Consultation								
4.2	Characterization Campaign								
4.3	Recharge Experiment								
4.4	Data Analysis								
4.5	Data Interpretation / Final Report / Scientific Paper Publication								